TECHNO-ECONOMIC ANALYSIS OF HYDROGEN-INTEGRATED SUSTAINABLE ENERGY SYSTEMS

by

Honglin Li

APPROVED BY SUPERVISORY COMMITTEE:

Jie Zhang, Chair

Rotea A. Mario

D. Todd Griffith

Xinfang Jin

Copyright © 2025

Honglin Li

All rights reserved

To my family.

TECHNO-ECONOMIC ANALYSIS OF HYDROGEN-INTEGRATED SUSTAINABLE ENERGY SYSTEMS

by

HONGLIN LI, BA, ME, MS

DISSERTATION

Presented to the Faculty of

The University of Texas at Dallas

in Partial Fulfillment

of the Requirements

for the Degree of

DOCTOR OF PHILOSOPHY IN

MECHANICAL ENGINEERING

THE UNIVERSITY OF TEXAS AT DALLAS

December 2025

ACKNOWLEDGMENTS

I would like to express my deepest gratitude to my advisor, Professor Jie Zhang, for his invaluable guidance, encouragement, and support throughout my doctoral journey. His vision, insightful feedback, and continuous mentorship has shaped not only this dissertation but also my academic and professional growth.

I am also sincerely thankful to my committee members — Professor Mario Rotea, Professor Todd Griffith, and Professor Xinfang Jin — for their constructive advice, thoughtful feedback, and generous support. Their expertise and perspectives have greatly enriched this work and broadened my research outlook.

Beyond my committee, I wish to acknowledge my colleagues, collaborators, and friends at The University of Texas at Dallas and at the Idaho National Laboratory, whose discussions and encouragement have made this journey both intellectually rewarding and personally meaningful.

Finally, I would like to thank my family for their unwavering love, patience, and support. Their belief in me has been the foundation of my perseverance and success.

September 2025

TECHNO-ECONOMIC ANALYSIS OF HYDROGEN-INTEGRATED SUSTAINABLE ENERGY SYSTEMS

Honglin Li, PhD
The University of Texas at Dallas, 2025

Supervising Professor: Jie Zhang, Chair

The global energy transition is driven by the urgent need to achieve deep decarbonization while maintaining system reliability and economic viability. Yet, the variability of renewable resources and the limited flexibility of conventional baseload power remain key barriers to large-scale integration. Hydrogen has emerged as a versatile solution, capable of providing long-duration storage, enabling sector coupling, and enhancing the operational flexibility of energy systems. This dissertation develops three distinct techno-economic analysis (TEA) frameworks that integrate optimization modeling with lifecycle financial evaluation to systematically assess hydrogen's role in advancing sustainable energy systems.

The study explores three interconnected applications. It first examines the integration of hydrogen storage with renewable generation, showing how co-location strategies reduce curtailment and improve cost-effectiveness under diverse market and resource conditions. It then broadens the scope to the grid level, using the Texas power system as a case study to evaluate how hydrogen can mitigate uncertainty in renewable deployment and demand growth, while inter-regional hydrogen networks alleviate geographic mismatches and contribute to significant carbon reductions. Building on these insights, the framework is applied to nuclear power systems, where hydrogen production enhances operational flexibility, supports

participation in ancillary service markets, and creates new revenue streams—outcomes that are further reinforced under favorable policy incentives.

These analyses illustrate hydrogen's capacity to serve as a unifying energy carrier across renewable and nuclear contexts. The findings emphasize that the effectiveness of hydrogen-enabled systems depends not only on technological performance but also on evolving cost trajectories, market mechanisms, and policy frameworks. By establishing a coherent analytical foundation and offering actionable insights, this dissertation provides guidance for policymakers, industry leaders, and researchers in designing resilient, economically viable, and carbon-neutral energy pathways where hydrogen plays a central role.

TABLE OF CONTENTS

ACKNOWLEDGMENTS v

ABSTRACT vi

LIST OF FIGURES x

LIST OF TABLES xv

CHAPTER 1 INTRODUCTION 1

CHAPTER 2 LITERATURE REVIEW 4

2.1 Technical Analysis of Hydrogen as an Energy Storage Medium within Integrated Energy Systems 4

2.2 Techno-Economic Analysis (TEA) of Integrated Energy Systems (IESs) . . . 6

2.3 Technical and Economic Analysis of Hydrogen-Integrated Hybrid Energy Systems 8

CHAPTER 3 EVALUATE THE TECHNO-ECONOMIC FEASIBILITY OF HYDROGEN STORAGE FOR WIND ENERGY 10

3.1 Techno-Economic Analysis Methodology 10

3.2 Numerical Experiments 20

3.2.1 Results and Discussion 22

3.3 Sensitivity Analysis 25

3.3.1 Impact of Hydrogen Prices on System Configurations 26

3.3.2 Impact of Regional Variations on System Configurations 27

3.3.3 Impact of Future Component Prices on System Configurations 30

3.4 Summary 30

CHAPTER 4 ASSESS HYDROGEN'S ROLE IN INCREASING RENEWABLE ENERGY PENETRATION AND GRID DECARBONIZATION 33

4.1 A Stochastic Optimization Model for Renewable Energy Integration in the Electric Reliability Council of Texas (ERCOT) Power Grid 35

4.2 Results 41

4.2.1 Optimization of The Power System 41

4.2.2 Analysis and Optimization of Hydrogen Systems 46

4.2.3 Carbon Dioxide (CO2) Emission Abatement Analysis 50

4.3 Summary 54

CHAPTER 5 TECHNO-ECONOMIC ANALYSIS OF HYDROGEN STORAGE WITH NUCLEAR ENERGY FOR GRID ANCILLARY SERVICES 57
5.1 Nuclear-Hydrogen Ancillary Service Optimization Model 60
5.1.1 Optimization Model Formulation 60
5.1.2 Techno-Economic Analysis Framework 65
5.1.3 Data Generation and Collection 72
5.1.4 System Parameter Formulation 72
5.1.5 Time-Series Data Generation Collection 74
5.2 Results 76
5.2.1 Economic Viability and Revenue Diversification of Integrated Nuclear-Hydrogen Systems 76
5.2.2 Operational Flexibility and Ancillary Service Provision under High-resolution Dispatch 77
5.2.3 Sensitivity Analysis 80
5.3 Summary 84
CHAPTER 6 CONCLUSIONS AND FUTURE WORK 86
APPENDIX A NOMENCLATURE 90
APPENDIX B SYSTEM PARAMETERS OF CHAPTER 5 98
APPENDIX C TECHNO-ECONOMIC ANALYSIS PARAMETERS OF CHAPTER 5 102
APPENDIX D ANCILLARY SERVICES LIST OF CHAPTER 5 106
APPENDIX E ABBREVIATIONS 108
REFERENCES 110
BIOGRAPHICAL SKETCH 124
CURRICULUM VITAE

LIST OF FIGURES

3.1 TEA framework for the integrated wind and hydrogen system (modified from [81]) 11

3.2 Model architecture of the Renewable Energy Integration and Optimization tool (REopt) modules adopted/created in this study (modified from [81]) 12

3.3 Overall structure of the grid-connected IES with wind, battery, hydrogen, and fuel cells 14

3.4 The annual wind power generation of the simulated wind farm in 2020 21

3.5 Monthly output energy of the IES for each component in the four cases 24

3.6 Hourly wind power allocation and state of charge (SOC) of battery and hydrogen tank within the IES over a randomly selected 168 consecutive hour period. Battery, Grid, and Electrolyzer in the legend represent the hourly wind power allocation to the battery, grid, and electrolyzer, respectively. Curtailed and Wind Generation represent wind energy curtailment and actual wind power generation, respectively. 25

3.7 Sensitivity analysis of the impact of hydrogen price on levelized cost of hydrogen (LCOH), capital expenditure (CAPEX), curtail rate price 27

3.8 Sensitivity analysis of the impact of wind profile in different regions on levelized cost of energy (LCOE), LCOH, CAPEX, and curtailed rate 29

3.9 Sensitivity analysis of future components' prices 31

4.1 Conceptual Diagram of the Future Texas Power System with Hydrogen Integration. The future Texas power system will rely on combined cycle gas-turbine (CCGT) plants, wind, and solar to meet ERCOT's demand, with batteries and hydrogen providing energy storage. Natural gas will also produce hydrogen via steam methane reforming (SMR) for industrial use, with CO2 emissions from both gas plants and SMR captured and stored through carbon capture, utilization, and storage (CCUS) technology to achieve zero carbon emissions. 34

4.2 Structural Diagram of the Stochastic Optimization Model. This model focuses on maintaining three key system balances: electricity demand, hydrogen demand, and carbon balance. The carbon balance addresses CCUS from CCGT and SMR processes. Hydrogen and electricity are interconverted via electrolyzers and hydrogen fuel cells to maintain equilibrium between electricity and hydrogen demand. The core influencing factors of these balances are the primary focus of the model, with the objective function aiming to minimize the total cost of maintaining these three critical balances. 42

4.3 Spatial and Temporal Differences Between Renewable Energy Generation and Electricity Demand in ERCOT. **a** shows that peak renewable energy generation in ERCOT occurs between 9am and 3pm, while peak electricity consumption is concentrated from 3pm to 7pm. Seasonally, **b** depicts renewable energy generation peaks in the second quarter, whereas electricity demand peaks in the third quarter. These mismatches highlight the need for both short- and long-term storage solutions to enhance renewable energy integration into the ERCOT grid. Figures **c** and **d** illustrate the spatial distribution of renewable energy generation and electricity demand across the eight weather zones within ERCOT (Both are results for 2023, in kW), with darker colors representing higher values. The data reveal a clear spatial disparity: renewable energy generation is primarily concentrated in the Midwest region, while electricity demand is predominantly focused in the Southeast and North regions, highlighting significant geographic differences in supply and demand. 43

4.4 Results of Power System Optimization. **a**, Stochastic optimization results showing power balance within the system. During peak clean energy generation, excess electricity is stored in batteries, while some is converted into green hydrogen via electrolyzers. In periods of low generation, stored energy from batteries and CCGT work together to meet power demand, maintaining system stability. **b**, The difference between original power demand and actual power supply after load regulation. Demand-side adjustments successfully shift peak demand periods to better align with the system's power generation profile. 44

4.5 Hydrogen demand (kg/Day) 47

4.6 Inter-Zone Hydrogen Network in ERCOT and Results. **a**, Hydrogen pipeline connections and distance assumptions. **b**, Strategic placement of electrolysis units and hydrogen distribution. **c** and **d**, Sensitivity analysis of system costs under equipment and tariff changes. **e**, Green hydrogen distribution across zones in power system optimization. 48

4.7 CO2 Emission Percentage. The figure illustrates the carbon emission shares from various energy sources across ERCOT's zones: Coast, East, Far West, North, North Central, South, South Central, and West. Direct combustion and electricity generation account for over 60% of total carbon emissions in each region. In Zone East, electricity generation contributes a staggering 93.3% of the region's emissions due to its low renewable energy penetration and distance from major wind and solar hubs in the Midwest. Zone Far West, a key fossil fuel production area, sees 33.9% of its emissions coming from oil-related activities. Meanwhile, Zone Coast, despite being a core petrochemical region, has minimal petroleum-related emissions, primarily because hydrogen used in its production processes is supplied from other Gulf Coast states, reducing reliance on local fossil fuels. These patterns underscore the regional differences in carbon emissions, driven by geographic, industrial, and energy resource factors across ERCOT's territory. 51

4.8 Results of Sensitivity Analysis on Carbon Emissions. **a**, Through demand-side load regulation, renewable energy utilization becomes significantly more efficient, leading to notable reductions in carbon emissions from both SMR and CCGT. Completion rates and electricity demand directly impact these emissions, with low completion rates and high demand increasing emissions from both sources. Reduced battery installation completion lowers renewable energy flexibility, decreasing utilization rates and raising CCGT emissions, while SMR emissions remain unaffected. **b**, Higher CCGT tariffs lead to increased conversion of green hydrogen to electricity, lowering overall electricity use efficiency. This shift raises carbon emissions from SMR and the overall system, despite a reduction in emissions from CCGT. 53

5.1 Installed capacity and costs of commercial nuclear power across countries. **a**, Overnight capital costs of nuclear construction in major countries. Most countries report values exceeding $2,000/kW, with the U.S. surpassing $4,000/kW [77, 69, 105]. **b**, Comparison of nuclear LCOE with other sources. In most countries, nuclear LCOE exceeds that of solar Photovoltaic (PV) ($47/MWh) and onshore wind ($40/MWh). In the U.S., initial capital expenditures account for over 50% of the total LCOE, highlighting investment cost as a dominant driver [152, 103]. **c**, Changes in global nuclear capacity over the past 20 years, reported in five-year intervals (A: added; R: retired). While total installed capacity has slightly increased, most traditional nuclear countries show declining trends [49, 67, 154]. **d**, Country-level nuclear capacity trends. Over the past two decades, nuclear additions have primarily occurred in China and other emerging markets, whereas traditional nuclear countries—led by the U.S.—have seen substantial retirements. Germany has fully phased out its nuclear fleet [67, 154, 49]. 58

5.2 Modeling framework for the nuclear-hydrogen energy system optimization. TEA framework consists of two main components. The first is an optimization model for the nuclear–hydrogen system, which incorporates system characteristics, electricity and ancillary service market data, and operational constraints to determine the optimal configuration and dispatch strategy. The second component uses the optimization outputs, policy incentives, and cost parameters to evaluate the system's techno-economic performance and compute key financial metrics, including net present value (NPV). 60

5.3 Economic performance of the nuclear–hydrogen system. **a**, Comparison of NPV across two cases, before and after tax credits. In the Business-as-Usual (BAU) case (Case 1), the average NPV across 42 reactors is negative, lowest in ERCOT. After the Section 45U Production Tax Credit (45U PTC), some regions (e.g., Independent System Operator New England (ISONE), New York Independent System Operator (NYISO)) turn positive, though the overall average remains negative—showing most reactors still struggle. In the hybrid system (Case 2), the national average NPV is positive even without policy support, though ERCOT, Midcontinent Independent System Operator (MISO), and Southwest Power Pool (SPP) stay negative. With 45U, all reactors achieve positive NPV. **b**, LCOH breakdowns for hybrid systems across seven Independent System Operators (ISOs), compared with U.S. Department of Energy (DOE) 2030 target, Small Modular Reactor, and renewable electrolysis. LCOH exceeds the DOE target and SMR but is below renewable electrolysis. Electricity costs dominate, followed by capital investment. **c**, NPV of new nuclear–hydrogen systems with 60- and 80-year lifespans under three policy cases: no credit, Section 45Y Production Tax Credit (45Y PTC), and Section 48E Investment Tax Credit (48E ITC). NPVs stay negative under current costs. Shorter lifespans yield higher NPVs due to lower O&M escalation and fewer replacements. Revenues from extended years cannot offset rising expenses. Among policies, 48E ITC is most favorable, followed by 45Y. **d**, Revenue composition of hybrid systems across seven regions. Electricity sales account for about half of total revenue. Hydrogen—split between direct sales and Section 45V tax credits (45V)—forms the second largest share. Both assume \$3/kg, though totals differ slightly by production vs. sales bases. Ancillary services, though small, provide extra income. 78

5.4 Operational flexibility of the nuclear–hydrogen system. **a**, Hourly heatmap of electricity exported to the grid by a nuclear–hydrogen system in the Pennsylvania-New Jersey-Maryland Interconnection (PJM) region over a full year. The system departs from a traditional baseload profile, exhibiting fluctuations exceeding 100 MW. Output closely follows grid demand, with near-maximum generation during morning and evening peaks and reduced output during off-peak hours, indicating strong load-following capability. **b**, Annual energy flow within the system. Reactor thermal output remains constant, primarily powering the turbine, with a smaller portion directed to the high-temperature electrolyzer (HTE). In the secondary energy allocation, most turbine-generated electricity is exported to the grid, with the remainder used to power the HTE, supply ancillary services, and meet balance of plant (BOP) demand. **c**, Hourly energy distribution breakdown. Consistent with the annual trend, most reactor energy is converted to electricity for export, followed by hydrogen production, ancillary services, and BOP, demonstrating efficient intra-system energy management. **d**, Average share of reactor energy used for ancillary services across regions. Most regions maintain a 5–8% share, reflecting the system's active participation in ancillary markets. In contrast, ISONE exhibits a lower share (2.7%) due to limited ancillary service offerings. 81

5.5 Sensitivity analysis of key system parameters. **a**, Nuclear fixed O&M and NPV. In BAU, NPV remains negative even as O&M falls from $230k/MW to $170k/MW. In the hybrid case, NPV rises 130% at $170k/MW but falls 370% at $290k/MW. **b**, HTE capacity limits. Relative to the 200 MW baseline, lower limits cut tank size and sales, while higher limits sustain output despite lower utilization. **c**, Revenues. Greater HTE capacity increases total and hydrogen revenues, though hydrogen peaks at 250 MW before declining. Ancillary revenues rise sharply with added flexibility. **d**, Ancillary services. Larger HTEs allow higher bids, especially beyond 200 MW, with regulation prioritized. Other bids shrink, but deployment rises. **e**, Grid output. Average output falls with larger HTEs, but variability grows, peaking at 120 MW under 250 MW, highlighting flexibility until system limits bind. **f**, Ramp rates. Higher HTE capacity raises ramp rates of both HTE and turbine; beyond a threshold, HTE slows from energy limits while turbine declines as flexibility shifts to HTE. 83

LIST OF TABLES

3.1 Key assumptions in the IES setup [122, 24, 121, 61, 109] 21

3.2 Integrated energy system component capacity and cost 23

3.3 The location of the four distinct wind farms located in different ISO regions . . 28

3.4 Annual technology baseline ($/kW for CAPEX, O&M except tank: $/kg) [103, 123, 106, 3] 29

4.1 Uncertainty scenarios for installed capacity and electricity demand growth . . . 36

4.2 Probability of stochastic scenarios 36

4.3 Key parameters used in the stochastic optimization model for the benchmark case study [13, 126, 28, 14, 81]. 37

4.4 Results for CCGT capacity, green hydrogen rate, and storage unit status for each region in the benchmark case. 42

4.5 Sensitivity analysis scenarios for optimization of the power system 45

4.6 Sensitivity analysis scenarios for analysis and optimization of hydrogen systems 49

4.7 The optimal capacity of hydrogen-related equipment 50

4.8 Optimal sizes of hydrogen related equipment for C4 52

4.9 Sensitivity analysis scenarios for CO2 emission abatement analysis 53

5.1 MACRS depreciation schedules 68

A.1 Nomenclature of Chapter 3 90

A.2 Nomenclature of Chapter 4 92

A.3 Nomenclature of Chapter 5 94

B.1 Advanced system parameters [151, 11, 64, 65, 66, 90, 50, 9, 98, 103, 37, 18, 154] 98

C.1 Core data and parameters for the TEA framework [151, 11, 64, 65, 66, 90, 33, 9, 98, 103, 37, 18, 49, 77] 102

D.1 Ancillary services across U.S. ISOs [17, 39, 96, 100, 71, 129, 113] 106

E.1 List of abbreviations used in the main text 108

CHAPTER 1

INTRODUCTION

The global energy system is undergoing a profound transformation driven by the urgent need to reduce greenhouse gas emissions and mitigate the impacts of climate change. The reliance on fossil fuels has long provided reliable and affordable energy but has also resulted in significant environmental and geopolitical challenges. With increasing international commitments to net-zero emissions by mid-century, nations are accelerating the deployment of renewable energy sources such as wind and solar. These resources are now growing at unprecedented rates, supported by technological advances, declining costs, and strong policy incentives. However, their variability and intermittency continue to pose substantial challenges for maintaining grid stability, reliability, and economic efficiency. Addressing these challenges requires innovative approaches that combine technological innovation, economic feasibility, and supportive policy frameworks.

Hydrogen has emerged as a promising energy carrier to complement and enhance renewable energy integration. Unlike batteries and other short-duration storage technologies, hydrogen offers long-term, large-scale storage potential. It can be produced via electrolysis using surplus renewable electricity, stored in tanks or pipelines, and converted back into power or used in diverse sectors including industry, transportation, and heating. This versatility makes hydrogen uniquely positioned to bridge the gap between variable renewable generation and steady energy demand, while also facilitating sector coupling and supporting deep decarbonization. At the same time, the economic feasibility of hydrogen-integrated hybrid systems remains uncertain, dependent on technology costs, infrastructure development, and policy incentives. Therefore, systematic TEA is essential to evaluate hydrogen's role in future energy systems and guide investment and policy decisions.

This dissertation aims to explore hydrogen's role in advancing sustainable and low-carbon energy systems through three distinct techno-economic frameworks. Each framework is designed to address specific contexts where hydrogen integration could provide operational, economic, and environmental benefits. Collectively, these frameworks offer a holistic view of how hydrogen can contribute to renewable integration, grid flexibility, and decarbonization, while also highlighting the conditions under which such systems become economically viable.

The first framework focuses on the integration of hydrogen with renewable energy at the project level. Wind power, one of the most rapidly expanding renewable sources in the United States, often experiences curtailment when generation exceeds demand or transmission

capacity. Co-locating hydrogen production facilities with wind farms presents an opportunity to convert excess electricity into hydrogen, thereby reducing curtailment, increasing project revenues, and enabling long-duration storage. This framework employs optimization models to compare system configurations involving batteries, electrolyzers, hydrogen storage, and fuel cells. The analysis reveals trade-offs between system cost, levelized cost of hydrogen (LCOH), levelized cost of energy (LCOE), and curtailment reduction. Sensitivity analyses further explore the impacts of hydrogen prices, regional resource variations, and future component cost trajectories, offering insights into the scalability and economic feasibility of renewable-hydrogen systems.

The second framework expands the analysis to the grid level, using the Electric Reliability Council of Texas (ERCOT) as a representative case study. Texas is uniquely positioned due to its vast wind and solar resources, growing hydrogen economy, and significant carbon emission profile. Yet, the state's grid faces challenges from renewable variability, geographic mismatches between supply and demand, and uncertainties in future capacity expansion and demand growth. A stochastic optimization model is developed to capture these uncertainties, while also incorporating hydrogen production, storage, and inter-regional transportation networks. The results demonstrate that hydrogen can play a critical role in balancing supply and demand across regions, enhancing renewable penetration, and reducing carbon emissions. Sensitivity analyses reveal the dependence of system outcomes on electricity prices, carbon costs, and hydrogen equipment costs, highlighting both opportunities and risks in large-scale hydrogen deployment. This framework underscores the importance of infrastructure development, regional planning, and policy support in realizing the potential of hydrogen-enabled grids.

The third framework highlights hydrogen's role in unlocking both the flexibility and economic potential of nuclear energy, which has long been constrained by its traditional baseload operation. While nuclear energy is a high-capacity, low-carbon resource that stabilizes power systems, its rigidity in the face of growing renewable penetration limits its contribution to a dynamic clean grid. By coupling nuclear generation with hydrogen production, excess output can be redirected toward marketable hydrogen, with the addition of electrolyzers providing greater operational flexibility to the hybrid system, enabling it to more effectively participate in grid services and revenue diversification. In this way, hydrogen enables nuclear plants to participate in ancillary service markets, thereby addressing a fundamental barrier to nuclear's broader role in a renewable-dominated system. A mixed-integer optimization model is combined with a lifecycle TEA to evaluate the economic and operational performance of nuclear-hydrogen-battery systems under different market and policy conditions. Case

studies of U.S. nuclear reactors demonstrate that hydrogen integration can create new revenue streams, improve nuclear plant profitability, and support grid stability. Policy incentives, such as the 45U production tax credit and 48E investment tax credit, are shown to significantly enhance project economics.

This dissertation contributes to the growing body of knowledge on hydrogen-integrated energy systems through four key areas. First, it develops three optimization-based frameworks tailored to different levels of hydrogen integration—project-level, grid-level, and hybrid nuclear systems—to systematically evaluate the techno-economic advantages that hydrogen brings to diverse energy configurations. Second, it presents a detailed case study of wind-hydrogen co-location projects, demonstrating the technical feasibility and economic benefits of using hydrogen as a storage medium to enhance renewable energy utilization. Third, using the ERCOT grid as an example, it assesses the role of hydrogen in mitigating supply-demand uncertainty and imbalance and enabling deeper decarbonization at the system level. Fourth, it explores how hydrogen can enhance the operational flexibility and economic performance of nuclear power plants, thereby expanding their contribution to high-renewable energy systems. Together, these contributions offer actionable insights for policymakers, energy planners, and industry stakeholders seeking to design resilient, economically viable, and low-carbon energy systems. This research advances a rigorous set of analytical tools and evidence-based conclusions that position hydrogen as a key enabler in the sustainable energy transition.

The remainder of this dissertation is organized as follows. Chapter 2 provides a literature review covering both technical and techno-economic studies of hydrogen as an energy storage medium within integrated energy systems. Chapter 3 introduces the first analytical framework, which evaluates the techno-economic feasibility of co-locating wind energy with hydrogen storage and conversion technologies, along with the corresponding results and sensitivity analyses. Chapter 4 expands the scope to grid-scale analysis, presenting a stochastic optimization framework applied to the ERCOT power system, accompanied by results on renewable penetration, hydrogen networks, and carbon reduction. Chapter 5 develops the third framework, which analyzes hydrogen integration with nuclear power systems. It focuses on evaluating how the incorporation of hydrogen production, combined with federal incentive policies, enhances both the economic viability and operational flexibility of existing nuclear power plants. These improvements strengthen the competitiveness of nuclear assets and expand their capacity to participate in electricity market operations and grid-balancing services. Finally, Chapter 2 concludes with key findings, policy implications, and directions for future research.

CHAPTER 2

LITERATURE REVIEW[1][2]

The literature review is structured into two distinct yet interrelated categories. The first encompasses the technical analysis of hydrogen as an energy storage medium within renewable integrated energy systems (IESs), analyzing the technical aspects of its production, storage, transportation and integration as an energy storage medium. The second focuses on the TEA of renewable IESs, evaluating the economic feasibility, cost-benefit trade-offs, and market dynamics that shape the integration of renewable energy with hydrogen storage solutions. Additionally, this review critically assesses the research gaps and limitations in existing studies, highlighting unresolved challenges and underscoring the need for further research to address technical inefficiencies, economic uncertainties, and policy constraints.

2.1 Technical Analysis of Hydrogen as an Energy Storage Medium within Integrated Energy Systems

Hydrogen Production Technologies for Renewable Energy Integration: The pursuit for efficient and sustainable energy solutions has spurred numerous studies exploring various hydrogen production methods that can seamlessly complement and enhance renewable energy systems. Among the prominent contenders, electrolysis, in particular, has emerged as a promising candidate, offering innovative avenues for harnessing excess renewable energy and converting it into valuable hydrogen resources. Two primary forms of electrolysis have taken the spotlight: proton exchange membrane electrolysis [107] and alkaline electrolysis [125]. Both methods have been subjected to thorough examination, highlighting their remarkable capabilities in facilitating the conversion of surplus renewable power into clean, storable hydrogen fuel. Apart from electrolysis, researchers have also delved into alternative avenues to achieve optimal hydrogen production alongside renewable energy integration. One such approach entails methane reforming [26], which has captivated attention for its potential to effectively harness renewable energy and convert methane into hydrogen, thereby presenting a compelling pathway for energy conversion and storage.

[1] ©2024 ASME. Reprinted, with permission, from Li, H. and Zhang, J., 2024. Towards sustainable integration: Techno-economic analysis and future perspectives of co-located wind and hydrogen energy systems. Journal of Mechanical Design, 146(2), p.020903.

[2] Li, H. and Zhang, J., 2025. Hydrogen's role in expanding renewable energy and reducing carbon emissions in Texas. International Journal of Hydrogen Energy, 113, pp.77-89.

Hydrogen Storage and Transportation: The efficient storage and seamless transportation of hydrogen constitute pivotal pillars in the pursuit of transforming it into a highly viable and effective option for power smoothing within the realm of renewable energy. Over the years, extensive research has diligently explored and evaluated a diverse range of hydrogen storage techniques, each holding the potential to unlock the full promise of this clean, abundant fuel source. One of the primary avenues investigated is compressed hydrogen storage [38], wherein hydrogen gas is compressed at high pressures and stored in specially designed containers. This approach offers an impressive balance between energy density and practicality, making it suitable for a variety of applications, including renewable energy power smoothing. The advancement in materials and engineering techniques has significantly enhanced the safety and efficacy of compressed hydrogen storage solutions, further solidifying its appeal. Another avenue of investigation lies in the domain of liquid hydrogen storage [56], wherein hydrogen is cooled and maintained at cryogenic temperatures to exist in a liquid state. This method capitalizes on the superior energy density of liquid hydrogen, allowing for increased storage capacity and extended usability. While presenting unique challenges due to the need for cryogenic systems, liquid hydrogen storage has shown great potential, especially in long-term energy storage scenarios where maximizing capacity is essential. In tandem with storage advancements, researchers have diligently explored various transportation methods, aiming to efficiently move hydrogen from production sites to end-users or dedicated energy storage facilities. Among these methods, pipelines [85] stand out as a primary choice for large-scale transportation, offering a cost-effective and reliable means of conveying hydrogen over significant distances. Investment in pipeline infrastructure for hydrogen has been growing, with the potential to form extensive networks that connect diverse regions and enable widespread adoption of hydrogen energy.

Hydrogen Electrolysis and Grid Ancillary Services: A study by Cl'ua et al. analyzed a grid-assisted wind power system for hydrogen production, evaluating different operation modes to optimize hydrogen output and grid stability [22]. Zenith et al. further investigated the economic viability of curtailed hydrogen as a grid-balancing service, finding that hydrogen production from curtailed wind energy can provide significant financial benefits [162]. Another research effort by Tavakoli et al. proposed using hydrogen electrolyzers not just as responsive loads but as grid-forming units capable of regulating voltage and frequency, enhancing the reliability of low-inertia power systems [135]. Raab et al. conducted a TEA showing that hydrogen production facilities benefit significantly from grid interaction, reducing installation costs and enhancing efficiency [117]. Furthermore, Andrade et al. developed an optimal control framework for PV-hydrogen production systems to minimize grid energy

consumption while maximizing hydrogen generation [5]. In another application, Meraj et al. demonstrated a hydrogen-based grid system that improves microgrid power quality through bidirectional energy storage, enhancing reliability [95]. Additionally, Gao et al. assessed the role of electric-hydrogen coupling systems in peak shaving and grid stabilization, confirming their effectiveness in reducing volatility and improving economic efficiency [52]. Oskouei and Mehrjerdi introduced an optimal allocation model for power-to-hydrogen units, showing that these units can enhance grid resilience and financial returns in renewable-dominated regions [108].

2.2 Techno-Economic Analysis (TEA) of Integrated Energy Systems (IESs)

Researchers use advanced techno-economic models and optimization frameworks to evaluate the feasibility and benefits of integrating hydrogen with wind power [119, 53, 27, 79]. These tools assess economic viability by analyzing capital and operational costs, including hydrogen production, storage, and utilization. They also compare these expenses with potential savings and revenue streams to determine financial feasibility. Additionally, energy efficiency is a key consideration, as the performance of hydrogen production, storage, and utilization technologies directly impacts system viability. By optimizing these factors, researchers identify cost-effective pathways for successful hydrogen integration.

Optimization Techniques: Optimization-based methodologies play a significant role in the TEA of IES. These methods facilitate the identification of cost-effective and energy-efficient configurations. Wu et al. [155] propose a bi-level optimization method that categorizes electrical loads and optimizes the output of micro sources, including gas-fired generators, energy storage systems, and renewable energy sources. Their findings demonstrate cost reductions and improved operational efficiency. A key advancement in optimization techniques is the integration of hybrid energy storage systems. Xie and Li [157] investigate the impact of life cycle assessment on optimizing hydrogen-based IES configurations. Their study highlights the role of carbon trading mechanisms in reducing operational costs and promoting cleaner energy integration. Additionally, Yan [158] introduces an improved ε-constraint method to balance multiple economic and environmental objectives in IES operation, offering a structured approach to decision-making in energy network optimization. Furthermore, stochastic optimization techniques are gaining traction in addressing the uncertainties in energy demand and supply. Xiao et al. [156] propose a Markov-Chain-Monte-Carlo (MCMC) based scenario analysis method to model energy price fluctuations and their influence on IES operations. Their study demonstrates that incorporating uncertainty models enhances the

robustness of IES scheduling strategies. Similarly, Huang et al. [58] develop a parametric equation-based optimization method for energy price sensitivity analysis, offering a simplified yet effective approach to cost-benefit analysis in multi-energy networks.

Recent studies also highlight the role of multi-objective optimization methods in balancing conflicting goals such as cost, efficiency, and environmental impact. Su et al. [134] introduce a Pareto-based evolutionary algorithm for IES optimization, which simultaneously minimizes energy costs and carbon emissions. Their findings reveal that such techniques enable policy-makers and operators to identify optimal trade-offs between economic and environmental performance. Another crucial aspect of optimization in IES is the coordinated operation of multiple energy networks. Yan [159] proposes a novel integrated scheduling framework that optimizes the combined operation of electricity, gas, and district heating networks. Their approach improves system efficiency by dynamically adjusting energy flows based on real-time demand and supply conditions. Similarly, Wang et al. [149] present an agent-based optimization strategy for self-discipline economic operation of IES, which incorporates deep learning algorithms to enhance real-time decision-making.

Economic Evaluation Models: To assess IES viability, comprehensive economic evaluation models are necessary. Peng et al. [111] introduce a detailed economic evaluation framework that incorporates internal energy conversion, major cost factors, and revenue sources. Their model utilizes sensitivity analysis to identify critical economic indicators. Zhao et al. [164] develop an evaluation index system based on the G1-anti-entropy weight-TOPSIS method, applied to a school IES. This approach integrates both subjective and objective weights to enhance decision-making accuracy and reliability. Song et al. [128] conduct a comprehensive survey of IES economic evaluation methodologies, analyzing 243 highly relevant papers. Their study classifies IES modeling techniques into multiple categories and highlights key economic dispatch strategies. Additionally, Peng et al. [112] propose an evaluation method integrating life cycle analysis and sensitivity analysis to assess potential profit growth areas in IES deployment. Their findings provide valuable insights into revenue stream diversification in integrated energy services.

Risk and Reliability Assessment: Ensuring the reliability and resilience of IES under uncertainties is crucial for sustainable operation. Su et al. [134] propose a systematic reliability analysis framework that integrates stochastic modeling to evaluate IES performance under varying conditions. Their approach assesses the interaction of uncertainties in renewable energy supply, demand fluctuations, and operational constraints. Another approach by Su et al. [133] employs Value at Risk (VaR) to quantify potential service disruptions. This method provides insights into the economic impact of operational risks and helps in formulating

mitigation strategies. Jia et al. [73] investigate the applicability of multi-carrier energy flow analysis in IES, identifying key uncertainties that affect system stability. Their study proposes an improved integrated method for handling stochastic variations in energy supply. Moreover, Su et al. [134] present a two-stage stochastic optimization approach for evaluating supply reliability in complex IES, accounting for fluctuations in renewable generation and demand-side uncertainties.

2.3 Technical and Economic Analysis of Hydrogen-Integrated Hybrid Energy Systems

Hydrogen is increasingly employed as a complementary vector in renewable-dominant systems to mitigate variability, reduce curtailment, and enable revenue stacking under market exposure. Project-level TEA of co-located wind–hydrogen configurations show that appropriately sized electrolysis and storage can materially lower total system cost (nearly 30% in an optimal planning case), while converting otherwise curtailed energy into storable product and enhancing operational flexibility [81]. Beyond utility scale, studies of residential and remote applications (Photovoltaic (PV)–wind–hydrogen for buildings, islanded systems, and greenhouse reduction) report sizeable GHG reductions and competitive levelized costs when hydrogen provides long-duration storage and off-grid resilience [8, 140, 57]. Collectively, the renewables literature positions hydrogen as a long-duration sink that complements batteries, broadening the feasible design space for high variable renewable energy (VRE) systems [83].

For nuclear-integrated hybrids, hydrogen serves both as a flexibility outlet and as a product stream that diversifies revenue. Hybrid nuclear–wind systems with hydrogen storage demonstrate improved load-following with only modest impacts on cash flow and a measurable uptick in economic performance [163]. Market-coupled modeling further shows that profitability hinges on electricity price formation and hydrogen production constraints, with outcomes differing under price-taker versus price-maker assumptions [51]. On the technology pathway, high-temperature electrolyzer (HTE) coupled to operating nuclear plants expands product diversification and system flexibility [78], while comparative TEA indicates that in certain nuclear–renewable contexts low-temperature electrolyzer (LTE) can be more cost-effective despite lower efficiency [1]. Advanced fast-reactor concepts co-producing hydrogen and fuels via HTE report thermal efficiencies exceeding 40% and attractive project metrics at industrial scale [15]. Feasibility studies in South Africa and the Association of Southeast Asian Nations (ASEAN) region underscore the enabling role of policy, infrastructure, and

regional demand profiles in realizing nuclear–renewable–hydrogen systems for decarbonization and fuel independence [48, 137].

Despite rapid progress, the literature on hydrogen-integrated IESs remains fragmented across scales and methods, with several persistent gaps: (i) limited unification of short-interval operational scheduling with lifecycle TEA across project-, grid-, and nuclear-hybrid contexts; (ii) incomplete treatment of uncertainty—renewable variability, price formation, and demand imbalances are often stylized rather than embedded in stochastic, market-coupled models; (iii) insufficient representation of techno-physical constraints (electrolyzer part-load efficiency, ramping and degradation; nuclear ramping, minimum generation, and thermal coupling for HTE) and their economic consequences; (iv) narrow metrics and value streams, emphasizing LCOE/LCOH while underrepresenting revenue stacking, reliability/ancillary services, and curtailment mitigation; (v) sparse integration of policy mechanisms and regional market heterogeneity (e.g., IRA tax credits, MACRS, ISO/RTO rules) into cash-flow–consistent TEA; and (vi) a dearth of empirically anchored case studies at ISO resolution that link curtailment, prices, and system decarbonization outcomes. This dissertation addresses these gaps by developing three optimization-based frameworks that coherently connect hourly dispatch to TEA at the project, grid, and nuclear-hybrid levels; embedding stochastic supply–demand and price uncertainty with market participation for energy and ancillary services; explicitly modeling dynamic equipment constraints and degradation; and internalizing federal incentives and regional features. A co-located wind–hydrogen case quantifies curtailment reduction and revenue stacking; an ERCOT-scale analysis evaluates uncertainty mitigation and decarbonization; and a nuclear–hydrogen framework demonstrates flexibility enhancement and improved economics—together yielding policy-relevant, system-level evidence for hydrogen as a key enabler of resilient, low-carbon IESs.

CHAPTER 3

EVALUATE THE TECHNO-ECONOMIC FEASIBILITY OF HYDROGEN STORAGE FOR WIND ENERGY[1]

3.1 Techno-Economic Analysis Methodology

In this chapter, I will perform a TEA using wind energy as a representative example to explore the potential and viability of renewable-hydrogen co-location. The TEA for the sector-coupled wind-hydrogen IES is performed using the open-source techno-economic tool, Renewable Energy Integration and Optimization tool (REopt) (Renewable Energy Integration and Optimization), developed by the National Renewable Energy Laboratory (NREL) [97]. Fig. 3.1 depicts the overall framework of the REopt analysis for the integrated wind and hydrogen system. REopt takes into account various factors, including weather conditions, electrical load, wholesale electricity prices, and hydrogen prices at the system's location, to determine the capacity and dispatch decisions for the components of the IES. The primary objective is to optimize economic savings or profits from on-site energy production while maximizing stabilized power output. It should be noted that REopt is best suited for site-specific studies and is implemented through net export or import limits to the system, rather than for system-level analyses.

In our study, we have extended the capabilities of REopt by incorporating additional models for the electrolyzer, hydrogen tank storage, and hydrogen fuel cell. Fig. 5.2 illustrates the overall architecture of the REopt modules used in this study, along with the input and output parameters of each component and their respective constraints. To model the IES, certain user-inputs are provided to REopt, including the capital cost, operations and maintenance (O&M) cost, annual electricity consumption, battery charging and discharging efficiency, and other relevant performance parameters of the wind energy system. These inputs enable the estimation of power generation for the wind and battery components. For the hydrogen production model, the electrolyzer technology is employed, which utilizes electricity and a feedstock like water to produce hydrogen. User-inputs for the electrolyzer in REopt include the capital and O&M costs, feedstock type, electric energy consumed to hydrogen produced ratio, hydrogen sale price, and other relevant parameters [122, 24, 121, 61]. The

[1]©2024 ASME. Reprinted, with permission, from Li, H. and Zhang, J., 2024. Towards sustainable integration: Techno-economic analysis and future perspectives of co-located wind and hydrogen energy systems. Journal of Mechanical Design, 146(2), p.020903.

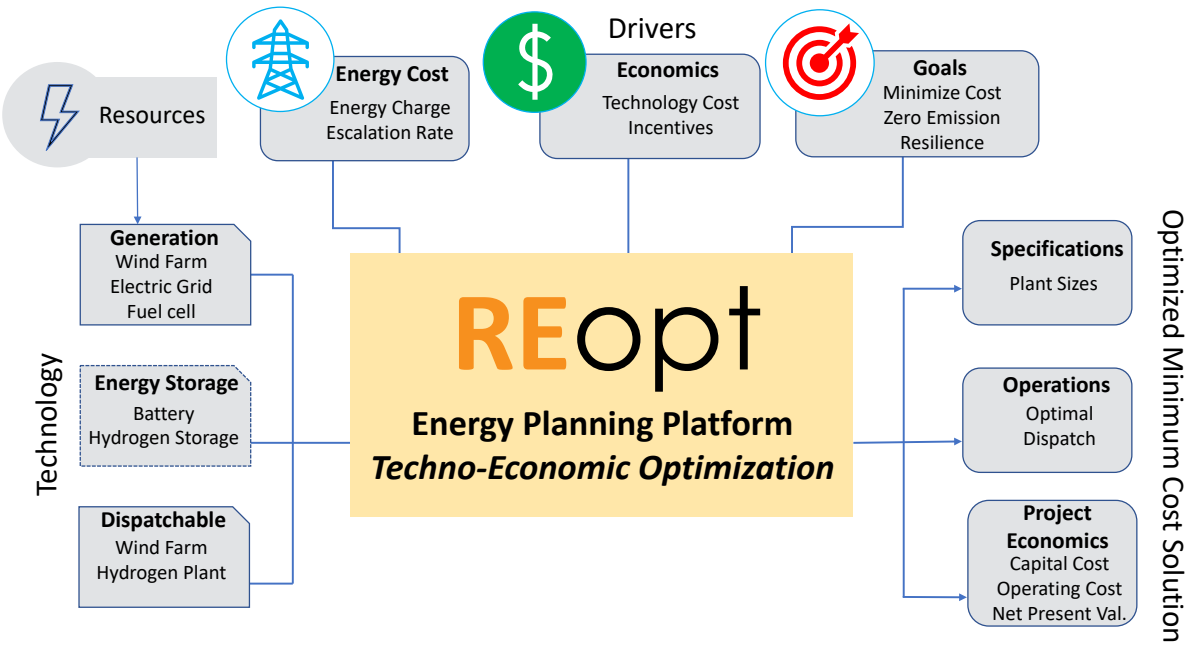


Figure 3.1: TEA framework for the integrated wind and hydrogen system (modified from [81])

hydrogen storage tank is modeled with considerations for minimum and maximum capacity limits, installation cost, and O&M cost [109, 24]. These inputs help determine the appropriate storage capacity for the hydrogen system. Various financial parameters, such as tax rates, investment-based incentives, capital-based incentives, production-based incentives, discount rate, and modified accelerated cost recovery system (MACRS), are also taken into account. These financial inputs are crucial for obtaining realistic results that consider the economic aspects of the integrated wind-hydrogen system.

By incorporating the electrolyzer, hydrogen tank, and fuel cell technology into the existing REopt capability, we can now assess the techno-economic performance of wind and hydrogen IES under various conditions, including different meteorological conditions, fluctuating electricity and hydrogen prices, and more. Fig. 3.3 depicts the overall structure of the grid-connected IES with wind, battery, hydrogen, and fuel cells in this study. We have comprehensively explored and compared the following four scenarios.

1. **Case I: Wind+Battery (Base Scenario)**: This case involves a wind power plant integrated with a conventional energy storage device. The objective is to minimize

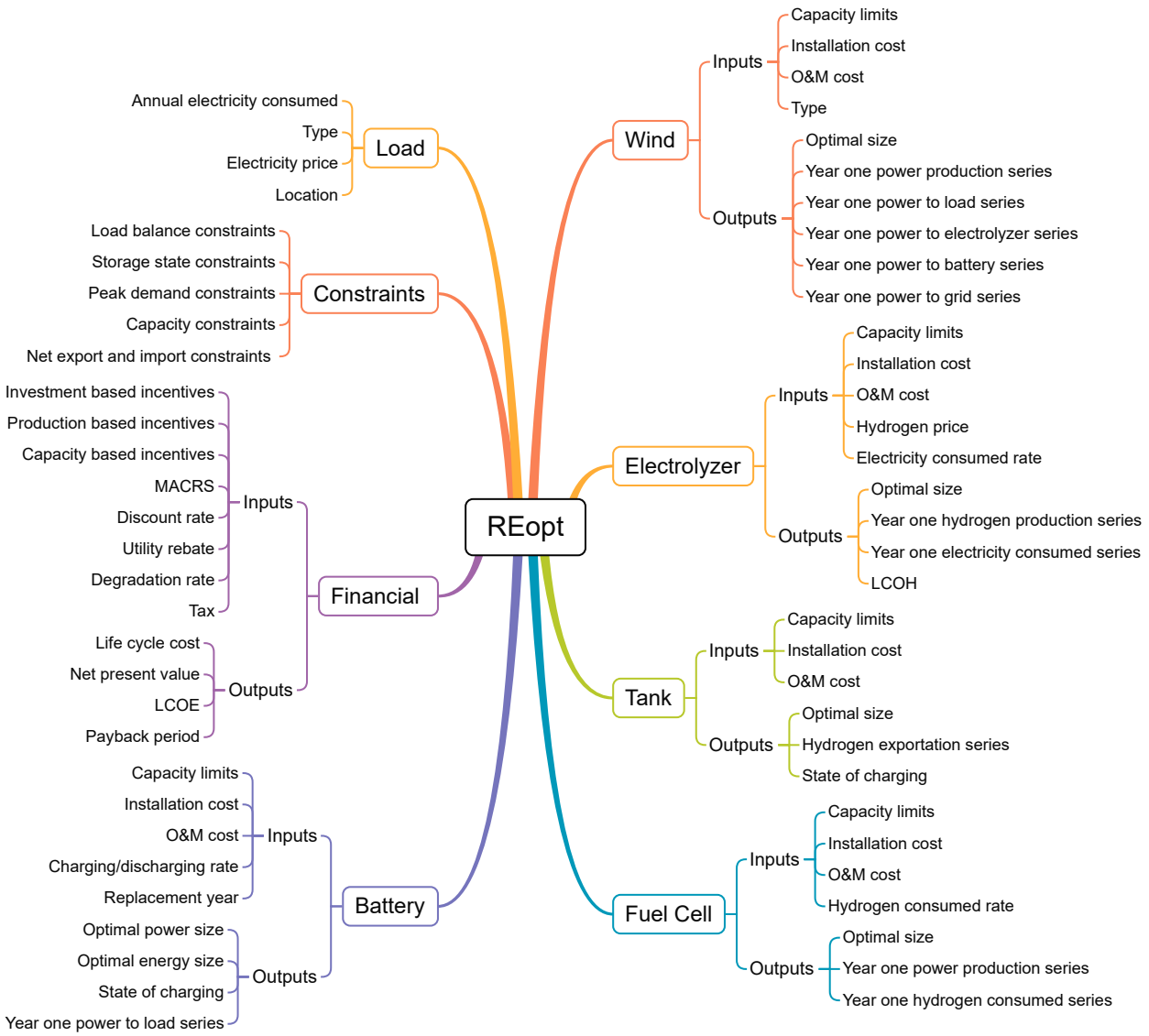


Figure 3.2: Model architecture of the Renewable Energy Integration and Optimization tool (REopt) modules adopted/created in this study (modified from [81])

system costs while achieving maximum stabilized output power. It is assumed in this study that the maximum stabilized output power of the system aligns with the grid demand. This approximation is derived from extensive empirical analyses. Thus, it's important to note that, within the scope of this study, we do not account for any potential grid demand deficits. The mathematical model optimizes the capacity and power size of the energy storage device, ensuring efficient utilization of wind energy and enhancing grid stability.

2. **Case II: Wind+Battery+Electrolyzer (Electrolyzer Integration)**: In this case, an electrolyzer is added to the system to convert excess wind energy into hydrogen, thereby increasing system revenue and energy versatility. The optimization process determines the optimal sizes of the electrolyzer and energy storage device to maximize hydrogen generation and storage while minimizing costs.

3. **Case III: Wind+Electrolyzer+Hydrogen Tank+Fuel Cell (Hydrogen Storage and Fuel Cell Integration)**: This case replaces conventional battery energy storage with hydrogen storage and a fuel cell. The economic feasibility of this combination is assessed, considering the lack of battery state-of-charge (SOC) limitations, ensuring optimal energy storage and utilization. The integration of hydrogen storage and fuel cells enhances energy conversion efficiency and offers a cleaner and sustainable energy option.

4. **Case IV: Wind+Battery+Electrolyzer+Hydrogen Tank+Fuel Cell (Comprehensive Integration)**: This case represents a holistic approach, incorporating electrolyzers, hydrogen tanks, fuel cells, and traditional battery storage. A sensitivity analysis examines the impact of future equipment cost reduction on system costs, providing valuable insights for long-term planning and investment strategies. Additionally, grid power integration is explored to enhance wind farm stability during low wind periods and maximize curtailed wind energy utilization. This comprehensive integration optimizes the synergies between different components, offering an efficient and resilient renewable energy system.

The modeling of the IES is a complex process that involves considering multiple technology, system, and financial constraints. These constraints encompass energy balance, battery and storage tank states, technology capacities, grid import/export limits, and stabilized output requirements. The primary objective of the optimization is to minimize the total cost of

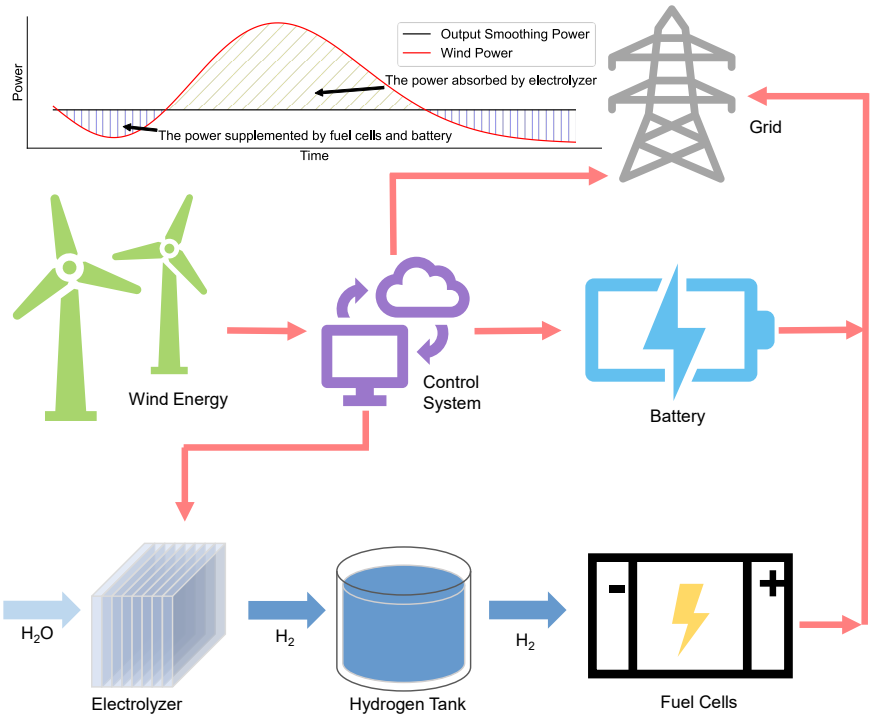


Figure 3.3: Overall structure of the grid-connected IES with wind, battery, hydrogen, and fuel cells

the IES, which includes installation costs for the electrolyzer, wind energy system, batteries, hydrogen storage, and fuel cells (if applicable), as well as O&M costs, electricity purchases, taxes, incentives, and profits from electricity and hydrogen sales. The objective function is formulated as:

$$
\begin{aligned}
\text{Minimize} \quad & \underbrace{\sum_{t\in\mathcal{T}} \left(c_t^{\mathrm{cm}} X_t^{\sigma} + c_t^{\mathrm{cb}} Z_t^{\sigma}\right)}_{\text{Generating Technology Capital Costs}} + \underbrace{\sum_{b\in\mathcal{B}} \left(c_b^{\mathrm{kW}} X_b^{\mathrm{bkW}} + (c_b^{\mathrm{kWh}} + c_b^{\mathrm{omb}}) X_b^{\mathrm{bkWh}}\right)}_{\text{Storage Capital Costs}} \\
& + (1 - f^{\mathrm{tow}})\, f^{\mathrm{om}} \left(\underbrace{\sum_{t\in\mathcal{T}} c_t^{\mathrm{om}\sigma} X_t^{\sigma}}_{\text{Fixed O\&M Costs}} + \underbrace{\sum_{t\in\mathcal{T}^{\mathrm{h}}, h\in\mathcal{H}} c_t^{\mathrm{omp}} X_{th}^{\mathrm{rp}}}_{\text{Variable O\&M Costs}} + \underbrace{c^{\mathrm{ome}} X_{eh}^{\mathrm{rp}}}_{\text{Electrolyzer O\&M costs}} \right) \\
& - (1 - f^{\mathrm{tow}})\, f^{e} \left(\underbrace{\sum_{h\in\mathcal{H}} \left(c_h^{\mathrm{e}} X_h^{\mathrm{stg}} + \sum_{t\in\mathcal{T}} c_h^{\mathrm{e}} X_{th}^{\mathrm{ptg}}\right)}_{\text{Energy Export Payment}} + \underbrace{\sum_{h\in\mathcal{H}} c_h^{\mathrm{hts}} X_{eh}^{\mathrm{sell}}}_{\text{Hydrogen profit}} \right) \\
& - (1 - f^{\mathrm{tow}}) \sum_{t\in\mathcal{T}} X_t^{\mathrm{pi}}
\end{aligned} \tag{3.1}
$$

The following constraints are considered in the optimization.

$$
X_{th}^{\mathrm{rp}} \leq \underbrace{\bar{b}_t^{\sigma} \cdot Z_{th}^{\mathrm{to}}}_{\text{Maximum Power Rating}} \qquad \forall t \in \mathcal{T}, h \in \mathcal{H} \tag{3.2}
$$

Constraint (3.2) ensures that the system's output is restricted to its maximum power rating when it is turned on, and it must be 0 when it is off.

$$
X_{b,0}^{\mathrm{se}} = \underbrace{w_b^0 \cdot X_b^{\mathrm{bkWh}}}_{\text{Initial State of Charge}} \qquad \forall b \in \mathcal{B} \tag{3.3}
$$

$$
\underline{w}_b^{\mathrm{bkWh}} \leq X_b^{\mathrm{bkWh}} \leq \bar{w}_b^{\mathrm{bkWh}} \quad \forall b \in \mathcal{B} \tag{3.4}
$$

$$
\underline{w}_b^{\mathrm{bkW}} \leq X_b^{\mathrm{bkW}} \leq \bar{w}_b^{\mathrm{bkW}} \quad \forall b \in \mathcal{B} \tag{3.5}
$$

Constraint (3.3) establishes the initial state of charge for each storage system as a fraction of its total energy rating. Constraints (3.4) and (3.5) further constrain the size of the storage system by imposing lower and upper bounds on its energy capacity and power output, respectively. These bounds limit the range within which the energy capacity and power output of the storage system can be optimized.

$$
X_{bh}^{\mathrm{se}} = X_{b,h-1}^{\mathrm{se}} + \underbrace{\sum_{t\in\mathcal{T}} \left(\eta_{bt}^{+} \cdot X_{bth}^{\mathrm{pts}}\right) - X_{bh}^{\mathrm{dfs}} / \eta_b^{-}}_{\text{Net Charging Energy}} \quad \forall b \in \mathcal{B}, h \in \mathcal{H} \tag{3.6}
$$

$$X_{bh}^{\mathrm{se}} \geq \underbrace{\underline{w}_b^{\mathrm{mcp}} \cdot X_b^{\mathrm{bkWh}}}_{\text{Minimum State of Charge}} \qquad \forall b \in \mathcal{B}, h \in \mathcal{H} \tag{3.7}$$

Constraint (3.6) ensures inventory balance for the state of charge of storage system b at the end of time period h. Constraint (3.7) enforces a minimum state of charge requirement for the energy stored in the battery. This constraint ensures that the energy in the battery does not fall below the specified minimum level.

$$X_b^{\mathrm{kW}} \geq \underbrace{\sum_{t \in \mathcal{T}_b} X_{bth}^{\mathrm{pts}} + X_{bh}^{\mathrm{dfs}}}_{\text{Charging and Discharging Power}} \qquad \forall b \in \mathcal{B}, h \in \mathcal{H} \tag{3.8}$$

$$X_b^{\mathrm{bkWh}} \geq X_{bh}^{\mathrm{se}} \quad \forall b \in \mathcal{B}, h \in \mathcal{H} \tag{3.9}$$

Constraint (3.8) restricts the power that can be charged or discharged from the storage system in each time step to the storage system's power rating. Additionally, constraint (3.9) sets a limit on the amount of energy stored in the storage system in each time step to the storage system's energy capacity.

$$X_t^{\mathrm{pi}} \leq \min \left\{ M \cdot Z_t^{\mathrm{pi}}, \underbrace{\sum_{h \in \mathcal{H}} i_t^{\mathrm{r}} \cdot f_t^{\mathrm{pi}} \cdot f_{th}^{\mathrm{p}} \cdot f_t^{\mathrm{li}} \cdot X_{th}^{\mathrm{rp}}}_{\text{Total Production Incentives}} \right\} \quad \forall t \in \mathcal{T} \tag{3.10}$$

$$X_t^{\sigma} \leq \underbrace{\bar{\imath}_t^{\sigma} + \bar{b}_t^{\sigma} \cdot \left(1 - Z_t^{\mathrm{pi}}\right)}_{\text{Upper Bound on the System Size}} \qquad \forall t \in \mathcal{T} \tag{3.11}$$

Constraint (3.10) computes the total production incentives, if they are available, for each technology. Constraint (3.11) sets an upper bound on the system size that qualifies for production incentives.

$$\underbrace{f_{eh}^{\mathrm{p}} \cdot f_e^1 \cdot X_{eh}^{\mathrm{rp}}}_{\text{Actual Power of Electrolyzer}} = X_{eh}^{\mathrm{p}} \quad \forall h \in \mathcal{H} \tag{3.12}$$

$$m_e \cdot X_{eh}^{\mathrm{p}} = \underbrace{\sum_{t \in \mathcal{T}} X_{th}^{\mathrm{pte}} + \sum_{b \in \mathcal{B}} X_{bh}^{\mathrm{ste}}}_{\text{Total Energy Input to the Electrolyzer}} \qquad \forall h \in \mathcal{H} \tag{3.13}$$

$$X_{eh}^{\mathrm{rp}} \leq X_e^{\mathrm{kg}} \quad \forall h \in \mathcal{H} \tag{3.14}$$

Constraints (3.12) and (3.13) give the input-output relationship and energy balance equations for the electrolyzer operation process, respectively. Constraint (3.14) sets a limit on the production of the eletrolyzer to the electrolyzer capacity.

$$X_{th}^{\mathrm{sh}} = X_{t,h-1}^{\mathrm{sh}} + \underbrace{X_{eh}^{\mathrm{p}} - X_{eh}^{\mathrm{sell}} - X_{eh}^{\mathrm{etf}}}_{\text{Net Hydrogen Storage}} \quad \forall h \in \mathcal{H} \tag{3.15}$$

$$X_{th}^{\mathrm{sh}} \leq X^{\mathrm{tank}} \quad \forall h \in \mathcal{H} \tag{3.16}$$

Constraint (3.15) ensures inventory balance for the state of charge of hydrogen storage system at the end of time period h. Constraint (3.16) sets a limit on the amount of hydrogen stored in the hydrogen storage system in each time step to the hydrogen storage system's capacity.

$$\underbrace{f_{fh}^{\mathrm{p}} \cdot f_{f}^{1} \cdot X_{fh}^{\mathrm{rp}} \cdot m_{f}}_{\text{Actual Hydrogen Consumption in Fuel Cells}} = X_{eh}^{\mathrm{etf}} \quad \forall f \in \mathcal{T}^{h}, h \in \mathcal{H} \tag{3.17}$$

$$\underbrace{f_{fh}^{\mathrm{p}} \cdot f_{f}^{1} \cdot X_{fh}^{\mathrm{rp}}}_{\text{Actual Energy Generation from Fuel Cells}} = X_{fh}^{\mathrm{ftg}} \quad \forall f \in \mathcal{T}^{h}, h \in \mathcal{H} \tag{3.18}$$

$$X_{fh}^{\mathrm{rp}} \leq X_{f}^{\mathrm{kW}} \quad \forall h \in \mathcal{H} \tag{3.19}$$

Constraints (3.17) and (3.18) give the relationship between the demand for hydrogen and the production of electricity and its capacity at each time point of the hydrogen fuel cells, respectively. Constraint (3.19) sets a limit that hydrogen fuel cells cannot generate more power per hour than their capacity.

$$\begin{aligned} &\underbrace{\sum_{t \in \mathcal{T}} f_{th}^{\mathrm{p}} \cdot f_{t}^{1} \cdot X_{th}^{\mathrm{rp}}}_{\text{Actual Wind Energy Generation}} + \sum_{b \in \mathcal{B}} X_{bh}^{\mathrm{dfs}} \\ &= \underbrace{\sum_{t \in \mathcal{T}} \left(\sum_{b \in \mathcal{B}} X_{bth}^{\mathrm{pts}} + X_{th}^{\mathrm{ptg}} + X_{th}^{\mathrm{pte}} + X_{th}^{\mathrm{ptc}} \right)}_{\text{Total Wind Energy Generation}} \\ &\quad + \underbrace{\sum_{b \in \mathcal{B}} \left(X_{bh}^{\mathrm{ste}} + X_{bh}^{\mathrm{stg}} \right)}_{\text{Total Battery Discharge}} \quad \forall h \in \mathcal{H} \end{aligned} \tag{3.20}$$

$$\underbrace{\sum_{t \in \mathcal{T}} X_{th}^{\mathrm{ptg}} + \sum_{b \in \mathcal{B}} X_{bh}^{\mathrm{stg}}}_{\text{Energy Delivered to the Grid}} = \delta_{\mathrm{h}}^{\mathrm{d}} \quad \forall h \in \mathcal{H} \tag{3.21}$$

$$\sum_{t\in\mathcal{T}} f^{\mathrm{p}}_{th}\cdot f^{1}_{t}\cdot X^{\mathrm{rp}}_{th}=\sum_{t\in\mathcal{T}}\left(\sum_{b\in\mathcal{B}} X^{\mathrm{pts}}_{bth}+X^{\mathrm{ptg}}_{th}+X^{\mathrm{pte}}_{th}+X^{\mathrm{ptc}}_{th}\right)\quad \forall h\in\mathcal{H} \tag{3.22}$$

$$\sum_{b\in\mathcal{B}} X^{\mathrm{stg}}_{bh}+\sum_{t\in\mathcal{T}} X^{\mathrm{ptg}}_{th}\leq \bar{\delta}^{\mathrm{g}}_{\mathrm{h}}\quad \forall h\in\mathcal{H} \tag{3.23}$$

Constraint (3.20) ensures that the load is balanced by equating the sum of power from all generation technologies and energy storage systems. Constraint (3.21) allows both storage X^{stg}_{h} and production X^{ptg}_{h} to contribute to the energy delivered to the grid, but the total contribution must equal the power demand, which is also the stabilized output power of the system. Constraint (3.22) limits the power allocation to all generation technologies at each point in time. Constraint (3.23) ensures the transmitted power to the grid does not exceed the interconnection limit.

$$X^{\mathrm{kWh}}_{b}, X^{\mathrm{kW}}_{b}\geq 0\quad \forall b\in\mathcal{B} \tag{3.24}$$

$$X^{\mathrm{stg}}_{h}, X^{\mathrm{ptg}}_{h}\geq 0\quad \forall h\in\mathcal{H} \tag{3.25}$$

$$X^{\mathrm{pi}}_{t}, X^{\sigma}_{t}\geq 0\quad \forall t\in\mathcal{T} \tag{3.26}$$

$$X^{\mathrm{pts}}_{bth}\geq 0\quad \forall b\in\mathcal{B}, t\in\mathcal{T}, h\in\mathcal{H} \tag{3.27}$$

$$X^{\mathrm{pte}}_{th}, X^{\mathrm{ptc}}_{th}, X^{\mathrm{sh}}_{th}, X^{\mathrm{rp}}_{th}\geq 0\quad \forall t\in\mathcal{T}, h\in\mathcal{H} \tag{3.28}$$

$$X^{\mathrm{ste}}_{bh}, X^{\mathrm{dfs}}_{bh}, X^{\mathrm{se}}_{bh}, X^{\mathrm{se}}_{b,0}\geq 0\quad \forall b\in\mathcal{B}, h\in\mathcal{H} \tag{3.29}$$

$$X^{\mathrm{rp}}_{eh}, X^{\mathrm{etf}}_{eh}, X^{\mathrm{p}}_{eh}, X^{\mathrm{sell}}_{eh}, X^{\mathrm{rp}}_{eh}\geq 0\quad \forall e\in\mathcal{T}^{gh}, h\in\mathcal{H} \tag{3.30}$$

$$X^{\mathrm{kg}}_{e}\geq 0\quad \forall e\in\mathcal{T}^{gh} \tag{3.31}$$

$$X^{\mathrm{rp}}_{fh}, X^{\mathrm{ftg}}_{fh}\geq 0\quad \forall f\in\mathcal{T}^{h}, h\in\mathcal{H} \tag{3.32}$$

$$X^{\mathrm{kW}}_{f}\geq 0\quad \forall f\in\mathcal{T}^{h} \tag{3.33}$$

$$Z^{\mathrm{to}}_{th}\in\{0,1\}\quad \forall t\in\mathcal{T}, h\in\mathcal{H} \tag{3.34}$$

$$Z^{\mathrm{pi}}_{t}\in\{0,1\}\quad \forall t\in\mathcal{T} \tag{3.35}$$

Finally, constraints (3.24-3.33) ensure all of the variables in our formulation assume non-negative values. In addition to non-negativity restrictions, constraints (3.34, 3.35) establish the integrality of the appropriate variables.

REopt extends its functionality to provide comprehensive runtime support for the IES optimization model. This encompasses tasks such as modeling and simulating the various

constituent modules within IES. Additionally, REopt plays a pivotal role in supplying coefficients to the optimization model, coordinating the entire optimization procedure, as well as efficiently handling the processing and dissemination of the resultant outcomes [97]. The problem is formulated as a mixed-integer linear program (MILP), and the FICO Xpress solver is utilized to find the optimal selection, sizing, and dispatch strategy of technologies from a candidate pool. Since the solver uses an exact algorithm rather than a heuristic algorithm to obtain the optimal solution, this optimal solution is also the global optimal solution. This approach ensures the maximization of stabilized power output at each time step while minimizing the overall life cycle cost of the system, encompassing both system costs and profit. The optimization process yields several important outputs, including the maximized stabilized output power, optimal component sizes, total system expenditure, capital expenditure (CAPEX) for each component, the trade-off between wind and hydrogen production, the LCOH, and the LCOE of the IES. Additionally, various financial parameters such as payback period, life cycle cost, and net present value (NPV) are provided, offering valuable insights for IES investment, planning, and operation decisions. This comprehensive modeling approach empowers stakeholders with critical information for designing, optimizing, and managing the IES effectively, supporting the development of sustainable and economically viable energy solutions.

In this research, a single-year optimization approach is employed to estimate cash flows over an extended 25-year period, assuming constant production and consumption throughout the entire analysis period. This approach assumes perfect foresight in predicting all future events, encompassing factors like weather conditions and energy demand. While this method provides valuable insights, it is subject to several inherent limitations that can influence the results and their real-world applicability. These limitations stem from various assumptions made in the analysis, including the presumption of consistent wind energy generation, fixed electrolyzer efficiency, stable hydrogen storage costs, and simplified grid integration. Additionally, these analyses often rely on historical or estimated data, potentially introducing uncertainties into the findings. Furthermore, they may not fully account for the influence of technological advancements, environmental impacts, changing policies, or economic factors.

Key limitations of these studies include the omission of environmental costs and the oversight of potential technology breakthroughs. Regulatory changes, such as alterations in government policies or incentives, can significantly affect project economics, but these analyses often overlook such dynamics. Moreover, it's important to acknowledge that these studies are typically location-specific and may not readily generalize well to different regions with varying resource availability, infrastructure, and market conditions.

3.2 Numerical Experiments

In this study, the IES is assumed to be located in Snyder, TX, with a planned wind farm capacity of 253 MW, thus, the decision variable of wind farm size in this model will be fixed at 253 MW. Historical meteorological data from the year 2020, along with wholesale market prices from the ERCOT, serve as inputs for the study. Fig. 3.4 visually represents the annual wind power generation obtained from the simulation. The essential assumptions for setting up the hybrid energy system are summarized in Table 3.1, with a planning horizon of 25 years. To conduct the TEA, the analysis employs 8,760 hourly data points for the modeled year (2020).

To enhance the conciseness of this paper while maintaining its focus, we have carefully selected key parameters for inclusion in Table 3.1. Our criteria for choosing these parameters are as follows:

- **Relevance to Key Components:** We have included parameters that are essential for understanding the key components of our study.

- **Impact on Key Results:** Parameters that significantly influence critical outcomes, such as LCOE and total cost, have been prioritized.

- **Focus on New Modules:** In particular, we have focused on parameters related to the newly added module, the hydrogen system. For original modules like the wind system, we have relied on default parameters as described in [97].

For future projections, the study takes into account changes in grid energy costs and O&M expenses with a constant rate of change. This approach incorporates discounting factors to account for anticipated cost escalation or de-escalation rates. The study assumes perfect predictions of all future events, encompassing weather conditions and failure rates. Moreover, all costs and benefits are discounted using a specified discount rate to present values, following standard economic practices.

Capital and operating costs for wind, battery storage, various hydrogen generation technologies, fuel cell, and other system components are referenced from the NREL Annual Technology Baseline (ATB) [103]. This comprehensive approach allows for a robust analysis of the IES, enabling strategic decision-making and evaluation of economic viability and long-term sustainability over the planning period.

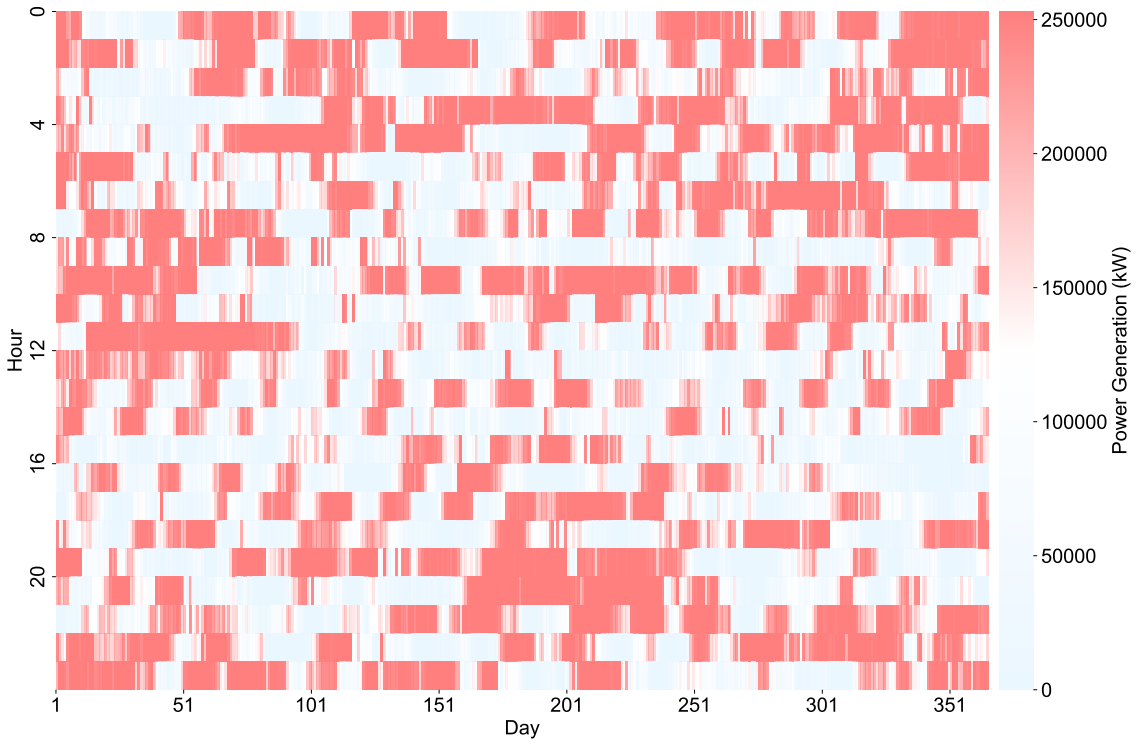


Figure 3.4: The annual wind power generation of the simulated wind farm in 2020

Table 3.1: Key assumptions in the IES setup [122, 24, 121, 61, 109]

Parameter	Cost
Electricity consumed per kg of hydrogen produced (low thermal energy)	55 kWh/kg
Hydrogen sale price	$2/kg
Hydrogen slope for fuel cell	0.076 kg/kWh
Electrolyzer installation cost	$48,000/kg/yr
Fixed electrolyzer O&M cost	$3,600/kg/yr
Variable electrolyzer O&M cost	$0.24/kg
Fuel cell installation cost	$500/kW
Fuel cell fixed O&M cost	$30/kW
Planning period	25 years
Minimum allowable battery SOC	0.2

3.2.1 Results and Discussion

Table 3.2 presents a comprehensive overview of the optimal sizing of various components within the IES, including wind, electrolyzer, battery, tank, and hydrogen fuel cell, along with the corresponding total system costs for all four cases. The results indicate significant cost reductions in Case II (Electrolyzer Integration) and Case III (Hydrogen Storage and Fuel Cell Integration) by 7% and 26%, respectively, compared to the benchmark Case I. Particularly in Case III, battery storage is excluded and replaced by the integration of a hydrogen storage tank and fuel cell system.

In Case IV (Comprehensive Integration), the higher total system cost is attributed to the increased stabilized IES power output (i.e., 57 MW). In order to further evaluate the economic advantages of the Case IV combination, we added two additional sub-cases, which have the same stabilized IES output power as Case II and Case III, respectively, namely Case IV(a) and Case IV(b). When comparing the stabilized IES power outputs of 28.3 MW (Case IV(a)) and 39 MW (Case IV(b)) to Cases II and III, respectively, the total system cost in Case IV can be reduced by 23% and 26%. Notably, the curtailed rate of wind energy is lower in Case IV, suggesting the more efficient utilization of the electrolyzer, which was deliberately chosen to be smaller to meet the objective of minimizing the total system cost while maintaining maximum stabilized output. Indeed, Case III exhibits the lowest curtailed rate among all the cases due to its installation of the largest electrolyzer and its concerted effort to maximize the utilization of wind energy. However, it is essential to note that this configuration may not be the most economical option, as the utilization of the electrolyzer is not optimized sufficiently. This observation is further validated by the LCOH results, which indicate that Case III has the highest LCOH among all cases. Therefore, while the wind curtailed rate in Case III appears favorable, it must be cautiously interpreted in light of the higher LCOH and potential inefficiencies in the utilization of the electrolyzer. This information is crucial for the IES planning, as it highlights the trade-offs between curtailed rates and overall system economics and efficiency in the decision-making process.

These findings shed light on the cost-effective configurations and strategic component selections within the IES to achieve optimal performance and address energy demands efficiently. The outcomes provide valuable insights for decision-makers seeking to strike a balance between system costs, renewable energy utilization, and curtailment rates, while striving for a sustainable and economically viable integrated energy solution.

Fig. 3.5 provides a detailed view of the monthly energy output distribution for each component in the four cases. A comparison between Case I and Case II reveals that the

Table 3.2: Integrated energy system component capacity and cost

Technology	Case I	Case II	Case III	Case IV	Case IV (a)	Case IV (b)
Wind	253 MW	253 MW	253 MW	253 MW	253 MW	253 MW
Stabilized IES power	28.3 MW	28.3 MW	39 MW	57 MW	28.3 MW	39 MW
LCOE of wind	$0.0479/kWh	$0.0479/kWh	$0.0479/kWh	$0.0479/kWh	$0.0479/kWh	$0.0479/kWh
Fuel cell	N/A	N/A	39,000 kW	32,284 kW	25,823 kW	33,001 kW
Hydrogen tank	N/A	N/A	185,236 kg	208,565 kg	59,247 kg	128,573 kg
Battery energy capacity	1,064,030 kWh	1,064,030 kWh	N/A	867,950 kWh	54,217 kWh	160,555 kWh
Battery power capacity	224,497 kW	224,497 kW	N/A	183,127 kW	11,439 kW	33,875 kW
Electrolyzer	N/A	1,965 kg/h	3,888 kg/h	1,908 kg/h	2,157 kg/h	2,214 kg/h
Total system cost	$1,112,071,117	$1,033,978,268	$822,851,256	$1,193,795,109	$633,249,296	$767,428,831
Wind curtailment rate	79.1%	21%	0.02%	13.1%	27.4%	21%
LCOH	N/A	$4.07	$5.01	$4.38	$4.52	$4.56

addition of the electrolyzer in Case II, a power consumer component, results in a portion of the wind power being allocated to supply the electrolyzer. Despite the unchanged battery capacity compared to Case I, the batteries in Case II occupy a larger share of the output, leading to an increase in their utilization rate. In Case III, the hydrogen fuel cell fully replaces the function of the conventional battery pack. The results show that the hydrogen fuel cell in Case III effectively substitutes the conventional battery pack and is capable of delivering higher stabilized power output. Comparing Case IV with Case I, the combination of the fuel cell and the battery further optimizes the IES's potential, resulting in higher stabilized power output. Nevertheless, the installed capacity of both the fuel cell and the battery is reduced compared to the previous cases.

These findings underscore the system's adaptability and the strategic allocation of components to achieve higher power output and efficiency. The integration of the hydrogen fuel cell and battery in Case IV demonstrates the potential for improved performance while optimizing component sizes to achieve a balance between system capabilities and resource utilization. The detailed monthly energy output distribution offers valuable insights into the system's performance under varying conditions throughout the year. It highlights how different configurations impact the overall energy distribution among components, providing a clearer understanding of the IES's operation and potential energy savings.

To strike a balance between generality and specificity, the analysis encompasses the system's overall behavior while also zooming in on its specific operational state. Fig. 3.6 provides insights into the wind power allocation and the SOC of battery and hydrogen tanks within the IES over a randomly selected 168 consecutive hour period for the four cases. This

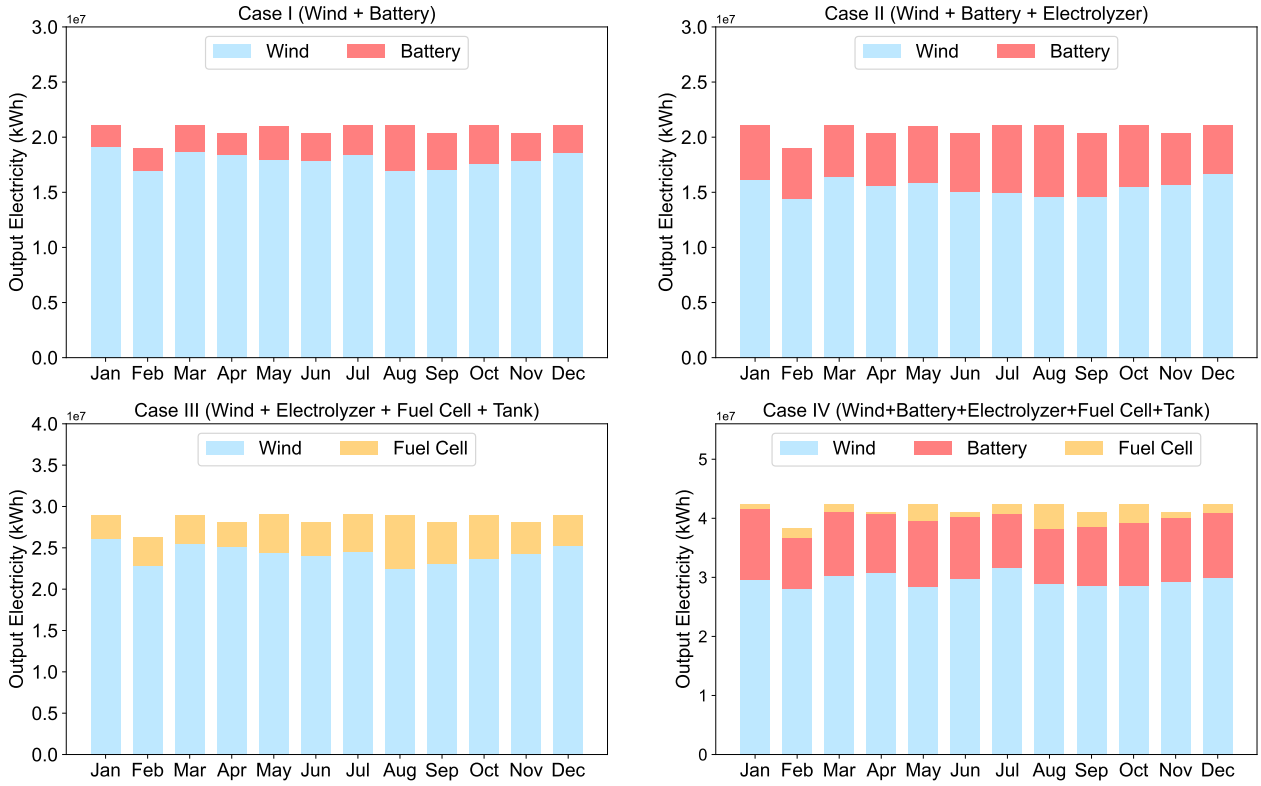


Figure 3.5: Monthly output energy of the IES for each component in the four cases

view offers a more detailed perspective on the operational behavior of system components. Notably, the SOC of the battery in Case II exhibits more frequent fluctuations, which is consistent with the observations in Fig. 3.5. This highlights the dynamic nature of the energy storage system in Case II, where the battery's charge and discharge cycles respond to the variable wind power generation and hydrogen production.

Examining the curtailed rate, the figure reveals that Cases II and III effectively utilize substantial portions of wind energy that would have been curtailed, directing it to the electrolyzer for hydrogen production. This observation aligns with the lower curtailed rates reported in Table 3.2 for these cases compared to Case I. Furthermore, when comparing wind energy allocation to the electrolyzer in Cases II and IV, it is evident that more curtailed wind energy is efficiently utilized by the electrolyzer in Case IV, in line with the earlier mentioned higher utilization efficiency of the electrolyzer in that case.

Additionally, the SOC of energy storage devices in all four cases during the Hours 40-80 time period, characterized by a relative shortage of wind energy resources, indicates that both batteries and hydrogen tanks play crucial roles in compensating for the IES power output

gap during such wind energy shortages. This comprehensive analysis of operational details sheds light on the dynamic behavior and synergistic functioning of system components within the IES.

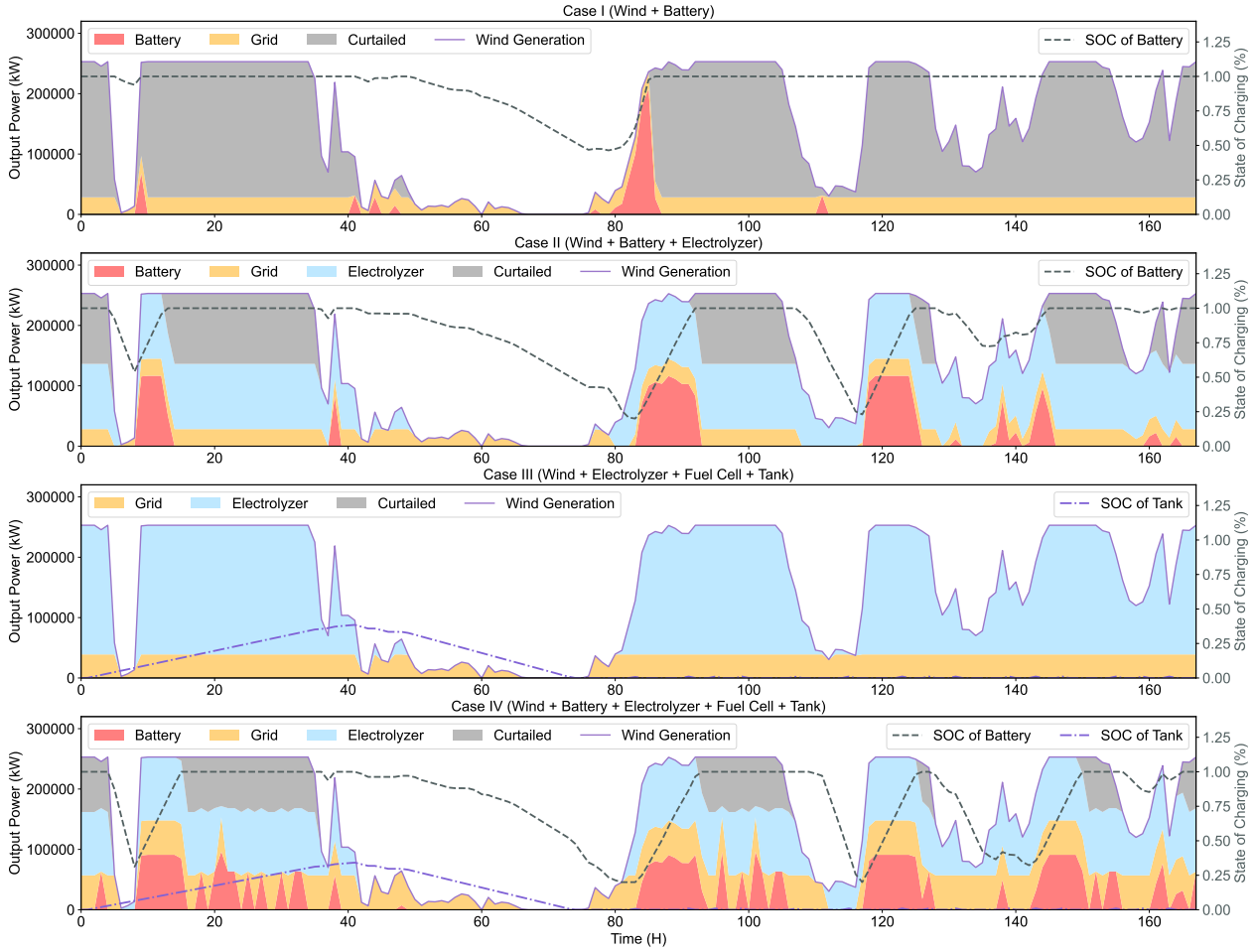


Figure 3.6: Hourly wind power allocation and state of charge (SOC) of battery and hydrogen tank within the IES over a randomly selected 168 consecutive hour period. Battery, Grid, and Electrolyzer in the legend represent the hourly wind power allocation to the battery, grid, and electrolyzer, respectively. Curtailed and Wind Generation represent wind energy curtailment and actual wind power generation, respectively.

3.3 Sensitivity Analysis

In Case IV (Comprehensive Integration), three sets of sensitivity analyses were conducted on the IES to assess the impacts of various factors. Firstly, we explored the influence of hydrogen

prices on system configurations and parameters. This analysis provided valuable insights into key metrics such as LCOH, total system cost, size of the electrolyzer, and curtailed wind energy rates. Secondly, we examined how different regional wind resources affected the IES. Lastly, we assessed the effects of future component prices on the IES, simulating different price scenarios for wind, battery, electrolyzer, fuel cell, and hydrogen tank installation costs. These analyses offered essential information for decision-making, risk mitigation, and optimized investment strategies, fostering sustainable planning and shaping policies for a resilient and environmentally friendly energy future within the IES.

3.3.1 Impact of Hydrogen Prices on System Configurations

Regarding the impact of hydrogen selling price on the IES, our investigation focused on four key parameters: LCOH, CAPEX of the IES, size of the electrolyzer in the IES, and the curtailed rate of wind energy within the system. In the baseline Case IV, the selling price of hydrogen was fixed at \$2/kg. However, for the sensitivity analysis, we introduced variations in the hydrogen sale price, ranging from \$2/kg to \$5.5/kg. This allowed us to explore the effects of different price levels, resulting in a total of 8 new simulated cases to assess the influence of these changes.

Fig. 3.7 illustrates a comprehensible result that emerged from this analysis: as the price of hydrogen increases, the total cost of the IES decreases. This outcome is understandable because the higher hydrogen price leads to increased IES hydrogen revenues, partially offsetting the total system cost. It is also relatively intuitive to observe how the size of the electrolyzer and the curtailed rate of wind energy are affected by the higher hydrogen price. As the hydrogen price rises, the IES tends to install larger electrolyzers to produce more hydrogen, aiming to reduce the total system cost and, consequently, decreasing the amount of wind energy curtailed.

However, one important finding is that the increase in LCOH is mainly due to the larger size of the electrolyzer, which results from the higher hydrogen price. As the size of the electrolyzer increases, the utilization rate of the electrolyzer gradually decreases, leading to a decrease in the hydrogen produced per unit of installed capacity. Consequently, this increase in the LCOH metric is observed. These insights are valuable for understanding the trade-offs and interconnections between hydrogen selling price, system cost, electrolyzer size, and curtailed wind energy within the IES. It informs decision-makers on how to strike a balance between these parameters to achieve cost-effective and efficient operation while ensuring a sustainable and economically viable IES.

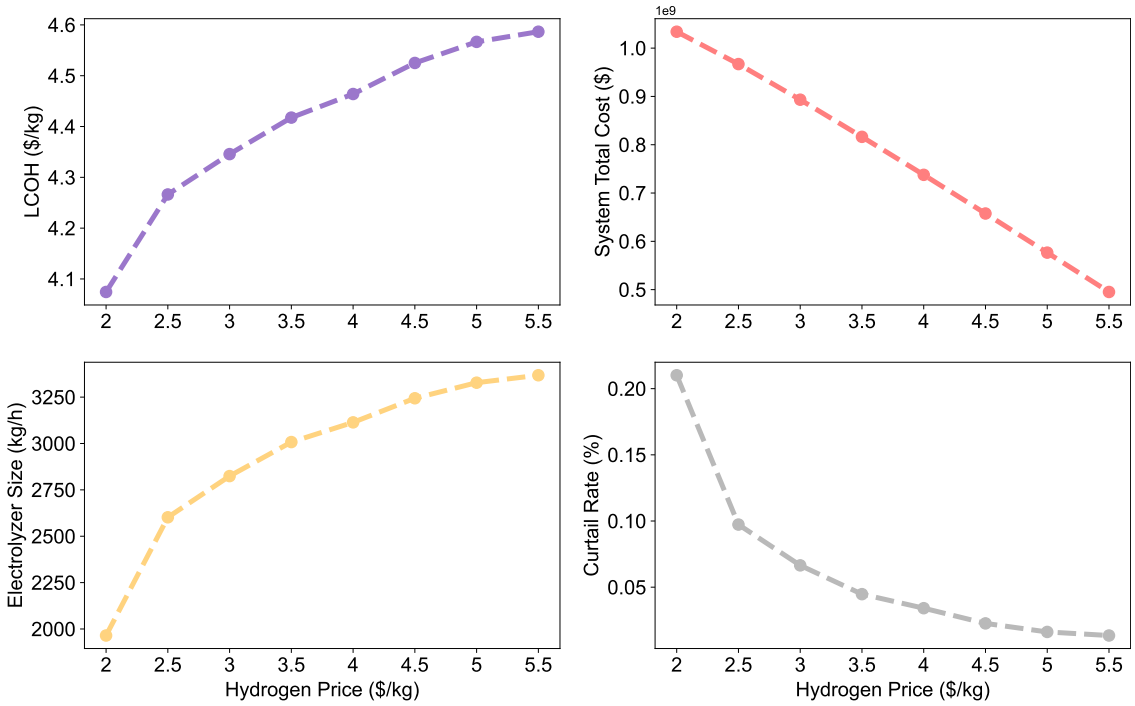


Figure 3.7: Sensitivity analysis of the impact of hydrogen price on levelized cost of hydrogen (LCOH), capital expenditure (CAPEX), curtail rate price

3.3.2 Impact of Regional Variations on System Configurations

To capture regional variations, we consider four distinct wind farms located in strategic regions: the ERCOT, the Midcontinent Independent System Operator (MISO), the Southwest Power Pool (SPP), and the Pennsylvania-New Jersey-Maryland Interconnection (PJM). These locations were chosen to represent diverse Independent System Operators (ISOs) with unique wind resource characteristics. For a comprehensive representation, we have provided the geographic coordinates of these locations in Table 3.3. In this particular sensitivity analysis, we investigate how different wind profiles from diverse regions impact the IES. By thoroughly examining key performance metrics, such as LCOE, LCOH, CAPEX, and curtailed rates under various wind scenarios, this study reveals crucial insights into the system's overall performance and economic viability.

The outcomes of this sensitivity analysis are depicted in Fig. 3.8, which showcases how the different wind profiles in each region affect the IES metrics. Among the four wind farms, the one situated in ERCOT stands out with the most abundant wind resource, resulting in the lowest LCOE, LCOH, and CAPEX, while concurrently exhibiting the highest curtailed rate. This valuable information aids in understanding the strengths and challenges associated

Table 3.3: The location of the four distinct wind farms located in different ISO regions

	ERCOT	MISO	SPP	PJM
Lon.	-100	-93	-94	-87
Lat.	32	46	40	40

with each region's wind resources, guiding strategic decision-making and potential investment opportunities for achieving enhanced system performance and cost-effectiveness within the IES.

The ERCOT wind farm's favorable outcomes highlight its potential as an attractive location for renewable energy integration and hydrogen-based storage. The abundance of wind resources leads to lower LCOE and LCOH, making the electricity and hydrogen produced in this region more competitive in the energy market. Additionally, the reduced CAPEX indicates that the initial investment required for establishing the IES is relatively lower in ERCOT, potentially attracting investors and stakeholders interested in sustainable energy projects. However, the high curtailed rate observed in ERCOT suggests a challenge in efficiently utilizing the surplus wind energy. This finding calls for innovative energy storage strategies, such as hydrogen production and storage, to effectively capture and store excess energy during periods of high wind generation.

Conversely, wind farms in other regions, such as MISO, SPP, and PJM, exhibit different trade-offs. While these regions may have higher LCOE, LCOH, and CAPEX due to relatively lower wind resources, they also experience reduced curtailed rates, indicating better utilization of wind energy. These regions may have a higher focus on optimizing energy storage solutions and balancing mechanisms to align electricity supply with demand. To offer decision makers a more comprehensive grasp of the interrelationships among the four systematic evaluation metrics, we have further summarized their connections as follows. **LCOE and Wind Resource:** Our analysis reveals that LCOE remains consistent across all cases, signifying its primary association with the wind resource available at a specific location. Areas with superior wind resources tend to exhibit lower LCOE, and vice versa. **LCOH and LCOE Correlation:** There exists a positive correlation between LCOH and LCOE due to the significant influence of electricity, a major cost component in hydrogen production, shared by both metrics. **CAPEX and Cost Metrics:** CAPEX is found to be lower when both LCOE and LCOH exhibit lower values, although the correlation is not extremely strong. This suggests that reducing operational costs can potentially lead to reduced capital costs. **Curtailment Rate:** The curtailment rate is influenced by various factors such as wind resource volatility and system configuration. It is suggested that considering wind curtailment

rate as an additional optimization objective in future research could facilitate multi-objective optimization and provide deeper insights.

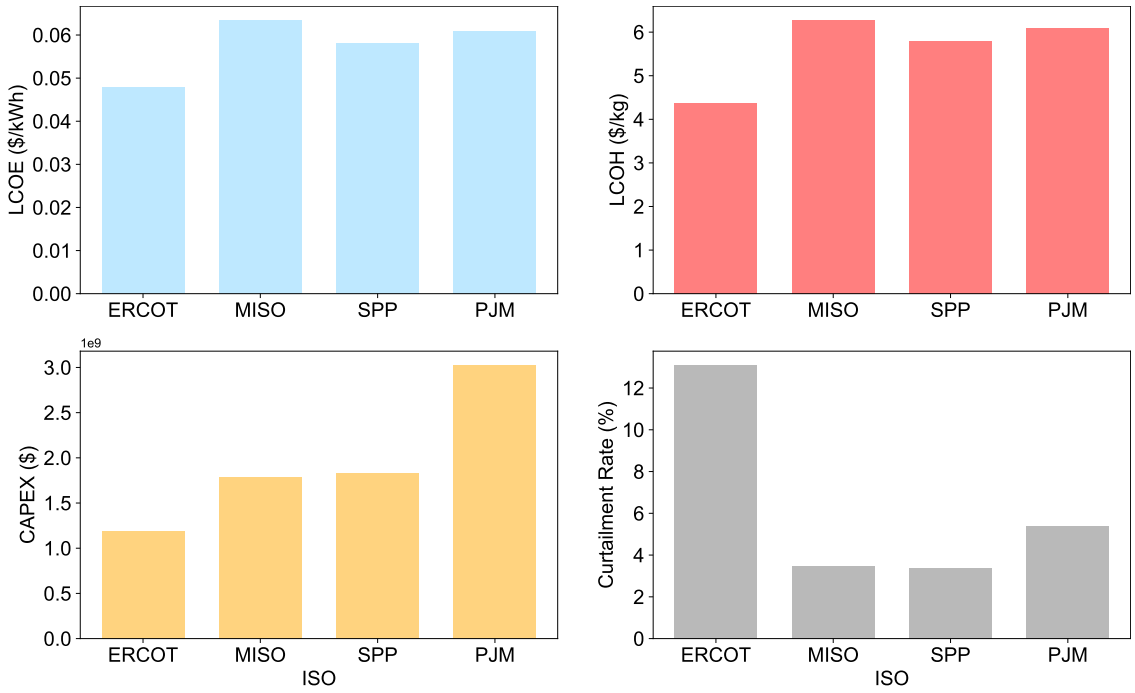


Figure 3.8: Sensitivity analysis of the impact of wind profile in different regions on levelized cost of energy (LCOE), LCOH, CAPEX, and curtailed rate

Table 3.4: Annual technology baseline ($/kW for CAPEX, O&M except tank: $/kg) [103, 123, 106, 3]

Year	CAPEX					O&M				
	Wind	Batt.[a]	Elec.	FC	Tank	Wind	Batt.[b]	Elec.	FC	Tank[c]
2020	1,874	840	48,000	500	1,168	40	410	3,600	30	117
2025	1,323	838	46,000	450	1,110	35	400	3,500	28	111
2030	1,274	620	44,000	400	1,070	34	340	3,400	26	107
2035	1,231	512	42,000	350	1,040	33	328	3,300	25	104
2040	1,188	454	40,000	300	1,010	32	313	3,200	24	101
2045	1,145	410	38,000	250	980	31	300	3,100	23	98
2050	1,102	346	36,000	200	950	30	289	3,000	22	95

[a] Battery CAPEX: Total upfront battery power capacity costs; energy capacity cost is half.
[b] Battery O&M: Replacement cost at replacement year.
[c] Tank: $/kg.

3.3.3 Impact of Future Component Prices on System Configurations

The final set of sensitivity analyses investigates the influence of component prices within the IES on key performance metrics over a thirty-year horizon [103, 123, 106, 3], as presented in Table 3.4. As technology matures, the prices of these components are expected to decline. This analysis aims to assess how fluctuations in prices for components like wind, battery, electrolyzer, fuel cell, and hydrogen tank installation costs impact critical IES metrics, including LCOE, LCOH, CAPEX, wind curtailed rate, and system component sizes.

By understanding the implications of future component prices on the IES, stakeholders can make informed decisions, mitigate risks, and devise optimized investment strategies. It facilitates sustainable planning, policy formation, and ensures long-term sustainability. Moreover, this analysis offers competitive advantages, fosters public acceptance, and aids in resource allocation. The comprehension of how price fluctuations influence key IES metrics enables the development of cost-effective, resilient, and environmentally friendly energy solutions for a sustainable future.

Fig. 3.9 illustrates the temporal evolution of each key IES metric and component sizes as prices decrease. Financial metrics, such as LCOE, LCOH, and CAPEX, exhibit a progressive reduction. As component prices decrease, the overall cost of electricity and hydrogen production decreases, leading to more economically viable solutions. Additionally, the electrolyzer size increases with decreasing prices, enabling better utilization of curtailed wind energy and consequently lowering the wind curtailed rate. The larger electrolyzer capacity allows for more efficient conversion of excess wind energy into hydrogen, maximizing the system's energy utilization. However, the sizes of storage devices and hydrogen fuel cells remain unchanged, primarily due to their limited sensitivity to price variations as essential support components for IES operations.

3.4 Summary

In this research, we conducted a comprehensive TEA of co-located wind and hydrogen energy within an IES to explore cost-effective and sustainable energy solutions. It was found that comparing to configurations that only have wind and conventional battery combinations, incorporating an electrolyzer results in a 7% reduction in the total cost of the IES, and utilizing hydrogen as the energy storage medium for hydrogen fuel cells leads to a 26% cost reduction.

The sensitivity analysis of hydrogen prices revealed that higher hydrogen selling prices led to reduced total system costs due to increased hydrogen revenues, thus partially offsetting

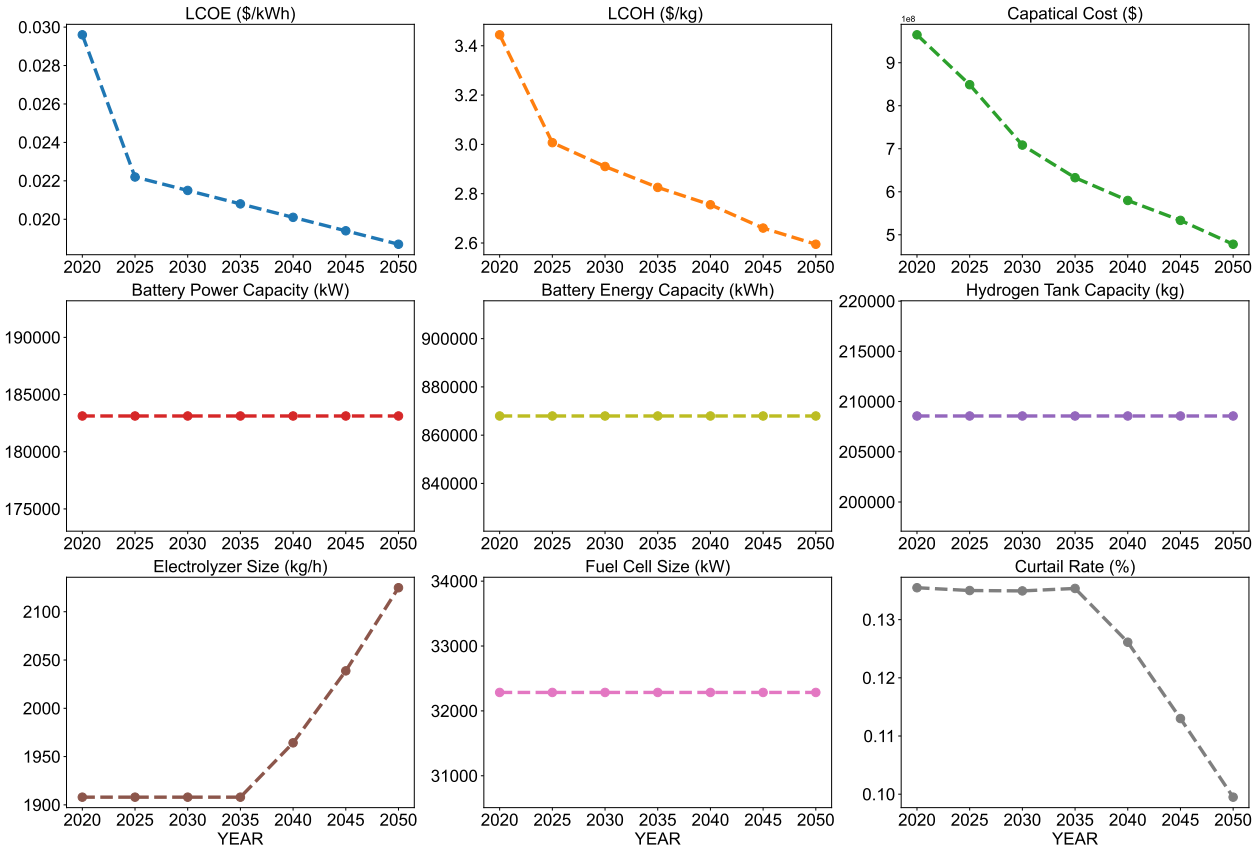


Figure 3.9: Sensitivity analysis of future components' prices

IES expenses. Moreover, as the hydrogen price increased, the IES strategically installed larger electrolyzers to convert excess wind energy into hydrogen, resulting in a significant reduction of wind curtailment rates.

Investigating regional wind profiles allowed us to identify ERCOT as a region with the most abundant wind resource, resulting in the lowest LCOE. However, the high curtailed rate in ERCOT indicated the need for further consideration of grid limitations and operational challenges in the region.

The analysis of future component prices illustrated a progressive reduction in financial metrics, such as LCOE, LCOH, and CAPEX, with decreasing costs over the thirty-year horizon. The increase in the size of the electrolyzer with decreasing prices led to improved utilization of excess wind energy and a decrease in wind curtailment rates. This demonstrates the system's adaptability to changing technology costs and its potential for enhanced cost-effectiveness over time.

Overall, our research offers valuable insights for decision-makers and planners seeking to develop sustainable, resilient, and environmentally friendly energy solutions within an IES. By considering diverse scenarios and specific data findings, stakeholders can strategically allocate resources, optimize component selections, and devise investment strategies that align with long-term objectives and market dynamics. This holistic approach to TEA empowers stakeholders to make informed decisions, mitigate risks, and shape policies that foster a sustainable and economically viable energy future. By harnessing the potential of co-located wind and hydrogen energy, we pave the way for a greener and more sustainable energy landscape, contributing to a resilient and carbon-neutral future.

Future research directions in the field of co-located wind and hydrogen energy within IES hold significant potential for advancing sustainable energy solutions. Continued investigation into the optimization of component configurations and sizing strategies can further enhance system performance and economic feasibility. Additionally, exploring advanced energy storage technologies, such as advanced batteries and novel hydrogen storage solutions, can improve the overall efficiency and reliability of the IES. Integration of advanced forecasting and control algorithms can also be explored to better manage the variability of renewable energy sources and enhance grid stability. Furthermore, research on the scalability and replicability of IES models in different geographic regions will be valuable for widespread implementation and adoption. Lastly, considering the social and environmental impacts of IES deployment can contribute to fostering community acceptance and promoting sustainable development in the energy sector.

CHAPTER 4

ASSESS HYDROGEN'S ROLE IN INCREASING RENEWABLE ENERGY PENETRATION AND GRID DECARBONIZATION[1]

In the previous chapter, we investigated the techno-economic feasibility of utilizing hydrogen as an energy storage medium within renewable energy integration systems, emphasizing a multi-scenario case study of wind-hydrogen co-located systems. Building upon these insights, this chapter broadens the analytical scope to examine the potential benefits of hydrogen within a grid-scale context, particularly addressing the challenges associated with renewable energy uncertainties and carbon reduction targets. Specifically, a comprehensive case study centered on the ERCOT is presented, offering detailed analyses and scenario evaluations to elucidate hydrogen's strategic role in facilitating renewable energy expansion and achieving substantial carbon emission reductions.

The international community has set ambitious goals for reducing carbon emissions and controlling climate change [2, 94, 70], with the United States aiming for net-zero emission electricity by 2035 [32]. In alignment with these objectives, Texas, endowed with vast renewable energy resources, has committed to significantly expand its wind and solar power capacities [35, 46, 7]. However, the intermittent nature of these renewable energy sources presents significant challenges to grid stability and reliability, compounded by the uncertainty of the actual total installed capacity in the future and the uncertainty of the growth of future demand for electricity. Without effective solutions, these challenges could lead to potential power outages and inefficiencies in energy supply, undermining the state's renewable energy goals. To address these difficulties, Texas needs to implement additional measures, such as advanced energy storage solutions and grid management technologies [46, 47, 84]. Specifically, integrating hydrogen production and utilization can play a crucial role in stabilizing the grid and enabling more renewable energy generation. This approach not only addresses the current limitations of renewable energy integration but also positions Texas as a leader in the emerging hydrogen economy, with potential economic and environmental benefits (Fig. 4.1).

Robust energy storage solutions are critical for large-scale renewable deployment, and hydrogen offers a promising option due to its capacity for long-term storage and versatility. Furthermore, Texas has a large-scale industrial demand for hydrogen, particularly in the Gulf

[1]Li, H. and Zhang, J., 2025. Hydrogen's role in expanding renewable energy and reducing carbon emissions in Texas. International Journal of Hydrogen Energy, 113, pp.77-89.

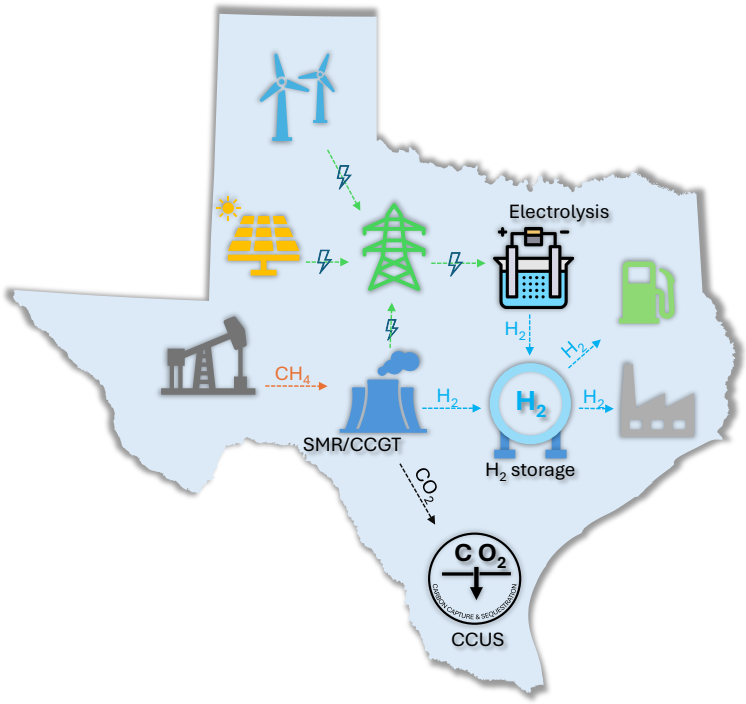


Figure 4.1: Conceptual Diagram of the Future Texas Power System with Hydrogen Integration. The future Texas power system will rely on combined cycle gas-turbine (CCGT) plants, wind, and solar to meet ERCOT's demand, with batteries and hydrogen providing energy storage. Natural gas will also produce hydrogen via steam methane reforming (SMR) for industrial use, with CO2 emissions from both gas plants and SMR captured and stored through carbon capture, utilization, and storage (CCUS) technology to achieve zero carbon emissions.

of Mexico, where it is used in refining, ammonia production, and chemical processes [13, 81]. Currently, the hydrogen economy is in its nascent stage, with hydrogen production primarily used in industrial applications and accounting for less than 1% of the global energy mix [101]. Scaling hydrogen to support renewable energy development requires substantial investment and technological advancements. Challenges include the high cost and limited capacity of electrolyzers, the need for extensive Carbon Capture, Utilization, and Storage (CCUS) for steam methane reforming (SMR) processes, and policy and market acceptance hurdles.

To address these uncertainties and challenges, this chapter introduces a stochastic optimization model that considers different scenarios of future renewable energy deployment completions and electricity demand growth. Past studies have often focused on changes in renewable energy generation due to meteorological factors [13, 126, 30, 21] and hydrogen's role in decarbonization through infrastructure development and regional hydrogen hubs [74, 148]. Studies have also examined stochastic optimization to address energy uncertainties [161, 160]

and the economic implications of hydrogen deployment [132]. Furthermore, advancements in grid flexibility, CCUS technologies, and global case studies on hydrogen integration highlight the potential for achieving cross-sectoral decarbonization [31, 86]. However, this study takes a more macro view, considering the impact of total installed capacity and the growth rate of total energy demand on the energy supply-demand balance. Additionally, it examines the construction of a hydrogen network across Texas within the context of the regional hydrogen hub to address the uneven geographic distribution of energy supply and demand. By incorporating these scenarios, the model provides a more comprehensive and realistic framework for planning and optimizing hydrogen integration. This innovation enhances the resilience and flexibility of the energy system by accounting for uncertainties in future deployment and demand.

4.1 A Stochastic Optimization Model for Renewable Energy Integration in the Electric Reliability Council of Texas (ERCOT) Power Grid

This study covers the entire ERCOT jurisdiction, dividing it into eight weather zones based on ERCOT's climate zoning. Each zone shares the same meteorological data, meaning generating resources within each zone have the same capacity factor, applicable to both installed and planned resources. The methodology involves a stochastic scenarios design, considering three scenarios for the completion of planned installed capacity: low (0%, status quo, no new equipment installed), medium (30% completion rate), and high (80% completion rate). The probabilities of low, medium, and high scenarios occurring are assumed to be 0.1, 0.7, and 0.2, respectively [118]. For the analysis of electricity demand growth, we added or subtracted 2% from ERCOT's projected 2030 electricity demand for the low and high demand cases, respectively, and projected values for the medium case [44]. The probabilities for the the cases are 0.2, 0.5, and 0.3 (Table 4.1). By combining these cases, we end up with nine stochastic scenarios and the probability of each occurring is summarized in Table 4.2. In this study, we focus on addressing the uncertainties associated with future electricity supply and demand. While we acknowledge that future hydrogen demand is also subject to significant uncertainty, obtaining reliable and accurate data on hydrogen demand remains challenging at this time. Additionally, the inherent unpredictability of future hydrogen trends further complicates its modeling. To balance computational complexity with the goal of producing meaningful and referable results, we have assumed a fixed value for future hydrogen demand within the stochastic optimization model.

Table 4.1: Uncertainty scenarios for installed capacity and electricity demand growth

Parameters	Scenarios	Description	Probability
Power demand	Low	2% decrease in ERCOT projections for 2030	0.2
	Medium	ERCOT projections for 2030	0.5
	High	2% increase in ERCOT projections for 2030	0.3
Completion rate of planned installed capacity	Low	0	0.1
	Medium	30%	0.7
	High	80%	0.2

Table 4.2: Probability of stochastic scenarios

Scenarios	Power demand[a]	Power generation	Probability
1	L	L	0.02
2	L	M	0.14
3	L	H	0.04
4	M	L	0.05
5	M	M	0.35
6	M	H	0.1
7	H	L	0.03
8	H	M	0.21
9	H	H	0.06

[a] L for low case, M for medium case, H for high case.

For the planned additional battery capacity, we assume a 100% completion rate. We also assume that hydrogen demand will remain relatively stable over the next few years, considering factors such as the progress of hydrogen hub completion, penetration of hydrogen vehicles, and changes in hydrogen demand in heavy industry and the petrochemical sector.

The primary data used in the analysis include the existing installed capacities of solar, wind, and battery storage in each region [42], the capacities of various types of equipment scheduled to come online by 2030 [118], and the demand for electricity and hydrogen in each region [35, 43, 13]. This comprehensive approach allows us to accurately model the impacts of different scenarios on the energy system, providing valuable insights into the future integration of renewable energy and hydrogen in Texas. Some of the key data used in the stochastic optimization model are summarized in Table 4.3.

Table 4.3: Key parameters used in the stochastic optimization model for the benchmark case study [13, 126, 28, 14, 81].

Category	Items	Value	Unit
General	Electricity to hydrogen (λ^{e2h})	55	kWh/kg
	Hydrogen to electricity (λ^{h2e})	17	kWh/kg
	Battery efficciency ($\eta^{\mathrm{cha//dis}}$)	0.95	-
	Hydrogen price (ρ^{h})	4	\$/kg
	Project discount rate (δ)	5%	-
	Life time	30	Year
	Oxygen selling price (ρ^{o})	0.007	\$/kg
	Carbon capture and storage cost (c^{p})	500	\$/T
	Deionized water cost (c^{w})	0.4	\$/kg
	Emission factor (SMR) (f^{smr})	10	T/T
	Emission factor (Power) (f^{power})	0.45	T/MWh
Electrolyzer	CAPEX cost (c_1^{ins})	588	\$/kW
	O&M cost (c_1^{om})	3.50%	-
	water rate (r^{w})	14.48	\$/kW-year
H_2 Storage	CAPEX cost (c_2^{ins})	74.8	\$/kW
	O&M cost (c_2^{om})	5%	-
	Transportation cost per unit (c^{tr})	3	\$/km·T^{-1}
Fuel cell	CAPEX cost (c_3^{ins})	994	\$/kW
	Fixed O&M (c_3^{om})	13.43	\$/kW-year

The Optimization Model

This stochastic optimization model aims to optimize the design and operation of a renewable energy system integrated with hydrogen storage and power generation technologies under various stochastic scenarios. The model captures the interplay between energy demand, hydrogen generation, and storage technologies under uncertain future scenarios [82, 80]. The core objective is to minimize the overall costs associated with the energy system, subject to constraints related to energy balance, hydrogen and battery storage, and resource availability.

The objective of the optimization model is to minimize the total system cost, $\mathbb{E}_s(\mathrm{ATC})$, which comprises CAPEX for installing technologies like electrolyzers, fuel cells, and hydrogen storage tanks across regions. These costs are discounted over the lifetime of the technologies using a discount rate, accounting for the time value of money. Additionally, the total cost includes fixed and operational expenditures, $\mathbb{E}_s(\mathrm{O\&M}_s)$, which cover hydrogen transportation, water and oxygen costs, hydrogen production, carbon costs, and penalties for emissions and unmet demand, while also factoring in revenue from the sale of hydrogen and oxygen. The

operational expenses, occurring during the runtime phase, are based on expected values across all stochastic scenarios, ensuring that uncertainties in system performance and costs are captured (Eqs. 4.10, 4.2, and 4.3).

Objective Function

$$\min \ \mathbb{E}_s(\text{ATC}) = \text{CAPEX} + \mathbb{E}_s(\text{O\&M}_s) \tag{4.1}$$

Here, ATC stands for the average total cost (sum of the CAPEX and the expected operating & maintenance costs). The operator $\mathbb{E}_s(\cdot)$ represents the scenario-weighted expectation over all scenarios s. CAPEX is the total capital cost, while $\text{O\&M}_s$ denotes the operating & maintenance costs under scenario s.

$$\text{CAPEX} = \sum_{i=1}^{I} \sum_{k=1}^{K} x_{i,k} \cdot \frac{c_k^{\text{ins}}}{\sum_{\tau=1}^{\text{lifetime}} \frac{1}{(1+\delta)^\tau}} \tag{4.2}$$

In this expression, $x_{i,k}$ is the installed capacity of technology k in region i, where $k = 1$, 2, and 3 represent the electrolyzer, hydrogen storage tank, and hydrogen fuel cell, respectively. c_k^{ins} is the installation cost per technology, while δ is the discount rate. The denominator $\sum_{\tau=1}^{\text{lifetime}} \frac{1}{(1+\delta)^\tau}$ is the present-worth factor over the lifetime of the technology.

$$\begin{aligned}
\mathbb{E}_s(\text{O\&M}_s) = & \sum_{i \in I} \sum_{k \in K} x_{i,k} \cdot c_k^{\text{om}} \\
& + \sum_{s \in S} \xi_s \left(\sum_{i \in I} \sum_{j \in I} \sum_{t \in T} c^{\text{tr}} \cdot h_{i,j,t,s}^{\text{tr}} \cdot d_{i,j} \right) \\
& + \sum_{i \in I} \sum_{t \in T} c^{\text{w}} \cdot w_{i,t,s} \\
& + \sum_{i \in I} \sum_{t \in T} (c^{\text{s}} \cdot f^{\text{smr}} + h^{\text{cost}}) \cdot h_{i,t,s}^{\text{smr}} \\
& + \sum_{i \in I} \sum_{t \in T} (c^{\text{p}} \cdot f^{\text{power}} + c^{\text{pen}}) \cdot \epsilon_{i,t,s}^{\text{n}} \\
& - \sum_{i \in I} \sum_{t \in T} \rho^{\text{h}} \cdot h_{i,t,s}^{\text{se}} - \sum_{i \in I} \sum_{t \in T} \rho^{\text{o}} \cdot o_{i,t,s}
\end{aligned} \tag{4.3}$$

Here, c_k^{om} is the fixed O&M cost per technology per year, and ξ_s is the probability of scenario s. c^{tr} is the hydrogen transportation cost per unit, $h_{i,j,t,s}^{\text{tr}}$ is the hydrogen flow from region i to region j at time t and scenario s, and $d_{i,j}$ is the distance between regions i and j. c^{w} is the water cost; $w_{i,t,s}$ is the water usage in region i; c^{s} is the SMR carbon cost; f^{smr} is the SMR emission factor; h^{cost} is the hydrogen price of SMR; c^{p} is the CCS cost; f^{power} is the

gas power emission factor; c^{pen} is the penalty cost per MWh; $\epsilon^{\text{n}}_{i,t,s}$ is the purchased electricity; $\rho^{\text{h}}, \rho^{\text{o}}$ are the prices of hydrogen and oxygen, respectively; $h^{\text{se}}_{i,t,s}$ is the hydrogen sold; and $o_{i,t,s}$ is the oxygen usage.

Constraints

The constraints ensure feasible system operation, respecting physical limits and balancing energy/resources. They are grouped for clarity: energy balance, hydrogen balance, storage limits, resource usage, and demand constraints.

$$\epsilon^{\text{h}}_{i,t,s} + \epsilon^{\text{dis}}_{i,t,s} + \epsilon^{\text{n}}_{i,t,s} - \epsilon^{\text{cha}}_{i,t,s} - \epsilon^{\text{e2h}}_{i,t,s} = \chi_{i,t,s} - \epsilon^{\text{r}}_{i,t,s}, \quad \forall i, t, s \tag{4.4}$$

Equation (4.4) states the energy balance, where $\epsilon^{\text{h}}_{i,t,s}$ is electricity generated from hydrogen, $\epsilon^{\text{dis}}_{i,t,s}$ is battery discharging, $\epsilon^{\text{n}}_{i,t,s}$ is purchased electricity, $\epsilon^{\text{cha}}_{i,t,s}$ is battery charging, $\epsilon^{\text{e2h}}_{i,t,s}$ is electricity used for hydrogen production, $\chi_{i,t,s}$ is the electricity demand, and $\epsilon^{\text{r}}_{i,t,s}$ is the renewable generation.

$$\theta^{\text{h}}_{i,t,s} = \theta^{\text{h}}_{i,t-1,s} + \sum_{j \neq i} \left(h^{\text{tr}}_{j,i,t,s} - h^{\text{tr}}_{i,j,t,s} \right) + \frac{\epsilon^{\text{e2h}}_{i,t,s}}{\lambda^{\text{e2h}}} - h^{\text{se}}_{i,t,s} - \frac{\epsilon^{\text{h}}_{i,t,s}}{\lambda^{\text{h2e}}}, \quad \forall i, t, s \tag{4.5}$$

Equation (4.5) captures hydrogen balance. $\theta^{\text{h}}_{i,t,s}$ is the hydrogen tank's state of charge, λ^{e2h} is the efficiency of electricity-to-hydrogen conversion, and λ^{h2e} is the hydrogen-to-electricity efficiency.

$$\theta^{\text{b}}_{i,t,s} = \theta^{\text{b}}_{i,t-1,s} + \eta^{\text{cha}} \cdot \epsilon^{\text{cha}}_{i,t,s} - \frac{\epsilon^{\text{dis}}_{i,t,s}}{\eta^{\text{dis}}}, \quad \forall i, t, s \tag{4.6}$$

Equation (4.6) is the battery storage balance. $\theta^{\text{b}}_{i,t,s}$ is the battery state of charge, η^{cha} and η^{dis} are charging and discharging efficiencies, respectively.

$$\theta^{\text{h}}_{i,t,s} \leq x_{i,2}, \quad \forall i, t, s \tag{4.7}$$

$$\theta^{\text{b}}_{i,t,s} \leq \beta_i, \quad \forall i, t, s \tag{4.8}$$

Equations (4.7) and (4.8) impose capacity limits on hydrogen tanks $x_{i,2}$ and battery storage β_i, respectively.

$$w_{i,t,s} = r^{\mathrm{w}} \cdot \frac{\epsilon^{\mathrm{e2h}}_{i,t,s}}{\lambda^{\mathrm{e2h}}}, \quad \forall i, t, s \tag{4.9}$$

$$o_{i,t,s} = r^{\mathrm{o}} \cdot \frac{\epsilon^{\mathrm{e2h}}_{i,t,s}}{\lambda^{\mathrm{e2h}}}, \quad \forall i, t, s \tag{4.10}$$

Equations (4.9) and (4.10) specify water and oxygen consumption for hydrogen production, where r^{w} and r^{o} are the water and oxygen rates per unit of hydrogen produced, respectively.

$$\sum_{s \in S} \xi_s \sum_{t \in T} h^{\mathrm{se}}_{i,t,s} = \psi_i \cdot hd_i, \quad \forall i \in I \tag{4.11}$$

$$\sum_{s \in S} \xi_s \big(h^{\mathrm{se}}_{i,t,s} + h^{\mathrm{smr}}_{i,t,s}\big) \geq \kappa_{i,t}, \quad \forall i, t \tag{4.12}$$

Equations (4.11) and (4.12) enforce hydrogen demand satisfaction. $h^{\mathrm{se}}_{i,t,s}$ is hydrogen sold, $h^{\mathrm{smr}}_{i,t,s}$ is hydrogen from SMR, ψ_i is the demand satisfaction rate, hd_i is the total hydrogen demand, and $\kappa_{i,t}$ is the hourly hydrogen demand.

$$\epsilon^{\mathrm{h}}_{i,t,s} \leq x_{i,3}, \quad \forall i, t, s \tag{4.13}$$

$$\epsilon^{\mathrm{e2h}}_{i,t,s} \leq x_{i,1}, \quad \forall i, t, s \tag{4.14}$$

Equations (4.13) and (4.14) limit electricity generation from hydrogen and electricity-to-hydrogen conversion by the installed capacities $x_{i,3}$ and $x_{i,1}$, respectively.

$$\theta^{\mathrm{b}}_{i,0,s} = 0.8 \cdot \beta_i, \quad \forall i, s \tag{4.15}$$

$$\theta^{\mathrm{b}}_{i,0,s} = 0, \quad \forall i, s \tag{4.16}$$

Equations (4.15) and (4.16) set initial conditions for battery and hydrogen storage, respectively.

$$\epsilon^{\mathrm{n}}_{i,t,s} \leq \max\big(\chi_{i,t,s} - \epsilon^{\mathrm{r}}_{i,t,s},\, 0\big), \quad \forall i, t, s \tag{4.17}$$

Equation (4.17) restricts hourly power purchase $\epsilon^{\mathrm{n}}_{i,t,s}$ by ensuring it does not exceed the gap between the demand $\chi_{i,t,s}$ and renewable generation $\epsilon^{\mathrm{r}}_{i,t,s}$. This promotes maximum use of renewables while allowing necessary flexibility via Combined Cycle Gas Turbine (CCGT) power.

4.2 Results

4.2.1 Optimization of The Power System

We optimize the energy mix for each zone within the ERCOT [45] by minimizing the total system cost of hydrogen-assisted storage for renewable energy, considering future total installed renewable energy capacity and the capacity of backup CCGT plants under the uncertainties of both total expected installed capacity of renewable energy and electricity demand growth. The objective is to achieve an optimal balance between renewable and non-renewable energy sources throughout the year. The total system cost includes the capital and operational costs of hydrogen-related equipment, such as electrolyzers, hydrogen storage tanks, and hydrogen fuel cells, as well as the costs associated with hydrogen transportation, and the capture and storage of carbon dioxide (CO2) produced by SMR processes used for hydrogen production and CCGT for power generation. For electricity from CCGT, we focus solely on the wholesale tariffs and the costs of CO2 mitigation from these plants, rather than the expenses of constructing new gas-fired power plants. This approach ensures a comprehensive assessment of the economic implications of integrating hydrogen storage into the renewable energy framework, providing a clear understanding of the trade-offs and benefits associated with different energy mix scenarios, and enabling the development of a cost-effective and sustainable energy strategy for Texas (Fig. 4.2).

Taking into account the planned installed capacity of each region, the possible percentage of completion, the demand for electric energy, the uncertainty in the growth rate of electric energy, the capacity factor of wind and other resources, we prioritized renewable energy [118, 43, 42]. In this study, we assume that renewable energy is first supplied to meet the demand for electric energy, and any surplus is used for hydrogen production. Additionally, we consider the carbon dioxide factor of CCGT, hydrogen demand, and the efficiency of the conversion between hydrogen and electricity. Based on these factors, we determined the optimal values for required installed capacity of CCGT, the green hydrogen (electrolyzers with renewable energy) fulfillment rate, the state of charge of the battery, and the state of the hydrogen tanks in each region, as summarized in Table 4.4. As shown in Fig. 4.4**a**, the stochastic optimization effectively balances the system's power supply. During peak renewable energy generation, excess electricity is stored in batteries, while a portion is converted to green hydrogen via electrolyzers. In low generation periods, the system meets demand by drawing on stored energy from both batteries and CCGT, ensuring continuous stability.

It is observed that there are spatial and temporal differences in power generation between regions, such as hourly and seasonal variations (Fig. 4.3 **a, b**), and differences in geographic

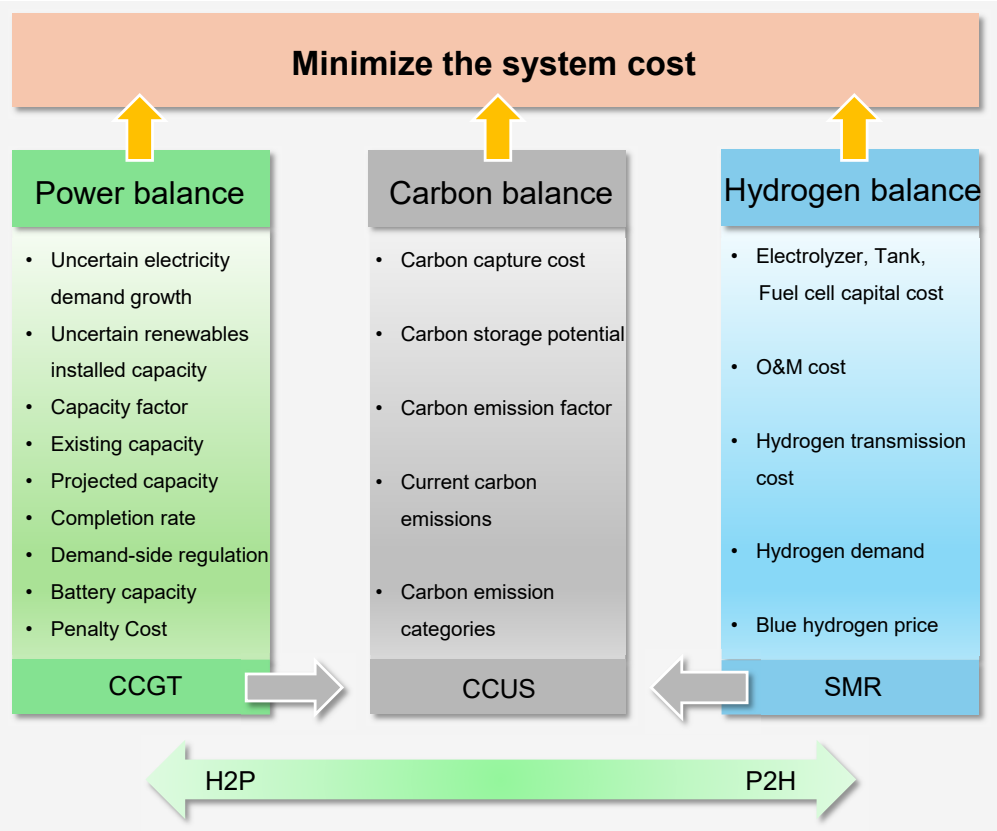


Figure 4.2: Structural Diagram of the Stochastic Optimization Model. This model focuses on maintaining three key system balances: electricity demand, hydrogen demand, and carbon balance. The carbon balance addresses CCUS from CCGT and SMR processes. Hydrogen and electricity are interconverted via electrolyzers and hydrogen fuel cells to maintain equilibrium between electricity and hydrogen demand. The core influencing factors of these balances are the primary focus of the model, with the objective function aiming to minimize the total cost of maintaining these three critical balances.

Table 4.4: Results for CCGT capacity, green hydrogen rate, and storage unit status for each region in the benchmark case.

	Coast	**East**	**Far west**	**North**	**North center**	**South**	**South center**	**West**
CCGT (MW)	22,719	3,116	11,258	26,535	2,488	16,571	7,777	1,865
Green H2 rate	0	87.78%	59.33%	5.20%	NA	0	92.93%	NA
State of charge	55.99%	60.14%	60%	24.47%	69.37%	60.88%	46.62%	73.71%
State of tank	NA	36.11%	NA	NA	34.3%	NA	NA	NA

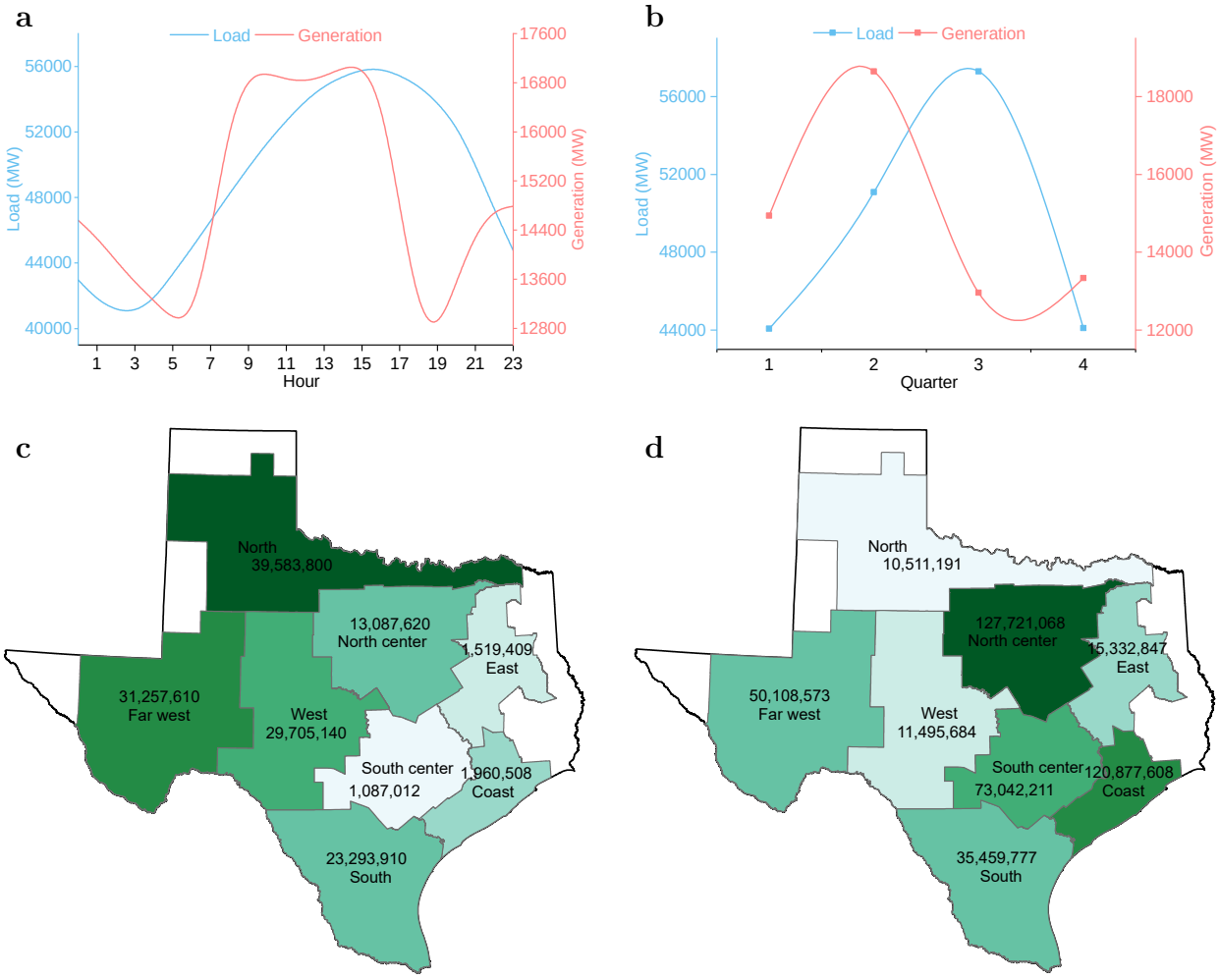


Figure 4.3: Spatial and Temporal Differences Between Renewable Energy Generation and Electricity Demand in ERCOT. **a** shows that peak renewable energy generation in ERCOT occurs between 9am and 3pm, while peak electricity consumption is concentrated from 3pm to 7pm. Seasonally, **b** depicts renewable energy generation peaks in the second quarter, whereas electricity demand peaks in the third quarter. These mismatches highlight the need for both short- and long-term storage solutions to enhance renewable energy integration into the ERCOT grid. Figures **c** and **d** illustrate the spatial distribution of renewable energy generation and electricity demand across the eight weather zones within ERCOT (Both are results for 2023, in kW), with darker colors representing higher values. The data reveal a clear spatial disparity: renewable energy generation is primarily concentrated in the Midwest region, while electricity demand is predominantly focused in the Southeast and North regions, highlighting significant geographic differences in supply and demand.

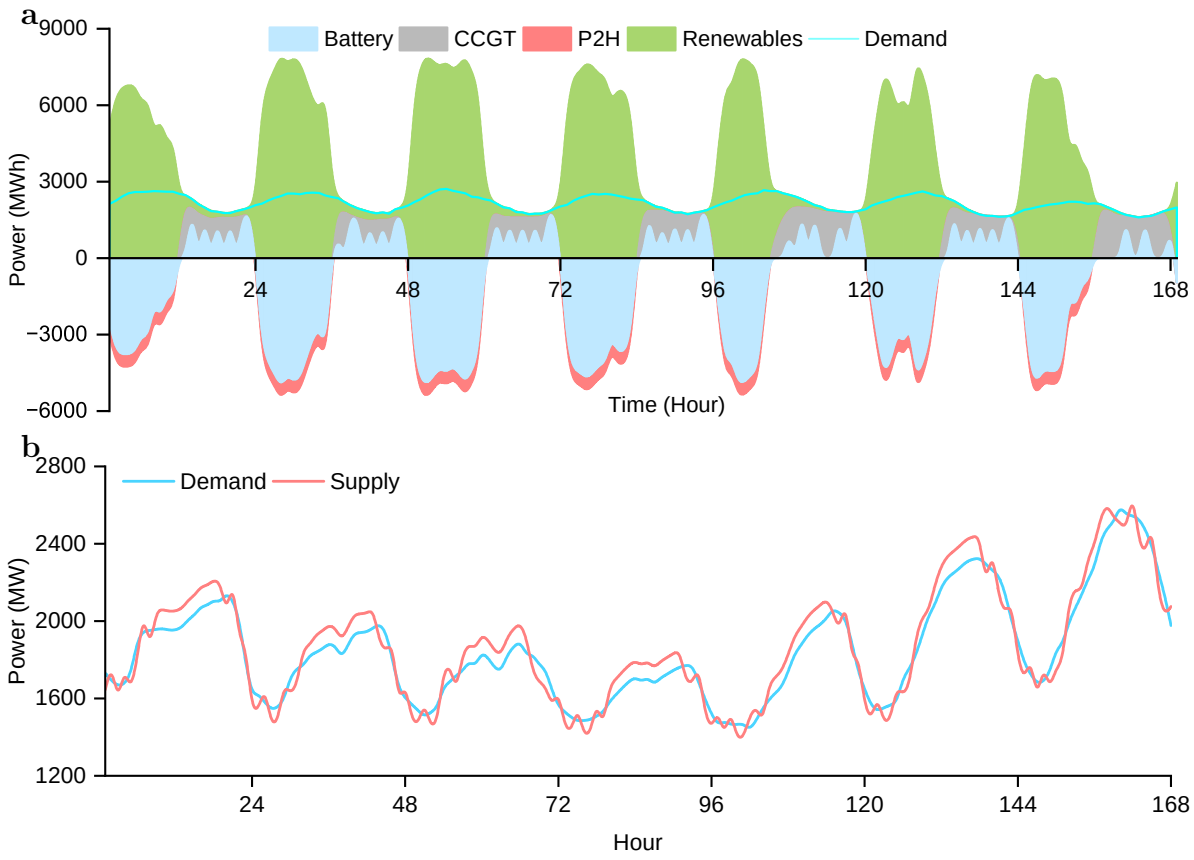


Figure 4.4: Results of Power System Optimization. **a**, Stochastic optimization results showing power balance within the system. During peak clean energy generation, excess electricity is stored in batteries, while some is converted into green hydrogen via electrolyzers. In periods of low generation, stored energy from batteries and CCGT work together to meet power demand, maintaining system stability. **b**, The difference between original power demand and actual power supply after load regulation. Demand-side adjustments successfully shift peak demand periods to better align with the system's power generation profile.

location (Fig. 4.3 **c, d**). These differences are influenced by the climatic variations across regions and the different proportions of solar and wind energy installations. As a result, power generation in these regions is often out of sync with the electricity demand curve. To address this, our model incorporates the scenario of load demand flexibility. By adding an acceptable range (±5% power demand) to the hourly power demand while maintaining the total power demand constant, we shift power demand to align more closely with the characteristics of renewable energy generation. This approach maximizes the use of renewable energy and minimizes reliance on non-renewable sources. The total annual electrical energy demand for CCGT across the entire ERCOT region experienced a slight decline, dropping

from 389,785,123 MWh to 389,164,389 MWh. Similarly, the total annual demand for blue (SMR with CCUS) hydrogen showed a marginal reduction, decreasing from 3,309 kilotons (KT) to 3,307 KT. Fig. 4.4**b** illustrates the difference between the original power demand and the adjusted power supply curve following load regulation. The visualization clearly shows that demand-side load regulation effectively shifts the demand peaks, aligning them more closely with the system's generation profile. This adjustment improves the balance between generation and consumption, optimizing efficiency and easing the strain on resources during peak demand.

To refine our analysis, we designed several sensitivity experiments to explore the robustness of our model under varying conditions. For scenarios A1 and A2, we varied the completion rate of the planned installed renewable energy capacity by ±10% for both medium and high completion cases. In scenarios A3 and A4, we analyzed the effects of adjusting the growth rate of electricity demand by ±5% for each case. Lastly, for scenarios A5 and A6, we reduced the final installed capacity of the planned energy storage systems to 80% and 60% of the target levels. These sensitivity analyses provide insights into the impact of key variables on overall system performance, helping us identify potential risks and opportunities(Table 4.5).

Table 4.5: Sensitivity analysis scenarios for optimization of the power system

Scenarios	**Description**
A1	+ 10% completion rate of projected renewables installation
A2	- 10% completion rate of projected renewables installation
A3	+ 5% final power demand
A4	- 5% final power demand
A5	80% completion rate of projected battery installation
A6	60% completion rate of projected battery installation

The results reveal the impact of completion rates (defined in the Methods section) of planned renewable energy capacities on future energy system operating costs and the operation of other equipment within the system. Higher completion rates of planned renewable energy capacities significantly decreased the total system cost by utilizing more low-cost renewable energy sources (i.e., from $150.5 billion to $146.8 billion). Conversely, lower completion rates increased costs (i.e., from $150.5 billion to $154.4 billion), highlighting the economic benefits of higher renewable energy penetration. At the same time, the supply of green hydrogen within ERCOT increases by 10,844 tons (+8%) in the higher completion rate scenario, and decreases by 15,412 tons (-12%) in the lower completion rate scenario. Meanwhile, the circulation of hydrogen increases by 5,979 tons (+5%) and 9,035 tons (-7%) in the higher and

lower completion rate scenarios, respectively. In terms of the utilization of energy storage and hydrogen storage equipment, the increased completion rate has simultaneously driven a more efficient use of these storage systems. Notably, battery utilization has reached an average of 64.8%, corresponding to 68,698 MWh of stored energy, up from a previous average of 56.3% or 59,312 MWh. This trend highlights the critical role of energy storage in accommodating the growing penetration of renewable energy sources. As renewable energy continues to expand, the need for higher capacity storage systems becomes increasingly evident to manage and balance the inherent fluctuations in energy supply, ensuring a stable and reliable energy system.

4.2.2 Analysis and Optimization of Hydrogen Systems

This study investigates the dual role of hydrogen in increasing renewable energy penetration and supporting decarbonization in Texas. Hydrogen acts as an energy storage medium for managing renewable intermittency and as a clean fuel to reduce emissions. We analyzed hydrogen demand across eight weather zones, detailed in Fig. 4.5. The Gulf Coast, a major hub for U.S. hydrogen demand, driven by ammonia, methanol, and refinery industries, consumes over 3 megatons annually ($\mathrm{MT \cdot yr^{-1}}$), over a quarter of the national demand [138, 41]. About half of U.S. hydrogen production is concentrated in this region, where Air Products operates the world's largest hydrogen pipeline network [116]. The region also hosts a significant portion of the nation's hydrogen pipelines. As of December 2020, the U.S. had over 1,600 miles of hydrogen pipelines, nearly all of which are located in Texas and Louisiana[124]. These factors position the Gulf Coast as a foundation for a cleaner hydrogen market. However, geographical discrepancies between hydrogen demand and renewable generation prompted the design of a green hydrogen transportation network within ERCOT (Fig. 4.6**a**). Hydrogen is transported between neighboring zones. Electrolyzers, storage tanks, and fuel cells are installed at zone nodes to optimize hydrogen's energy storage potential, with surplus renewable energy converted to hydrogen. While hydrogen demand is met by SMRs, we accounted for carbon capture costs. Electrolyzer capacity was capped at 500 MW, considering spatial constraints.

The results of the stochastic optimization reveal that 3.8% of the hydrogen demand within ERCOT will be met by green hydrogen. The results also revealed an unexpected strategy: instead of installing the electrolyzer in the region with the highest hydrogen demand, the system opted to place the electrolyzer in areas with minimal or even no hydrogen demand. This decision was driven by the economic efficiency of inter-regional hydrogen transportation

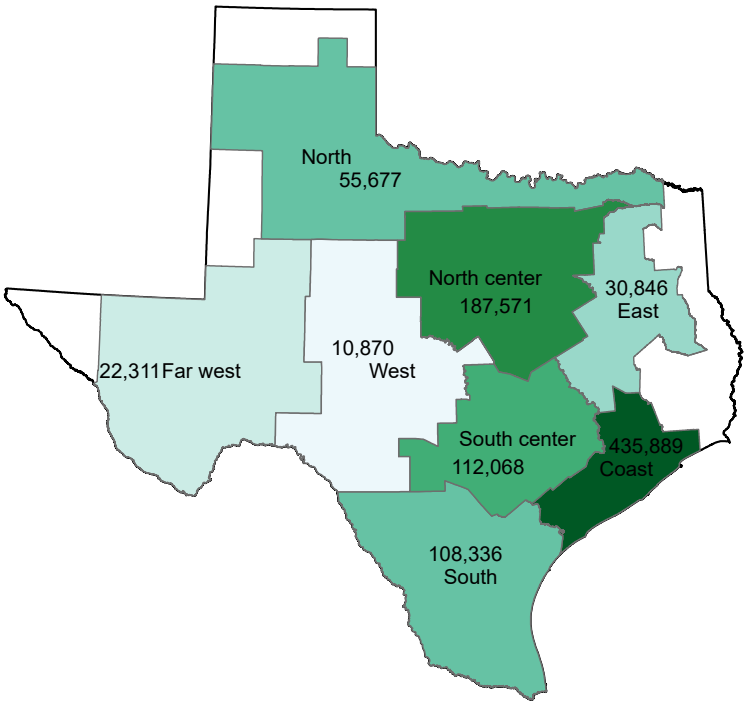


Figure 4.5: Hydrogen demand (kg/Day)

(Fig. 4.6**a**), and the availability of renewable energy (Fig. 4.3**c**). This conclusion is supported by the economically optimal results generated by the stochastic optimization model, which aims to minimize total system costs. In Zone East and Zone North Center, 49 tons and 14 tons hydrogen storage tanks were strategically installed to address the mismatch between hydrogen production and demand. Fig. 4.6**b** illustrates the hydrogen transfer between the eight regions, showing a predominant flow direction from west to east and from north to south. Notably, Zone South Center meets 92.9% of its total hydrogen demand through supply from the two green hydrogen production zones. However, despite Zone Coast and Zone South being the regions with the highest hydrogen demand, the most economical solution to meet their needs, given the current green hydrogen production capacity, is to rely entirely on gray hydrogen. This approach highlights the complex interplay between production capabilities, regional demands, and economic viability within the hydrogen supply network.

A series of sensitivity analyses were conducted to assess the impact of technological advancements on cost reductions. In the first category of scenarios, we examined the effects of reducing the initial costs of hydrogen-related equipment, including electrolyzers, hydrogen storage tanks, and hydrogen fuel cells, by incremental percentages of 5%, 10%, 15%, 30%, and 50%. These scenarios are designed to assess how these cost reductions influence the economic

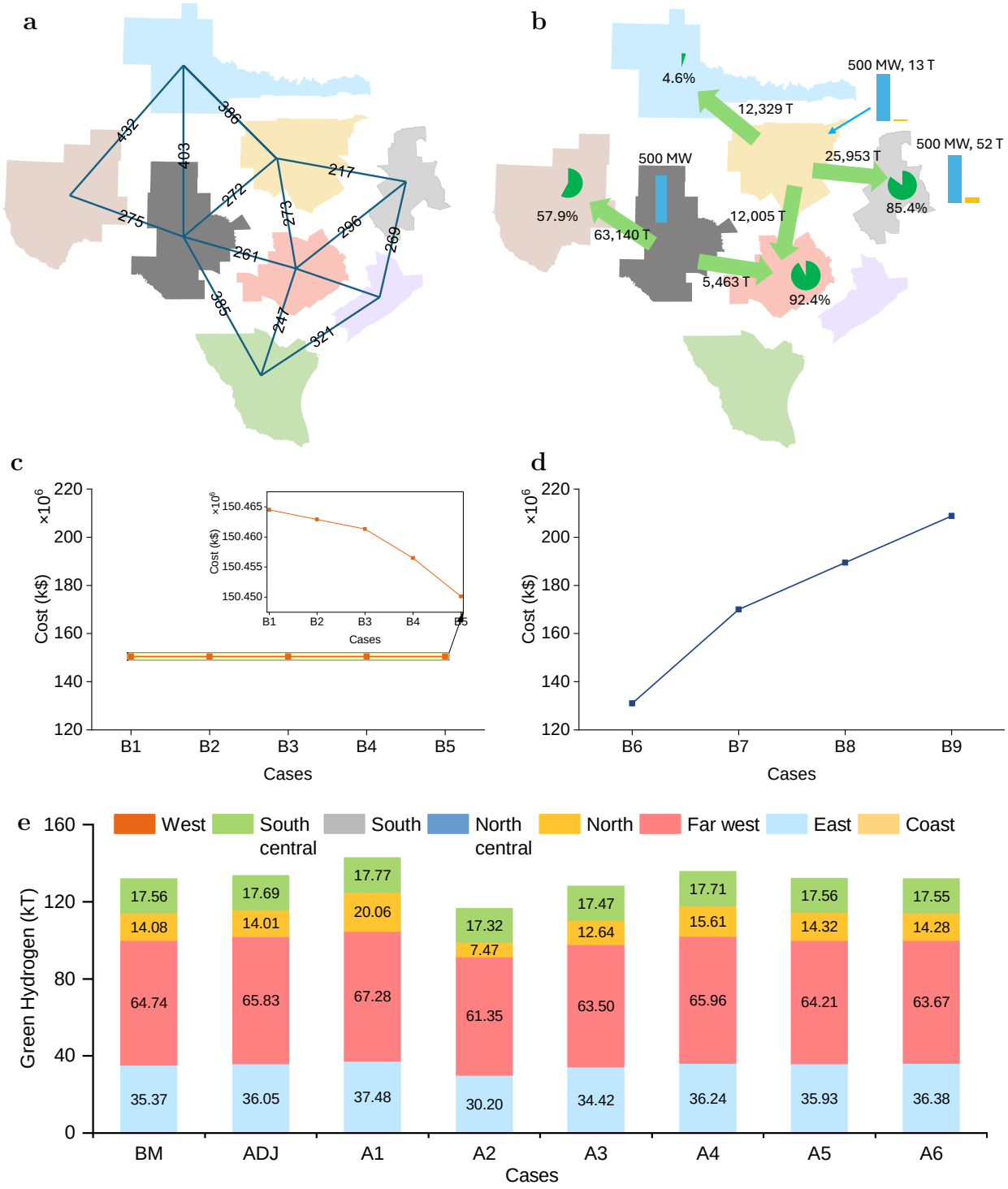


Figure 4.6: Inter-Zone Hydrogen Network in ERCOT and Results. **a**, Hydrogen pipeline connections and distance assumptions. **b**, Strategic placement of electrolysis units and hydrogen distribution. **c** and **d**, Sensitivity analysis of system costs under equipment and tariff changes. **e**, Green hydrogen distribution across zones in power system optimization.

viability and adoption rates of green hydrogen technologies within the energy system. In the second category of scenarios, we modified the electricity tariff of the backup gas-fired power plants to explore how increases in this tariff affect the overall system configuration. This scenario allowed us to observe the shifts in the energy mix and the reallocation of resources within the system as the cost of backup electricity rises. (Table 4.6).

Table 4.6: Sensitivity analysis scenarios for analysis and optimization of hydrogen systems

Scenarios	**Description**
B1	- 5% CAPEX of hydrogen-related equipment
B2	- 10% CAPEX of hydrogen-related equipment
B3	- 15% CAPEX of hydrogen-related equipment
B4	- 15% CAPEX of hydrogen-related equipment
B5	-50% CAPEX of hydrogen-related equipment
B6	\$50MWh^{-1} wholesale electricity price
B7	\$150MWh^{-1} wholesale electricity price
B8	\$200MWh^{-1} wholesale electricity price
B9	\$250MWh^{-1} wholesale electricity price

The results show that reducing the cost of hydrogen equipment alone did not significantly alter the system's configuration, changes in electricity prices from CCGT had a profound effect on the energy mix and deployment strategy. When electricity prices rose to \$200 MWh^{-1}, the total installed capacity of CCGT plants dropped from 92,329 to 92,176 MW, while hydrogen fuel cell capacity increased from 0 to 296 MW. This led to greater use of green hydrogen as an energy reserve, with stored hydrogen being converted to electricity during periods of low renewable generation. Consequently, the total green hydrogen supply fell from 131,748 T to 40,232 T, while hydrogen-to-electricity conversion surged to 1,789,688 MWh. Despite a 50% cost reduction in hydrogen technologies, they still struggle to compete with gas-fired backup electricity. The system's sensitivity to electricity prices highlights its reliance on gas-fired plants, emphasizing the need for further cost reductions and advancements in hydrogen technologies to enhance their competitiveness and influence in the energy mix. It is worth noting that the focus of this study is to optimize the structure of the energy system under the uncertainty of future electricity supply and demand, and the adjustment of electricity prices in the sensitivity analysis is only intended to show the direct impacts it brings to the energy system, but it does not take into account the possible secondary economic effects of the electricity price increase, such as the impacts on household incomes or industrial productivity, which require further in-depth analysis beyond the scope of this study. Table 4.7 shows the difference in capacity of hydrogen-related equipment in each case of the sensitivity analysis

Table 4.7: The optimal capacity of hydrogen-related equipment

	B1	B2	B3	B4	B5	B6	B7	B8	B9
East 1[a,b]	500	500	500	500	500	500	500	500	500
East 2	51	47	47	47	53	49	47	47	99
East 3	0	0	0	0	0	0	0	134	178
East 1	0	0	0	0	0	0	0	0	0
Far west 2	0	0	0	0	0	0	0	0	0
Far west 3	0	0	0	0	0	0	0	0	0
North 3	0	0	0	0	0	0	0	0	0
North center 1	500	500	500	500	500	500	500	500	500
North center 2	15	19	19	22	22	15	17	27	3
North center 3	0	0	0	0	0	0	0	2	0
South center 2	0	0	0	0	0	0	0	0	14
South center 3	0	0	0	0	0	0	0	153	271
West 1	500	500	500	500	500	500	500	500	500
West 2	0	0	0	0	0	0	0	0	19

[a] The first two digits are the weather zone code, the last digit is the technology, 1 is the electrolyzer, 2 is the hydrogen tank, and 3 is the fuel cell.
[b] Electrolyzers are measured in MW, hydrogen tank in T, and fuel cells in MW.

4.2.3 Carbon Dioxide (CO2) Emission Abatement Analysis

Most of the world's environmental challenges stem from carbon emissions [29]. Global energy-related CO2 emissions surged by 1.1% in 2023, rising by 410 MT to hit an unprecedented record of 37.4 GT [60, 87]. As such, a key goal in energy system development is to reduce carbon emission, and increasing the penetration of renewable energy sources is a crucial part of this effort. However, the volatility of renewable energy necessitates reliable energy storage solutions, and hydrogen emerges as a versatile option. It not only serves as a medium for long-term energy storage but also acts as an industrial feedstock, particularly useful in hard-to-decarbonize sectors, further aiding in the reduction of carbon emissions. This section of the study focuses on this context, using Texas's 2022 carbon emissions data as a reference [40]. As illustrated in Fig. 4.7, direct combustion and power generation contribute 28% and 54% of Texas's total carbon emissions, respectively, while other sectors account for only 18%. Therefore, targeting carbon reductions in the areas of power generation and direct combustion presents the most impactful strategy for significantly lowering Texas's overall carbon emissions.

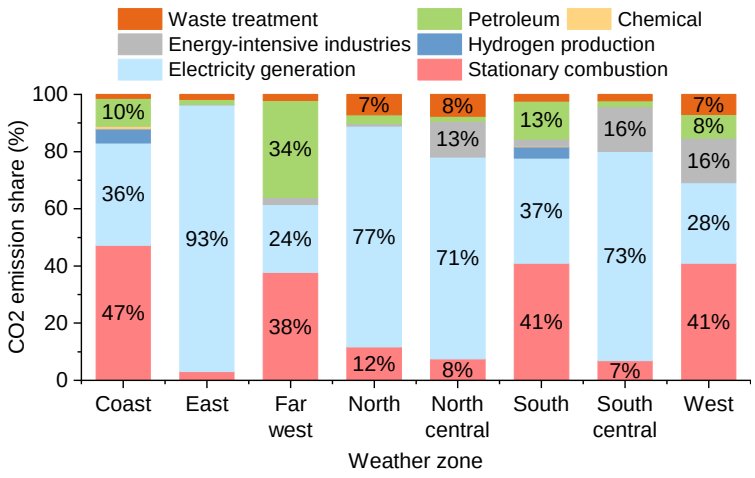


Figure 4.7: CO2 Emission Percentage. The figure illustrates the carbon emission shares from various energy sources across ERCOT's zones: Coast, East, Far West, North, North Central, South, South Central, and West. Direct combustion and electricity generation account for over 60% of total carbon emissions in each region. In Zone East, electricity generation contributes a staggering 93.3% of the region's emissions due to its low renewable energy penetration and distance from major wind and solar hubs in the Midwest. Zone Far West, a key fossil fuel production area, sees 33.9% of its emissions coming from oil-related activities. Meanwhile, Zone Coast, despite being a core petrochemical region, has minimal petroleum-related emissions, primarily because hydrogen used in its production processes is supplied from other Gulf Coast states, reducing reliance on local fossil fuels. These patterns underscore the regional differences in carbon emissions, driven by geographic, industrial, and energy resource factors across ERCOT's territory.

At the current stage, the penetration of renewable energy sources remains relatively low (30% [34]), leaving the power system reliant on fossil fuels, either as a backup supply or as a direct part of the energy mix. Consequently, reducing carbon emissions from the energy supply side is critical, but CCUS also plays a pivotal role in emission reduction strategies [92]. Texas is particularly well-positioned to capitalize on its unique geologic structures for CCUS to further minimize its carbon footprint. The state's vast subsurface geology offers numerous potential sites for storing captured carbon dioxide, including depleted oil and gas fields, saline aquifers, and unmineable coal seams [75]. The Gulf Coast region stands out, offering opportunities for both enhanced oil recovery (EOR) and permanent CO2 storage within its expansive saline aquifers and depleted oil fields [91]. According to the National Energy Technology Laboratory (NETL), Texas's saline formations alone could store up to 20 billion metric tons of CO2 [54, 93]. Integrating CCUS with renewable energy and hydrogen solutions creates a comprehensive approach to achieving substantial carbon reductions. In

this study, we focus on the cost implications of implementing CCUS in CCGT and SMR units, examining how these factors affect the overall system cost, energy mix, and future composition of the energy system.

The results of our stochastic optimization reveal that by 2030, if ERCOT's electricity demand is met solely by a combination of wind, solar, and CCGT, the expected CO2 emissions from CCGT, considering various stochastic scenarios, would reach 175.4 MT per year. However, by implementing load regulation on the demand side, these emissions are reduced by 279 KT (Fig. 4.8**a**). Additionally, our analysis shows that in scenarios where the electricity price from CCGT remains below $200 per MWh, the structure and composition of the energy system remain unchanged, resulting in no reduction in overall carbon emissions. In contrast, when the price increases to $200 and $250 per MWh, the system compensates by installing more hydrogen fuel cells to meet electricity demand, reducing CO2 emissions from CCGT to 174.6 MT and 174.4 MT, respectively. However, this shift necessitates greater reliance on gray hydrogen to meet hydrogen demand, which subsequently raises CO2 emissions (Fig. 4.8**b**). Furthermore, the inefficiency in converting electricity to hydrogen and then back to electricity results in energy losses, leading to an overall increase in total system CO2 emissions. In sensitivity analyses that adjust the cost of hydrogen-related equipment (Table 4.6), we observe no significant change to the energy system configuration, and thus the total carbon emissions remain unchanged. This underscores the complexity of balancing cost, emissions, and system efficiency in future energy scenarios. The carbon emissions reduction results presented in this study should be interpreted as an indicator of the effectiveness of the stochastic optimization approach rather than its ultimate goal. The relatively modest reduction of 1,300 tons of CO2 reflects the structural challenges within ERCOT's energy system, where limited renewable energy penetration and a reliance on fossil fuels drive high baseline emissions. While the optimization framework minimizes system costs rather than maximizing emissions reductions, these results provide valuable insights into the interplay between carbon mitigation and system economics, offering a foundation for further exploration of clean energy deployment strategies.

Table 4.8: Optimal sizes of hydrogen related equipment for C4

	Coast	**East**	**Far west**	**North**	**North center**	**South**	**South center**	**West**
Electrolyzer (MW)	0	500	500	0	500	0	0	500
Tank (T)	0	117	33	0	28	0	9.8	18
Fuel cell (MW)	0	219	22	105	2.5	0	237	0

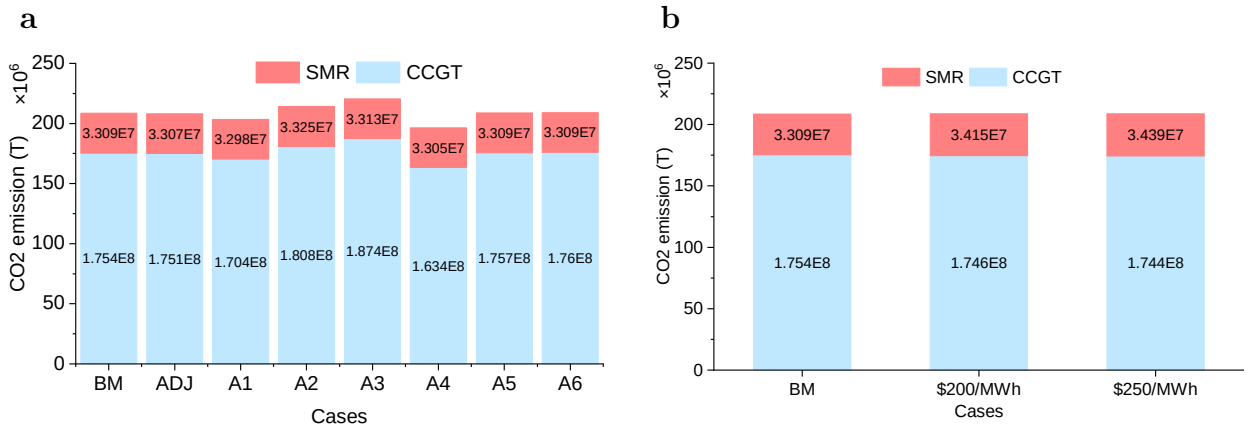


Figure 4.8: Results of Sensitivity Analysis on Carbon Emissions. **a**, Through demand-side load regulation, renewable energy utilization becomes significantly more efficient, leading to notable reductions in carbon emissions from both SMR and CCGT. Completion rates and electricity demand directly impact these emissions, with low completion rates and high demand increasing emissions from both sources. Reduced battery installation completion lowers renewable energy flexibility, decreasing utilization rates and raising CCGT emissions, while SMR emissions remain unaffected. **b**, Higher CCGT tariffs lead to increased conversion of green hydrogen to electricity, lowering overall electricity use efficiency. This shift raises carbon emissions from SMR and the overall system, despite a reduction in emissions from CCGT.

To better understand the impact of CCUS costs on the overall system performance, we conducted a sensitivity analysis by varying carbon pricing. In Scenarios 1 and 2, the cost of CCUS was increased to $100 and $150 per ton across the entire system, respectively. In Scenarios 3 and 4, we raised the CCUS cost to $150 per ton for either SMR or CCGT individually, while maintaining the cost at $5 per ton for the other, to assess the impact on system configuration (Table 4.9).

Table 4.9: Sensitivity analysis scenarios for CO2 emission abatement analysis

Scenarios	**Description**
C1	$100 Carbon capture and storage costs
C2	$150 Carbon capture and storage costs
C3	$50 Power, $150 SMR
C4	$150 Power, $50 SMR

In the first three scenarios, the higher CCUS cost for SMR prompted the system to install a 500 MW electrolyzer in the Far West region, reducing overall reliance on gray hydrogen and thus lowering total carbon emissions. However, in Scenario C4, where only the CCUS

cost for CCGT was increased (assumed the CCUS cost is higher than that for SMR), total carbon emissions rose. This was primarily due to the increased cost of CCUS for CCGT, making the system less efficient in managing emissions. Additionally, as shown in Table 4.8, a large number of hydrogen fuel cells were installed (586 MW), leading to more green hydrogen being converted to electricity to meet system demand. This shift forced the system to rely more heavily on gray hydrogen to satisfy hydrogen demand. As previously discussed, the inefficiency of the hydrogen-to-electricity cycle resulted in significant energy losses, further contributing to an overall increase in carbon emissions. This highlights the trade-offs between system configuration, energy efficiency, and emission outcomes as CCUS costs fluctuate.

4.3 Summary

This study underscores hydrogen's pivotal role in enhancing renewable energy integration and driving decarbonization within Texas's energy system. Through comprehensive modeling and analysis, we demonstrate that hydrogen, when integrated with renewable sources such as wind and solar, serves not only as a crucial energy storage medium but also as a versatile fuel that can address the intermittency of renewable generation. By strategically placing electrolyzers in high-renewable, low-demand regions, hydrogen can contribute significantly to grid stability and flexibility. Moreover, the development of a hydrogen transportation network enables efficient energy distribution across regions, meeting up to 92.4% of hydrogen demand in certain areas and reducing the need for fossil fuel-based generation.

Despite these promising results, several limitations must be acknowledged. The scenarios modeled, while extensive, contain inherent uncertainties, particularly related to the completion rates of planned renewable installations and the actual behavior of the market in future decades. These uncertainties, while managed through careful assumption-setting, suggest that our findings should be interpreted as directional insights rather than precise forecasts. At the same time, this study does not explicitly model future changes in renewable energy costs, such as increased land costs due to siting challenges or cost reductions from technological advancements. Instead, these factors are indirectly reflected in the planned installed capacity completion rate, assuming that cost dynamics will influence project implementation in a market-driven economy. This study specifically focuses on hydrogen transportation via pipelines, given its relevance to large-scale and long-term deployment within the Texas energy system. Other potential transportation methods, such as road transport (e.g., tube trailers) and rail, were not included in the current model to maintain a clear focus on the primary objective of addressing electricity supply-demand uncertainty and optimizing the role of

hydrogen in this context. However, we acknowledge that these alternative transport methods could significantly influence the economic and operational performance of the system. Future research will aim to incorporate these modes of transportation, along with additional storage options such as salt caverns, to develop a more comprehensive and integrated hydrogen energy system model. Furthermore, while we accounted for the costs of CCUS in our carbon emissions analysis, we did not fully address the installation and capacity constraints of CCUS infrastructure. This represents another area for future investigation to ensure the feasibility of large-scale CCUS deployment. Given the focus and scope of this study, we have conducted our analysis of carbon emission reduction results at the level of the entire ERCOT system, rather than delving into the detailed emissions across the full lifecycle of the system. While this approach aligns with the primary objectives of our research, we recognize the importance of a more granular and comprehensive evaluation. In future studies, particularly when examining the environmental and social value of hydrogen, we plan to conduct a more thorough and detailed analysis of carbon emission reductions, encompassing lifecycle considerations to provide a holistic perspective. As previously mentioned, this study does not incorporate the uncertainty of future hydrogen demand into the stochastic optimization model. This decision was made after carefully considering the limitations in the accuracy of available hydrogen demand data, the primary focus of this paper, and the challenges posed by computational complexity. However, we recognize the importance of addressing this uncertainty to enhance the comprehensiveness of our analysis. In future studies, we plan to integrate hydrogen demand uncertainty into our models to develop a more unified and holistic energy system framework.

Our sensitivity analyses reveal that reductions in hydrogen equipment costs alone are insufficient to drastically reshape the energy system. However, rising electricity prices from gas-fired plants do have a substantial impact on the system's configuration, emphasizing the need for policy-driven investments in hydrogen infrastructure and technological advancements. Policy support will be critical in fostering the growth of hydrogen and renewable energy, particularly in building regional hydrogen hubs and advancing CCUS technologies. These elements are essential for aligning Texas's energy system with its long-term decarbonization goals and national climate objectives.

In conclusion, hydrogen is positioned as a vital component in Texas's future energy landscape. Its dual role as an energy storage medium and a clean fuel allows it to effectively balance the variability of renewable generation, while its versatility extends to decarbonizing hard-to-electrify sectors such as heavy industry and transportation. Although uncertainties remain regarding the completion of renewable energy projects and the deployment of hydrogen

infrastructure, the potential benefits of hydrogen integration are clear. With continued policy support, investments in hydrogen infrastructure, and advancements in CCUS technologies, Texas has the opportunity to achieve a more resilient, flexible, and low-carbon energy system. Hydrogen stands as a key enabler of this transition, helping the state meet its renewable energy and carbon reduction targets, ensuring a sustainable energy future.

CHAPTER 5

TECHNO-ECONOMIC ANALYSIS OF HYDROGEN STORAGE WITH NUCLEAR ENERGY FOR GRID ANCILLARY SERVICES

Nuclear power, as a high–energy-density and highly reliable energy source, has historically played a vital role in providing firm baseload electricity and enhancing energy security [49, 130, 33]. Expanding its share can therefore contribute substantially to the stability and resilience of national energy systems [55, 20]. Although past concerns over the economic viability of existing nuclear plants in competitive markets have eased in recent years, the rapid transition toward high-penetration renewable energy systems continues to reshape operational requirements for nuclear generation—particularly the need to provide greater flexibility while maintaining cost competitiveness [115, 110, 147].

In today's U.S. power markets, new large nuclear units face steep overnight capital costs ($6,000–$12,000/kW) and long development timelines, even as electricity systems become more dynamic and price-volatile [77, 6, 62, 120]. At the same time, demand for firm, 24/7 supply is rising—driven in part by data-center growth—leading to higher regional load forecasts and renewed interest in long-term procurement of dependable capacity by utilities and large offtakers [145, 114, 25]. These countervailing forces mean that conventional baseload operation remains economically viable in many contexts—especially with policy support for the existing fleet—but also that there is growing opportunity for nuclear to augment its role through flexible configurations that can capture additional market and system value where merchant exposure is material [64, 59].

While the development of next-generation nuclear technologies continues, there is significant—yet underexplored—potential for retrofitting existing reactors [127]. Nevertheless, the economic and technical feasibility of such retrofits remains uncertain and highly context-dependent [110, 89]. A systematic evaluation of the economic viability, operational flexibility, and integration potential of nuclear plants—underpinned by policy support, technology readiness, and electricity market conditions—is urgently needed to inform the future role of nuclear power in the evolving energy landscape [150, 72, 77] (Fig. 5.1**a, b**).

As the role of nuclear power undergoes global reconfiguration, national contexts exhibit diverging trajectories and challenges [152, 19]. In the United States (U.S.)—home to the world's largest installed nuclear capacity—nuclear power is at a critical inflection point, facing pronounced concerns over cost competitiveness and system flexibility [68, 153]. The U.S. fleet currently comprises 93 operating reactors, contributing approximately 18% of national

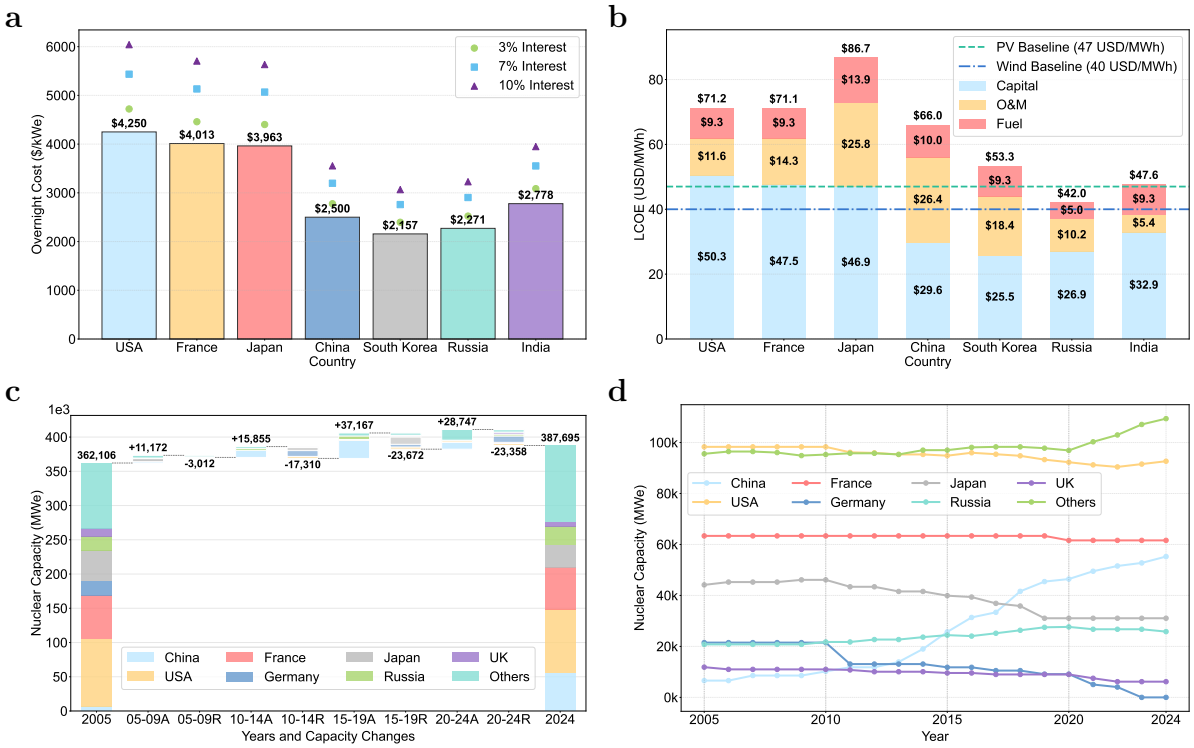


Figure 5.1: Installed capacity and costs of commercial nuclear power across countries. **a**, Overnight capital costs of nuclear construction in major countries. Most countries report values exceeding $2,000/kW, with the U.S. surpassing $4,000/kW [77, 69, 105]. **b**, Comparison of nuclear LCOE with other sources. In most countries, nuclear LCOE exceeds that of solar Photovoltaic (PV) ($47/MWh) and onshore wind ($40/MWh). In the U.S., initial capital expenditures account for over 50% of the total LCOE, highlighting investment cost as a dominant driver [152, 103]. **c**, Changes in global nuclear capacity over the past 20 years, reported in five-year intervals (A: added; R: retired). While total installed capacity has slightly increased, most traditional nuclear countries show declining trends [49, 67, 154]. **d**, Country-level nuclear capacity trends. Over the past two decades, nuclear additions have primarily occurred in China and other emerging markets, whereas traditional nuclear countries—led by the U.S.—have seen substantial retirements. Germany has fully phased out its nuclear fleet [67, 154, 49].

electricity generation[36, 99, 141]. Yet, the increasing penetration of subsidized renewable generation—despite its variable availability—has exerted significant downward pressure on electricity prices, rendering traditional baseload nuclear operations economically unsustainable [6]. Over the past decade, more than a dozen nuclear units have been prematurely retired, and new construction has stalled: aside from the recent connection of Vogtle Units 3 and 4 in Georgia, no new commercial nuclear units have come online in the last 15 years [143, 144]. Furthermore, limited ramping capability constrains the role of existing nuclear plants in systems with high shares of variable renewables. In this context, integrating hydrogen production technologies—such as L/HTE—into existing nuclear plants has emerged as a promising approach [12]. This strategy not only allows nuclear units to operate more flexibly by shifting output toward hydrogen production during low-price or low-demand periods, but also creates new revenue streams from hydrogen sales for industrial and transport applications, while enabling cross-sectoral solutions to energy adequacy challenges. Several pilot projects supported by the U.S. Department of Energy—including Nine Mile Point, Palo Verde, and Davis-Besse—have explored the coupled nuclear–hydrogen pathway, reflecting policy and industry interest at the time [142, 76, 104]. Concurrently, the U.S. government has announced ambitious expansion targets: an additional 35 GW of nuclear capacity by 2035 and 200 GW or more by 2050 [136]. Achieving these targets will require not only the deployment of advanced and small modular reactors, but also the lifetime extension, retrofit, and integration of existing plants with emerging technologies [88, 146]. A robust, techno-economic assessment of nuclear–hydrogen hybrid systems—accounting for market structures, policy incentives, and regional resource conditions—is therefore essential to determine their feasibility, cost-effectiveness, and deployment value (Fig. 5.1**c, d**).

To address these challenges, this study presents a system-level techno-economic assessment of integrating electrolysis-based hydrogen production into existing U.S. nuclear power plants [102]. This approach aims to evaluate the potential of nuclear–hydrogen hybrid systems to enhance operational flexibility and expand revenue opportunities. Focusing on the seven major U.S. ISOs — which feature heterogeneous electricity price structures and ancillary service market designs—the analysis quantifies how regional market mechanisms affect the economic performance of nuclear–hydrogen systems [17, 39, 96, 100, 71, 129, 113]. The dispatch model incorporates key operational constraints including ramping limits, start-up costs, variable efficiency, and part-load performance [9, 72]. Hourly simulations are used to characterize power allocation between electricity sales, hydrogen production, and grid service provision. The analysis compares the financial outcomes of baseline (business-as-usual) operations against retrofit and new-build hybrid configurations, evaluating differences

across 60- and 80-year plant lifetimes [50]. Results include the breakdown of revenue sources (electricity, hydrogen, ancillary services), estimates of levelized costs (energy and hydrogen), and the cost composition of hydrogen production. In addition, the study explores how policy incentives—such as investment and production tax credits—affect system profitability and deployment feasibility across diverse market contexts, providing quantitative decision support for regional nuclear–hydrogen integration strategies (Fig. 5.2).

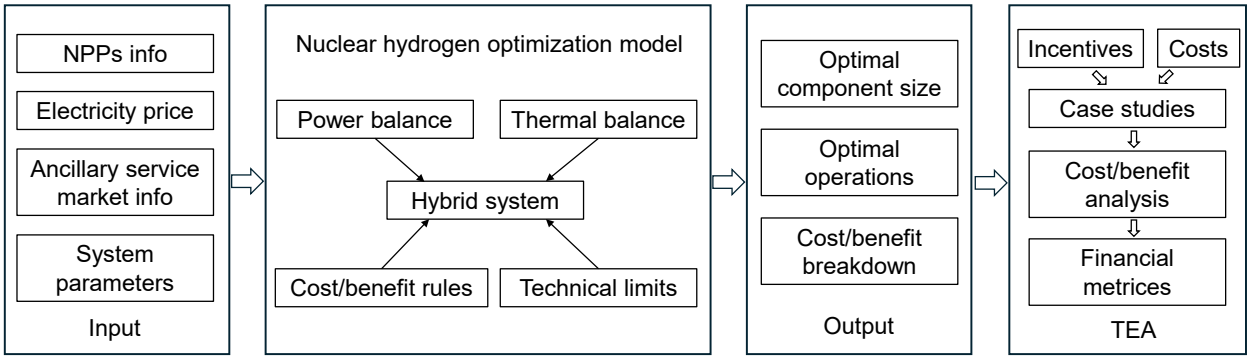


Figure 5.2: Modeling framework for the nuclear-hydrogen energy system optimization. TEA framework consists of two main components. The first is an optimization model for the nuclear–hydrogen system, which incorporates system characteristics, electricity and ancillary service market data, and operational constraints to determine the optimal configuration and dispatch strategy. The second component uses the optimization outputs, policy incentives, and cost parameters to evaluate the system's techno-economic performance and compute key financial metrics, including net present value (NPV).

5.1 Nuclear-Hydrogen Ancillary Service Optimization Model

5.1.1 Optimization Model Formulation

This section details the mathematical formulation of the techno-economic optimization model for an IES. The model is formulated as a MILP to maximize the annual profit of the system by co-optimizing its participation in various energy and ancillary service markets. The core of the model consists of an objective function to be maximized, subject to a series of physical, operational, and economic constraints that govern the behavior of the system components. These components include an NPP, a water electrolyzer for hydrogen production, a battery energy storage system (BESS), and hydrogen storage.

Objective Function

The objective of the model is to maximize the total profit (Π) over the optimization horizon. The profit is the sum of all revenues minus the sum of all operational and annualized capital costs.

$$\text{Maximize} \quad \Pi = (R^{E} + R^{H_2} + R^{AS}) - (C^{OPEX} + C^{CAPEX}) \tag{5.1}$$

Revenue Components

Revenue from selling electricity to the grid minus the cost of purchasing electricity from the grid.

$$R^{E} = \sum_{t \in T} \Delta t \cdot \lambda_t^{E} \cdot (p_t^{sale} - p_t^{buy}) \tag{5.2}$$

Revenue from selling hydrogen, including any production subsidies. This revenue is based on sales from storage, while subsidies are based on total production.

$$R^{H_2} = \sum_{t \in T} \Delta t \cdot \Big((\dot{m}_t^{stor,out} + \dot{m}_t^{H_2,market}) \cdot \lambda^{H_2} + \dot{m}_t^{H_2} \cdot \lambda^{H_2,sub} \Big) \tag{5.3}$$

Revenue from participating in ancillary service markets. This includes payments for capacity reservation, and energy/performance payments upon deployment. The formulation varies by market. For a generic reserve service s:

$$R_s^{AS} = \sum_{t \in T} \Delta t \cdot \Big(b_{t,s} \cdot w_{t,s} \cdot \lambda_{t,s}^{AS,cap} + \text{Energy Payment}_s \Big) \tag{5.4}$$

Where the energy payment $\text{Energy Payment}_s = b_{t,s} \cdot w_{t,s} \cdot \delta_{t,s} \cdot \lambda_t^{E}$.

Cost Components

The sum of all variable operational costs.

$$\begin{aligned} C^{OPEX} = \sum_{t \in T} \Delta t \cdot (& C^{turb,vom} \cdot p_t^{turb} + C^{elec,vom} \cdot p_t^{elec} + C^{H_2O} \cdot \dot{m}_t^{H_2} \\ & + C^{b,vom} \cdot \frac{p_t^{b,ch} + p_t^{b,dis}}{2} + C^{stor,vom} \cdot (\dot{m}_t^{stor,in} + \dot{m}_t^{stor,out})) \\ & + \sum_{t \in T} C^{elec,su} \cdot v_t^{elec} \end{aligned} \tag{5.5}$$

The annualized capital cost of all dynamically sized components, scaled to the simulation period.

$$\begin{aligned} C^{CAPEX} = \frac{|T| \cdot \Delta t}{8760} \big(& C^{elec,capex} P_{max}^{elec} + C^{b,capex,E} E_{max}^{b} \\ & + C^{b,capex,P} P_{max}^{b} + C^{stor,capex} M_{max}^{stor} \big) \end{aligned} \tag{5.6}$$

Constraints

System-Level Constraints

Power Balance: The net power generated by the IES must equal the net power exchanged with the grid.

$$p_t^{turb} + p_t^{b,dis} - p_t^{elec} - p_t^{b,ch} = p_t^{IES} \quad \forall t \in T \tag{5.7}$$

$$p_t^{IES} = p_t^{sale} - p_t^{buy} \quad \forall t \in T \tag{5.8}$$

Steam Balance: The total steam produced by the reactor must be consumed by the turbine and the HTE.

$$q_t^{turb} + q_t^{elec} = Q^{steam,total} \quad \forall t \in T \tag{5.9}$$

Nuclear Turbine Constraints

Operating Limits: Turbine power output is constrained by its operational limits.

$$P_{min}^{turb} \leq p_t^{turb} \leq P_{max}^{turb} \quad \forall t \in T \tag{5.10}$$

Ramp Rates: The change in turbine power output between consecutive time periods is limited.

$$p_t^{turb} - p_{t-1}^{turb} \leq R_{max}^{turb,up} \cdot \Delta t \quad \forall t \in T, t > 1 \tag{5.11}$$

$$p_{t-1}^{turb} - p_t^{turb} \leq R_{max}^{turb,down} \cdot \Delta t \quad \forall t \in T, t > 1 \tag{5.12}$$

Piecewise Efficiency: Turbine power output (p_t^{turb}) is a piecewise linear function of its steam consumption (q_t^{turb}).

$$q_t^{turb} = \sum_{k \in K_{turb}} \lambda_{t,k} \cdot Q_k^{turb,bp} \quad \forall t \in T \tag{5.13}$$

$$p_t^{turb} = \sum_{k \in K_{turb}} \lambda_{t,k} \cdot P_k^{turb,bp} \quad \forall t \in T \tag{5.14}$$

$$\sum_{k \in K_{turb}} \lambda_{t,k} = 1 \quad \forall t \in T \tag{5.15}$$

$$\{\lambda_{t,k}\}_{k \in K_{turb}} \text{ is an SOS2 set} \quad \forall t \in T \tag{5.16}$$

Electrolyzer Constraints

Operating Limits: Electrolyzer power consumption is constrained. If startup/shutdown logic is enabled, these limits are gated by the binary status variable u_t^{elec}.

$$p_t^{elec} \geq P_{min}^{elec,on} \cdot u_t^{elec} \quad \forall t \in T \tag{5.17}$$

$$p_t^{elec} \leq P_{max}^{elec} \cdot u_t^{elec} \quad \forall t \in T \tag{5.18}$$

Ramp Rates: The change in electrolyzer power consumption is limited.

$$p_t^{elec} - p_{t-1}^{elec} \leq P_{max}^{elec} \cdot R_{max}^{elec,up} \cdot \Delta t \quad \forall t \in T, t > 1 \tag{5.19}$$

$$p_{t-1}^{elec} - p_t^{elec} \leq P_{max}^{elec} \cdot R_{max}^{elec,down} \cdot \Delta t \quad \forall t \in T, t > 1 \tag{5.20}$$

Piecewise Efficiency (Hydrogen Production): Hydrogen production rate ($\dot{m}_t^{H_2}$) is a piecewise linear function of electrolyzer power consumption (p_t^{elec}).

$$p_t^{elec} = \sum_{j \in K_{elec}} \lambda_{t,j} \cdot P_j^{elec,bp} \quad \forall t \in T \tag{5.21}$$

$$\dot{m}_t^{H_2} = \sum_{j \in K_{elec}} \lambda_{t,j} \cdot \dot{M}_j^{H_2,bp} \quad \forall t \in T \tag{5.22}$$

$$\sum_{j \in K_{elec}} \lambda_{t,j} = 1 \quad \forall t \in T \tag{5.23}$$

$$\{\lambda_{t,j}\}_{j \in K_{elec}} \text{ is an SOS2 set} \quad \forall t \in T \tag{5.24}$$

A similar piecewise formulation links steam consumption (q_t^{elec}) to power (p_t^{elec}) for the HTE.

Startup/Shutdown Logic: These constraints manage the on/off state of the electrolyzer and enforce minimum uptime and downtime.

$$u_t^{elec} - u_{t-1}^{elec} = v_t^{elec} - w_t^{elec} \quad \forall t \in T, t > 1 \tag{5.25}$$

$$v_t^{elec} + w_t^{elec} \leq 1 \quad \forall t \in T \tag{5.26}$$

$$\sum_{i=t-T_{min}^{elec,up}+1}^{t} u_i^{elec} \geq T_{min}^{elec,up} \cdot v_t^{elec} \quad \forall t \geq T_{min}^{elec,up} \tag{5.27}$$

$$\sum_{i=t-T_{min}^{elec,down}+1}^{t} (1 - u_i^{elec}) \geq T_{min}^{elec,down} \cdot w_t^{elec} \quad \forall t \geq T_{min}^{elec,down} \tag{5.28}$$

Degradation Tracking: Tracks the cumulative degradation of the electrolyzer.

$$d_t = d_{t-1} + (D_{op} \cdot \frac{p_t^{elec}}{P_{max}^{elec}} \cdot \Delta t) + (D_{su} \cdot v_t^{elec}) \quad \forall t \in T, t > 1 \tag{5.29}$$

Battery Storage Constraints

State of Charge Balance: The battery's state of charge is tracked over time, accounting for charge/discharge efficiencies.

$$e_t^b = e_{t-1}^b + \Delta t \cdot (\eta^{b,ch} p_t^{b,ch} - \frac{p_t^{b,dis}}{\eta^{b,dis}}) \quad \forall t \in T, t > 1 \tag{5.30}$$

The equation is adjusted for $t = 1$ to use the initial state of charge E_{init}^b.

Operating and Sizing Limits:

$$p_t^{b,ch} \leq P_{max}^b \cdot u_t^{b,ch} \quad \forall t \in T \tag{5.31}$$

$$p_t^{b,dis} \leq P_{max}^b \cdot u_t^{b,dis} \quad \forall t \in T \tag{5.32}$$

$$u_t^{b,ch} + u_t^{b,dis} \leq 1 \quad \forall t \in T \tag{5.33}$$

$$E_{max}^b \cdot SOC_{min} \leq e_t^b \leq E_{max}^b \quad \forall t \in T \tag{5.34}$$

$$P_{max}^b = E_{max}^b \cdot \text{PowerRatio} \quad \text{(If sizing)} \tag{5.35}$$

Hydrogen Storage Constraints

Storage Balance: The mass of hydrogen in storage is tracked over time.

$$m_t^{stor} = m_{t-1}^{stor} + \Delta t \cdot (\eta^{stor,ch} \dot{m}_t^{stor,in} - \frac{\dot{m}_t^{stor,out}}{\eta^{stor,dis}}) \quad \forall t \in T, t > 1 \tag{5.36}$$

Production and Sales Dispatch: Hydrogen produced can be sent to storage or directly to the market.

$$\dot{m}_t^{H_2} = \dot{m}_t^{H_2,market} + \dot{m}_t^{stor,in} \quad \forall t \in T \tag{5.37}$$

Operating and Sizing Limits:

$$M_{min}^{stor} \leq m_t^{stor} \leq M_{max}^{stor} \quad \forall t \in T \tag{5.38}$$

$$\dot{m}_t^{stor,in} \leq \dot{M}_{max}^{stor,ch} \quad \forall t \in T \tag{5.39}$$

$$\dot{m}_t^{stor,out} \leq \dot{M}_{max}^{stor,dis} \quad \forall t \in T \tag{5.40}$$

When optimal H2 storage sizing is enabled, a constant sales rate is enforced ($\dot{m}_t^{stor,out} = \dot{m}_{const}^{H_2,sale}$) and production is forced through storage ($\dot{m}_t^{H_2,market} = 0$).

Ancillary Service Constraints

Component Capability: The bids for ancillary services from each component are limited by the component's physical headroom and ramp rates. For upward reserve from the turbine:

$$p_t^{turb} + \sum_{s \in S_{up}} b_{t,s}^{turb} \leq P_{max}^{turb} \quad \forall t \in T \tag{5.41}$$

For downward reserve from the electrolyzer (load increase):

$$p_t^{elec,sp} + \sum_{s \in S_{down}} b_{t,s}^{elec} \leq P_{max}^{elec} \cdot u_t^{elec} \quad \forall t \in T \tag{5.42}$$

Similar constraints exist for all services on all components, including ramp rates and battery state of charge.

Bid Aggregation: The total bid for each service is the sum of bids from all participating components.

$$b_{t,s} = \sum_{c \in C} b_{t,s}^c \quad \forall t \in T, s \in S \tag{5.43}$$

Regulation Balance: For certain markets, regulation up and down bids must be equal for each component.

$$b_{t,\text{RegUp}}^c = b_{t,\text{RegDown}}^c \quad \forall t \in T, c \in C \tag{5.44}$$

Dispatch Execution Mode Constraints

Deployed: In this mode, the deployed amount of an ancillary service is linked to the winning bid.

$$d_{t,s}^c = b_{t,s}^c \cdot w_{t,s} \cdot \delta_{t,s} \quad \forall t \in T, s \in S, c \in C \tag{5.45}$$

Actual Power Adjustment: The actual power of a component is adjusted based on its setpoint and the amount of ancillary service it deploys. For the electrolyzer:

$$p_t^{elec} = p_t^{elec,sp} - \sum_{s \in S_{up}} d_{t,s}^{elec} + \sum_{s \in S_{down}} d_{t,s}^{elec} \quad \forall t \in T \tag{5.46}$$

5.1.2 Techno-Economic Analysis Framework

This section details the methodology of the TEA framework developed to evaluate the financial viability of nuclear-hydrogen integrated energy systems. The framework is designed to be comprehensive, incorporating detailed cost models, operational simulations, and the impact of federal tax incentives. It analyzes various scenarios, from retrofitting existing NPPs to developing new greenfield projects with different operational lifetimes. The core of the framework is a discounted cash flow (DCF) analysis, which is used to calculate key financial performance indicators.

Core Financial Principles and Metrics

The primary financial evaluation is based on a DCF analysis over the project's entire lifecycle, from construction to decommissioning. The fundamental metric is the NPV, which represents the total value of the project in today's currency. The NPV is calculated as the sum of all discounted future cash flows:

$$\text{NPV} = \sum_{t=0}^{N} \frac{CF_t}{(1+r)^t} \tag{5.47}$$

where CF_t is the net cash flow in year t, r is the discount rate, and N is the total project lifetime in years.

The annual net cash flow (CF_t) for each operational year is determined by accounting for all revenues, operating expenditures (OPEX), and the tax implications of depreciation. The after-tax cash flow is calculated as:

$$CF_t = (R_t - C_{\text{OPEX},t} - D_t)(1-\tau) + D_t \tag{5.48}$$

where R_t is the total annual revenue, $C_{\text{OPEX},t}$ is the total annual operating expenditure, D_t is the annual depreciation allowance, and τ is the corporate tax rate. The term $D_t \cdot \tau$ represents the "tax shield" provided by depreciation, which is a non-cash expense that reduces the project's tax burden. Other key financial indicators derived from the cash flow analysis include:

- *Internal Rate of Return (IRR):* The discount rate at which the NPV of the project becomes zero. A project is considered financially attractive if its IRR exceeds the minimum acceptable rate of return or the cost of capital.
- *Payback Period:* The time required for the cumulative cash flows from a project to equal the initial investment. This metric provides insight into the project's risk and liquidity.
- *Levelized Costs:* The average net present cost of a technology per unit of output over its lifetime. The framework calculates the LCOH, LCOE and LCOS using a detailed, independent accounting methodology, as described in a later section.

CAPEX Modeling

The framework employs a detailed, component-based model for capital expenditures. The total CAPEX is disaggregated into major systems, including the nuclear island, turbine

generator, hydrogen production system (electrolyzer, storage), and battery storage system. For greenfield projects, this also includes site preparation and grid connection costs. This granular approach allows for the application of technology-specific cost-scaling and learning rates. The cost of a component is scaled from a reference size using a learning rate to account for economies of scale, calculated as:

$$C_{\text{adj}} = C_{\text{ref}} \left(\frac{S_{\text{actual}}}{S_{\text{ref}}} \right)^{\alpha} \tag{5.49}$$

where C_{adj} is the adjusted cost for the component, C_{ref} is the base cost for a reference size S_{ref}, S_{actual} is the actual capacity of the component, and α is the scaling exponent, derived from a specified learning rate. Capital investments are distributed over the construction period according to predefined payment schedules for each major component.

Major component replacements are modeled as capital outflows in the specific years they are scheduled to occur. The framework uses a detailed replacement schedule, for instance [103]: *Electrolyzer Stacks* are replaced every 10 years; *Battery Systems* are replaced every 10 years; *Major Hydrogen Storage Components* are replaced every 15 years.

Operating Expenditure (OPEX) Modeling

Annual operating costs are modeled with a similar level of detail. OPEX is separated into fixed and variable components.

- *Fixed OPEX:* Includes costs that do not vary with production, such as salaries, insurance, and routine maintenance. These are calculated on a per-megawatt-year basis (e.g., $/MW-year) and are subject to an annual inflation rate.

- *Variable OPEX (VOM):* Includes costs directly tied to system operation, such as consumables, water for electrolysis, and component wear. These are calculated on a per-megawatt-hour ($/MWh) or per-kilogram ($/kg) basis.

- *Nuclear Fuel Costs:* As a major component of nuclear OPEX, it is calculated per megawatt-hour of electricity generation in the baseline case, whereas for the retrofitted hybrid system, and the calculation is based on the actual energy output of the reactor.

Revenue and Opportunity Cost Modeling

The framework considers multiple revenue streams, including electricity sales to the grid, hydrogen sales, and ancillary services, with a particular emphasis on modeling opportunity costs. When the nuclear plant diverts electricity or heat to hydrogen production, it forgoes potential revenue from electricity sales to the grid, which is explicitly treated as an opportunity cost in assessing hydrogen production profitability. Similarly, providing ancillary services may require the plant or electrolyzer to operate at suboptimal levels for energy sales, and the resulting opportunity cost is also accounted for. In the case of HTE, the diversion of steam from the turbine reduces potential electricity generation, and the corresponding opportunity cost is quantified based on the plant's thermal efficiency and prevailing electricity prices.

Depreciation and Taxation

The framework implements the MACRS for asset depreciation, which provides a significant tax shield [63]. Assets are classified into different schedules based on their type, reflecting U.S. tax law:

- *15-Year MACRS:* Applied to NPP equipment and grid infrastructure.
- *7-Year MACRS:* Applied to hydrogen production and battery storage equipment.

The annual depreciation for each class is calculated according to the schedules provided in Table 5.1. The total depreciation allowance in any given year is the sum of the depreciation from all assets, which is then used to calculate the project's tax liability.

Table 5.1: MACRS depreciation schedules

7-Year Property		**15-Year Property**	
Year	Rate (%)	Year	Rate (%)
1	14.29	1	5.00
2	24.49	2	9.50
3	17.49	3	8.55
4	12.49	4	7.70
5	8.93	5	6.93
6	8.92	6	6.23
7	8.93	7-15	5.90
8	4.46	16	2.95

Federal Tax Incentive Analysis

An important feature of the framework is its capability to simulate the effects of several major U.S. federal tax incentives. In this study, particularly for hybrid systems combining nuclear power and hydrogen production, we assume that the system can simultaneously benefit from both hydrogen-related and nuclear-related incentive schemes, with each calculated according to its respective methodology and then aggregated.

- **45U Production Tax Credit (PTC):** This credit is specifically for existing NPPs. For electricity generated between 2024 and 2032, the credit amount is determined dynamically based on the hourly electricity market price, decreasing linearly as the price increases from \$25/MWh to \$43.75/MWh. The hourly credit value (C_{45U}) is computed as a function of the market price (P_{market}) as follows. In this study, a streamlined implementation of the 45U credit adjustment is used to reflect the policy's essential price-responsive structure in a form suitable for integrated system modeling [64]:

$$C_{45U}(P_{\text{market}}) = \begin{cases} \$15 & \text{if } P_{\text{market}} < \$25.0 \\ \$15 \times \left(1 - \frac{P_{\text{market}} - \$25.0}{\$18.75}\right) & \text{if } \$25.0 \leq P_{\text{market}} \leq \$43.75 \\ \$0 & \text{if } P_{\text{market}} > \$43.75 \end{cases} \tag{5.50}$$

- **45Y Clean Electricity Production Tax Credit (PTC):** This credit is for *new* zero-emission power facilities, including new nuclear plants. The framework models this as a credit of up to \$30/MWh for the first 10 years of the plant's operation. This credit is a direct addition to the project's annual cash flow [65].

- **48E Clean Electricity Investment Tax Credit (ITC):** As an alternative to the 45Y PTC for *new* facilities, the ITC provides an upfront tax credit based on the initial capital investment. The model implements a credit of up to 50% on qualified capital expenditures. Crucially, the model correctly applies this credit only to the nuclear power generation equipment, excluding hydrogen and battery assets. Furthermore, it implements the required depreciation basis reduction, where the asset's value for depreciation purposes is reduced by 50% of the claimed ITC value [65]:

$$\text{Depreciable Basis}_{\text{adj}} = \text{CAPEX}_{\text{original}} - 0.5 \times \text{ITC}_{\text{value}} \tag{5.51}$$

  This reduction lowers the total depreciation tax shield over the asset's life, partially offsetting the benefit of the upfront credit.

- **Hydrogen Production Subsidy:** The framework also includes a generic hydrogen production subsidy, modeled after policies like 45V, which provides a direct payment of up to \$3.00/kg of clean hydrogen produced for verified use during the first 10 years of operation. In this study, we assume the maximum rate of \$3.00 per kg applies uniformly across all scenarios. [66].

Case Study Design

The TEA framework is applied across four distinct case studies to provide a holistic view of the economic potential of nuclear-hydrogen systems.

Case 1: Existing Reactor Baseline

This case serves as the financial benchmark. It analyzes the business-as-usual operation of an existing NPP without any modifications for hydrogen production. The analysis uses the plant's actual remaining operational lifetime and calculates revenue based on selling all generated electricity to the grid at hourly market prices. The key objective is to determine the standalone profitability of the existing asset and to analyze the potential financial uplift from the 45U PTC.

Case 2: Existing Reactor Retrofit

This case evaluates the economic viability of retrofitting an existing NPP with an integrated hydrogen production and battery storage system. The analysis includes the CAPEX for the new hydrogen and battery assets but assumes the nuclear plant itself is a sunk cost. It calculates the combined revenue streams from electricity sales, hydrogen sales, and ancillary services. This case also considers the impact of the 45U PTC on the nuclear portion of the integrated system's revenue.

Case 3: Greenfield System (60-Year Lifecycle)

This case examines a newly constructed, fully integrated nuclear-hydrogen-battery system with a 60-year operational lifetime. It includes the complete capital investment for the nuclear reactor and all non-nuclear subsystems. Three distinct policy scenarios are evaluated: (1) no federal incentives, (2) the 45Y PTC, and (3) the 48E ITC. This case evaluates the economics of greenfield nuclear-hydrogen systems over a standard design lifespan, considering current U.S. tax incentives and system cost structure.

Case 4: Greenfield System (80-Year Lifecycle)

Building upon Case 3, this case extends the system's operational lifetime to 80 years to reflect the enhanced durability and lifespan potential of next-generation advanced reactors. The same three policy scenarios—no incentives, 45Y PTC, and 48E ITC—are analyzed to evaluate how extended operation alters the cost-effectiveness and policy impacts. This longer-term perspective captures additional revenue potential, offset by the need for more frequent equipment replacements and increased long-term maintenance costs, offering deeper insight into lifecycle financial dynamics.

Levelized Cost Calculation Methodology

To provide a clear and fair comparison of costs, the framework utilizes an independent accounting methodology for calculating levelized costs. This approach avoids cross-subsidization between different parts of the integrated system.

LCOE

The LCOE represents the cost of generating electricity from the nuclear plant only. It is calculated by considering only the costs and revenues directly attributable to the nuclear power island and turbine generator.

$$\text{LCOE} = \frac{\text{PV}(\text{Nuclear CAPEX} + \text{Nuclear OPEX} - \text{Turbine AS Revenue})}{\text{PV}(\text{Total Electricity Generation})} \tag{5.52}$$

LCOH

The LCOH is calculated for the hydrogen production system. Critically, the cost of electricity consumed by the electrolyzer is not assumed to be zero. It is valued at the LCOE calculated for the nuclear plant, representing a fair internal transfer price.

$$\text{LCOH} = \frac{\text{PV}\begin{pmatrix}\text{CAPEX}_{\text{H}_2} + \text{OPEX}_{\text{H}_2} + \text{Elec. Cost}_{\text{LCOE}} \\ + \text{HTE Cost} - \text{AS Revenue}_{\text{H}_2}\end{pmatrix}}{\text{PV}(\text{Total H}_2\text{ Production})} \tag{5.53}$$

Levelized Cost of Storage (LCOS)

Similarly, the LCOS for the battery system is calculated based on its own CAPEX, OPEX, and dedicated revenue streams, providing a clear picture of the cost per megawatt-hour of

energy discharged from the battery over its lifetime.

$$\text{LCOS} = \frac{\text{PV(Battery CAPEX} + \text{Battery OPEX} - \text{Battery AS Revenue)}}{\text{PV(Total Energy Discharged)}} \tag{5.54}$$

5.1.3 Data Generation and Collection

To facilitate the testing and validation of our nuclear-hydrogen production optimization model, a comprehensive synthetic dataset was generated. This process, implemented in Python, creates internally consistent time-series data and system parameters that mimic real-world operational conditions. The generation process is deterministic, using a fixed random seed (`np.random.seed(42)`) to ensure the replicability of the entire dataset. The generated data encompasses techno-economic system parameters, hourly electricity prices, and detailed ancillary service market data for various ISOs.

5.1.4 System Parameter Formulation

A foundational set of techno-economic parameters is generated to define the physical and economic characteristics of the IES. These parameters are technology-specific and crucial for the optimization model's constraints and objective function.

Common and Plant-Wide Parameters

To support system-level sensitivity analysis, a representative nuclear-hydrogen configuration was established using stylized core plant parameters: a 1000 MW_{th} thermal reactor coupled with a 380 MW steam turbine. This configuration defines the upper bounds for turbine power output ($P_{\text{turbine}}^{\max} = 380.0$ MW) and total available thermal steam ($Q_{\text{steam}}^{\text{total}} = 1000.0$ MW_{th}), and assumes a 30-year project lifetime with a discount rate of $r = 0.06$. The turbine's operational range is characterized by minimum and maximum power and steam input limits, a piecewise linear thermal-electric efficiency curve based on steam flow breakpoints, and ramp rate constraints [77, 11].

However, for the core optimization and techno-economic analysis performed across 42 actual nuclear power plants, all nuclear-related system parameters—such as reactor thermal capacity, turbine power ratings, and conversion efficiency—are based on real plant-specific data. These technical specifications were obtained directly from the U.S. Nuclear Regulatory Commission (NRC) database, ensuring that the modeled system configurations reflect the actual physical and operational characteristics of each reactor [102].

Electrolyzer Technology Parameters

The model incorporates two distinct electrolyzer technologies: an HTE, representative of Solid Oxide Electrolysis Cell (SOEC) technology. A detailed set of parameters is calculated.

Capital Cost

The annualized CAPEX is a critical cost component. It is derived from the overnight cost, the economic lifetime, and the discount rate using the Capital Recovery Factor (CRF). The CRF is calculated as:

$$\text{CRF} = \frac{r(1+r)^L}{(1+r)^L - 1} \tag{5.55}$$

where r is the discount rate and L is the lifetime in years.

Efficiency and Consumption

Electrolyzer efficiency is modeled as a piecewise linear function dependent on the electrical load. Four operating breakpoints are defined, starting from a minimum load of 10% of the maximum capacity (200 MW).

- *Electrical Consumption (k_e):* For HTE, from 44.0 to 41.0 kWh/kg, reflecting its higher efficiency at operating temperatures. These are converted to MWh/kg for the model [151].
- *Thermal Consumption (k_t):* HTE requires thermal energy input, which is modeled as a constant 0.008 MW_{th} per kg/hr of hydrogen produced across all operating points [151].

Operational Parameters

Other key parameters include variable O&M costs ($6.9/MWh for HTE), startup costs, ramp rates (as a percentage of maximum capacity per minute), and minimum up/down times. Degradation is also modeled, with distinct factors for steady operation and for each startup event [151].

BESS Parameters

A BESS is included as an optional system component. Its parameters are derived to reflect current technology costs and performance.

- *Capital Cost:* BESS costs are defined for both power and energy capacity. A total energy capital cost of $2.1M/MW and a 4-hour duration are assumed. The annualized power capacity cost is calculated using a 20-year lifetime and the CRF. The model is specifically configured to only consider the power capacity cost, setting the energy capacity cost to zero to analyze scenarios where power is the primary cost driver [103].

- *O&M Cost:* A fixed O&M cost is derived as a fraction of the power CAPEX (2.5%).

- *Performance:* Key performance metrics include charge/discharge efficiency (both 92%), a minimum state of charge of 10%, and a power-to-energy ratio (P/E) of 0.25, corresponding to the 4-hour duration [103].

5.1.5 Time-Series Data Generation Collection

Hourly data for a full year (8,760 hours) is generated to simulate market conditions. This includes ancillary services and operational factors. All electricity price inputs used in the model are based on the average 2024 locational marginal prices (LMPs) at hub or node level, published by each ISO at 15-minute resolution and aggregated to hourly values. Ancillary service price data were similarly obtained from each ISO's 2024 hourly publications. February 29th was excluded to ensure consistency with a 365-day calendar year, and missing values were linearly interpolated to obtain a complete dataset of 8,760 hourly entries [17, 39, 96, 100, 71, 129, 113].

Ancillary Service (AS) Market Data

AS Capacity Prices

The market clearing price for each ancillary service is generated based on the hourly LMP, assuming that AS prices are correlated with energy prices. The price is calculated as:

$$\text{Price}_{\text{AS}} = \max(0, \text{LMP} \times U(0.05, 0.4) + N(0, 3) + \text{Spike})$$

where U is a uniform distribution, N is a normal distribution for noise, and 'Spike' represents a 2% hourly probability of a price adder between $10 and $50. This creates AS prices that are fundamentally linked to energy scarcity but have their own distinct volatility.

Deployment, Mileage and Performance Factors

Due to the lack of publicly available high-resolution deployment records for ancillary services, all deployment-related inputs in this study were generated synthetically through a simulation-based framework. The generation process was informed by publicly available ISO documents, historical system operation data, and operational heuristics reported in prior literature [4, 139, 23, 16, 10, 131].

For regulation services (e.g., RegUp/RegDown), where deployment frequency and directionality are critical but rarely disclosed, a paired simulation strategy was adopted. Hourly deployment probabilities were constructed using smoothed stochastic time series, incorporating both intra-day (three cycles per day) and weekly seasonalities. These patterns were calibrated to yield an average directional deployment bias of 0.44 in favor of regulation-up, consistent with empirical expectations of net upward control effort. To ensure system feasibility, the combined hourly deployment activity for regulation-up and regulation-down was constrained below 0.98, and post-processing adjustments were made to preserve both the directional bias and total activation limits.

For non-regulation reserve services (e.g., spinning, non-spinning, supplemental, and ramping reserves), deployment factors were similarly generated using category-specific probability and magnitude ranges. These ranges were derived from ISO-published simulation assumptions, such as those used in planning reserve margin studies or operational flexibility assessments. For each service, hourly deployment was determined by sampling a Bernoulli process governed by its probability envelope, with activated magnitudes drawn from uniform distributions within the category-specific operational band. This framework enables the representation of diverse service behaviors while maintaining cross-ISO consistency and interpretability.

Mileage multipliers and performance factors, essential for modeling the operational burden of regulation services, were likewise generated synthetically due to the unavailability of full-year, service-level data from ISOs. All parameterization was based on public ISO reports, simulation templates, and historical estimates.

For each ISO, regulation-up and regulation-down services were jointly modeled using base mileage values extracted from ISO-published simulation data (e.g., PJM's RegD mileage of 5.4, CAISO's 12.5, etc.). To reflect temporal variability and measurement uncertainty, independent Gaussian noise (scaled to 5–10% of the base mileage) was applied, and resulting values were clipped to maintain operational realism. Paired services within the same ISO (e.g., RegUp/RegDown) were assigned consistent mileage profiles to reflect the shared system control dynamics.

Performance factors were generated from a normal distribution centered at 0.95, with truncation at 0.7 and 1.0, reflecting the high but variable fidelity observed in actual Automatic Generation Control (AGC) regulation. Identical hourly performance factors were used for regulation-up and -down in each ISO to capture their joint dependence on telemetry precision, AGC latency, and plant control capabilities.

5.2 Results

5.2.1 Economic Viability and Revenue Diversification of Integrated Nuclear-Hydrogen Systems

We analyzed 42 nuclear reactors from the 93 operating commercial units in the U.S., selecting those with over 10 years of remaining operational lifetime across all seven major ISO regions: ISONE, NYISO, PJM, MISO, SPP, ERCOT, and CAISO [102]. Each unit was modeled with integrated high-temperature electrolysis and optional energy storage, with hourly dispatch optimized under representative market conditions. The resulting operational strategies formed the basis for a discounted cash flow TEA under four scenarios: baseline operation (Case 1), retrofit with hydrogen and storage systems (Case 2), new-build integrated systems (Case 3), and lifecycle/policy comparisons (Case 4). This section examines the economic viability of existing nuclear assets and the incremental value introduced by hydrogen integration.

Conventional nuclear plants, operating as inflexible baseload resources under current electricity market structures, face significant economic headwinds. In Case 1, 41 of the 42 reactors exhibit negative NPVs over their remaining lifetimes, with an average deficit of $1.06 billion. While the 45U production tax credit improves the average NPV by $740 million, more than half of the units remain unprofitable. These findings indicate that federal incentives, though beneficial, do not address the fundamental structural limitations. Without enhanced flexibility or diversified revenue streams, conventional nuclear facilities are unlikely to achieve financial self-sufficiency (Fig. 5.3**a**).

Retrofit configurations with hydrogen systems (Case 2) mark a pivotal economic shift. A majority of units (61.9%) achieve positive NPVs even in the absence of subsidies, with the average NPV rising to $240 million and a mean internal rate of return (IRR) of 10.2%. Twenty-four reactors achieve payback within four years, reflecting both commercial viability and investment stability. Post-retrofit, average annual revenues reach $510 million, with contributions from hydrogen sales and ancillary service markets. Ancillary service revenues, averaging $12.3 million annually (approximately 2.4% of total revenue), demonstrate how

flexible dispatch enables nuclear plants to capture value during periods of low wholesale energy prices. These results underscore that hydrogen-enabled flexibility enhances asset utilization while establishing a compounding value mechanism anchored in market-responsive operations (Fig. 5.3**b**).

Federal incentives further enhance financial viability across scenarios. In Case 2, the 45U credit, in addition to increasing the average NPV by $740 million, further reduces payback periods to under two years and substantially improves project bankability. In new-build cases (Case 3 and 4), 45Y and 48E reduce the LCOH from $22.2/kg to $16.0/kg, narrowing financial gaps even as NPVs remain negative. Extending system lifetimes from 60 to 80 years reduces the LCOH by approximately $0.15/kg but further decreases the NPV by around $85 million for newly built nuclear–hydrogen systems. While the reduction in LCOH reflects improved capital cost amortization, the extended operational horizon increases cumulative long-term O&M expenses, resulting in more negative NPVs under current cost structures (Fig. 5.3**c**).

Significant economic heterogeneity is observed across ISO regions, influenced by electricity price dynamics, ancillary service market design, and dispatch opportunities. ISO-NE and CAISO units achieve the highest average NPVs ($570 million and $360 million, respectively), while MISO and SPP units remain negative on average. PJM assets benefit from relatively high ancillary service revenues (nearly 4% of total income), whereas ERCOT units—despite high capacity factors—are constrained by low price volatility and limited surplus capacity. These regional disparities underscore the importance of location-specific modeling for evaluating retrofit potential (Fig. 5.3**d**).

5.2.2 Operational Flexibility and Ancillary Service Provision under High-resolution Dispatch

To assess the flexibility enhancements enabled by system integration, a comprehensive analysis was conducted across all available ancillary services in the seven U.S. ISOs, considering each service's pricing structure, deployment frequency, and technical requirements. The modeling framework simulates bidding and deployment outcomes for Regulation Up/Down, Spinning/Non-Spinning Reserves, and Flex Ramp products where applicable. Reactor-specific technical constraints and operational limits of HTEs, including ramp rate limits, thermal inertia, and minimum stable load thresholds, are explicitly incorporated. The model also accounts for energy allocation trade-offs between electricity export, hydrogen production, and battery storage (where applicable). While some nuclear power plants in North America

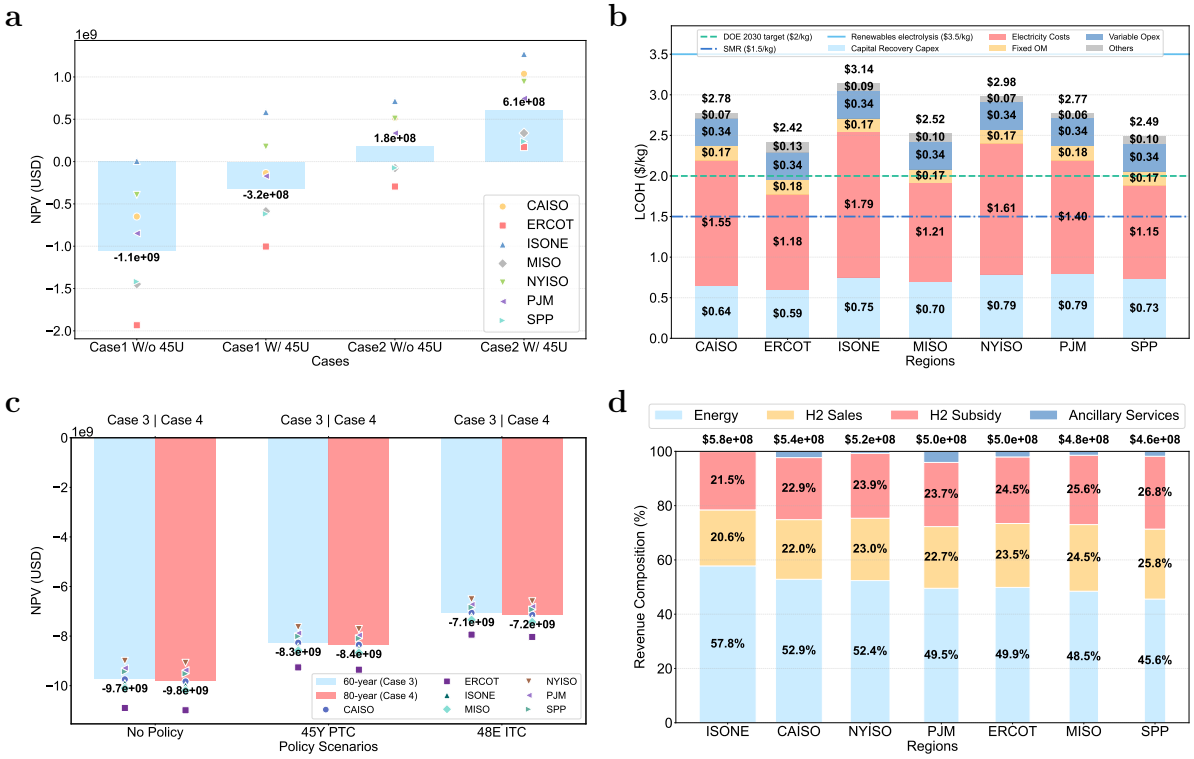


Figure 5.3: Economic performance of the nuclear–hydrogen system. **a**, Comparison of NPV across two cases, before and after tax credits. In the Business-as-Usual (BAU) case (Case 1), the average NPV across 42 reactors is negative, lowest in ERCOT. After the Section 45U Production Tax Credit (45U PTC), some regions (e.g., Independent System Operator New England (ISONE), New York Independent System Operator (NYISO)) turn positive, though the overall average remains negative—showing most reactors still struggle. In the hybrid system (Case 2), the national average NPV is positive even without policy support, though ERCOT, Midcontinent Independent System Operator (MISO), and Southwest Power Pool (SPP) stay negative. With 45U, all reactors achieve positive NPV. **b**, LCOH breakdowns for hybrid systems across seven Independent System Operators (ISOs), compared with U.S. Department of Energy (DOE) 2030 target, Small Modular Reactor, and renewable electrolysis. LCOH exceeds the DOE target and SMR but is below renewable electrolysis. Electricity costs dominate, followed by capital investment. **c**, NPV of new nuclear–hydrogen systems with 60- and 80-year lifespans under three policy cases: no credit, Section 45Y Production Tax Credit (45Y PTC), and Section 48E Investment Tax Credit (48E ITC). NPVs stay negative under current costs. Shorter lifespans yield higher NPVs due to lower O&M escalation and fewer replacements. Revenues from extended years cannot offset rising expenses. Among policies, 48E ITC is most favorable, followed by 45Y. **d**, Revenue composition of hybrid systems across seven regions. Electricity sales account for about half of total revenue. Hydrogen—split between direct sales and Section 45V tax credits (45V)—forms the second largest share. Both assume $3/kg, though totals differ slightly by production vs. sales bases. Ancillary services, though small, provide extra income.

have demonstrated the capability to adjust output—such as daily load-following within a limited range—most have historically operated primarily as baseload generators, with minimal operational flexibility and no participation in ancillary service markets. Therefore, any observed increase in ramping capability, output variability, or ancillary service engagement within the integrated system represents a fundamental departure from conventional nuclear operation.

The integrated system exhibits a pronounced improvement in operational flexibility compared to conventional nuclear plants. Grid output variability, historically negligible for baseload units, becomes significantly more dynamic: the average coefficient of variation across all systems reached 2.14%, with a maximum of 4.16%. The dispatchable output range exceeded 115 MW for most systems, with a peak of 162.3 MW. This was further supported by an average maximum ramping capability exceeding 121 MW/h and peak ramp rates surpassing 162 MW/h for the most responsive units. On average, the integrated systems experienced over 500 ramping events annually, with some registering more than 950 events, highlighting a substantial increase in sub-hourly dispatch activity. Collectively, the systems delivered over 145,000 MWh of energy annually through ancillary service deployment, representing approximately 1.7% of total generation across all units. This contribution, rising from a baseline of zero ancillary service participation, underscores the transition of integrated systems toward a service-responsive generation paradigm (Fig. 5.4**a**).

Turbine-level flexibility was similarly enhanced. The turbine output range averaged 7.33 MW, with several units exceeding 9 MW. The turbine flexibility factor—a normalized measure of ramping potential—averaged 0.0065, reaching a peak of 0.0114. These metrics indicate a shift from static baseload operation toward active participation in intra-hour balancing. The number of turbine-associated ramping events ranged from 260 to over 950 per year, evidencing a marked increase in short-term dispatch responsiveness.

HTEs played a pivotal role in system-level flexibility by operating as stable yet responsive loads. With a capacity factor averaging 97.95% and continuous operation across all 8,760 hours, HTEs effectively absorbed excess generation while maintaining operational stability. Despite this constant operation, the average cycling frequency was below 0.07 per hour, reflecting minimal operational stress. A strong correlation between HTE cycling and high-frequency grid ramping activity was observed in 75% of units, suggesting dynamic coordination between generation variability and load absorption. In aggregate, HTEs consumed over 630,000 MWh of electricity annually, representing more than 7% of total system output. This substantial share highlights their role in improving flexibility, stabilizing operations, and creating headroom for ancillary service participation without compromising reliability.

Together, turbines and HTEs form a tightly coupled flexibility backbone, enabling nuclear-hydrogen systems to meet grid balancing demands previously inaccessible to standalone reactors (Fig. 5.4**b, c**).

The flexibility gains extend beyond technical improvements to generate economic value via participation in ancillary service markets. Simulation results indicate that all reactors successfully submitted offers for Regulation Up and Down services, with average offer sizes ranging from 20 to 40 MW per unit and offer variability exceeding 25% in over 60% of reactors. More than 80% of reactors achieved deployment frequencies above 0.3 for at least one ancillary service. In regions such as MISO, where RegDown products are available, deployment frequencies surpassed 0.6, significantly higher than median values in other regions. In ERCOT, some reactors secured over 3,000 MWh of annual deployment through Non-Spinning Reserves. These patterns demonstrate that system flexibility interacts with ISO-specific service structures to create differentiated revenue streams. Therefore, the observed flexibility is both measurable and monetizable, with regionally dependent economic benefits (Fig. 5.4**d**).

5.2.3 Sensitivity Analysis

We conducted two groups of sensitivity analyses to assess how key technical and economic parameters shape the performance of the nuclear–hydrogen integrated system, assuming a $1000\,\mathrm{MW_{th}}$ ($380\,\mathrm{MW_e}$) nuclear facility operating within the ERCOT market framework. The first analysis explores the impact of nuclear fixed O&M costs on NPV and LCOE. The second investigates how upper bounds on HTE capacity in the optimization model affect system operations and market performance.

In the first analysis, we varied nuclear fixed O&M costs from \$170k/MW to \$290k/MW. Under the BAU (Case 1) scenario, even the lowest cost level fails to yield a positive NPV without tax credits, underscoring the inherent economic limitations of traditional nuclear systems. In contrast, the hybrid system shows strong economic sensitivity to this parameter. At \$170k/MW, NPV increases by over 130% compared to the baseline, reaching \$182 million. However, at \$290k/MW, NPV declines by more than 370%, turning negative. These results suggest that cost control of fixed O&M is critical for realizing economic gains from hybridization. Although the LCOE of the BAU system is less sensitive to this variable, a modest decrease is observed with lower O&M costs, as O&M accounts for only a small share of the LCOE while its effect on NPV accumulates over time (Fig. 5.5**a**).

In the second analysis, we examined the effect of varying the upper bound on HTE capacity in the optimization model, ranging from 100 MW to 300 MW. Although the model

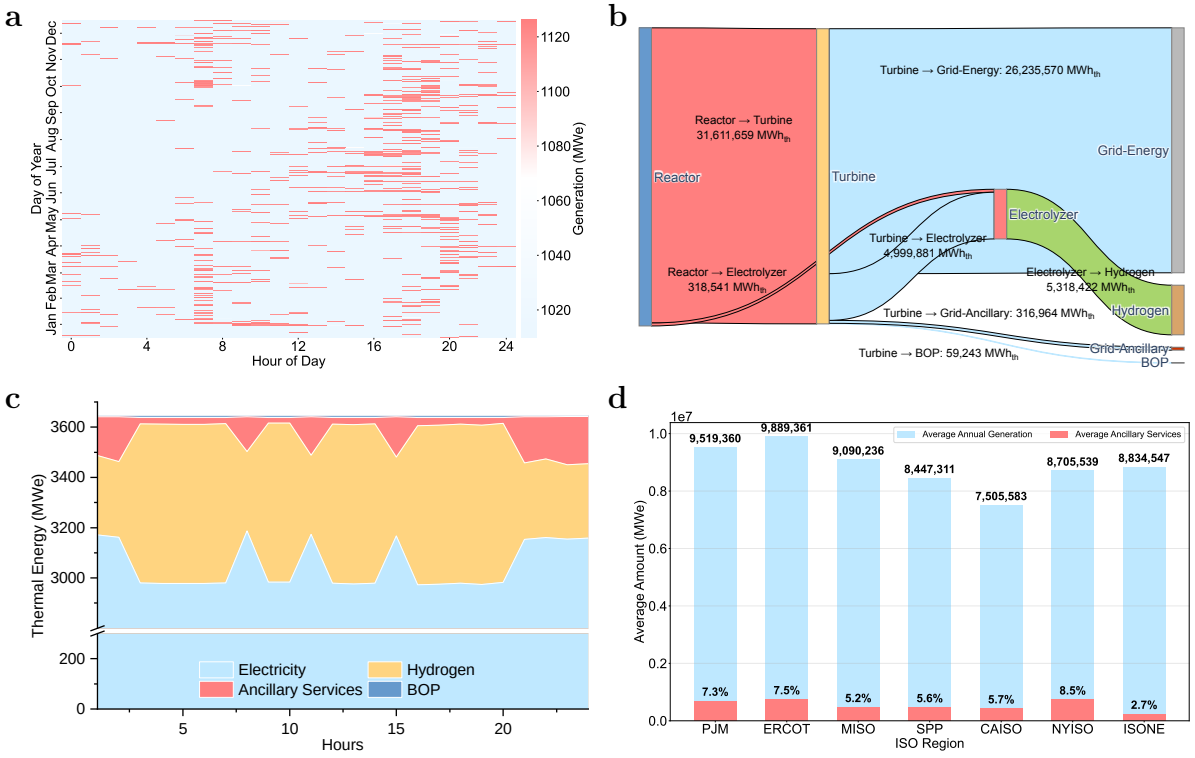


Figure 5.4: Operational flexibility of the nuclear–hydrogen system. **a**, Hourly heatmap of electricity exported to the grid by a nuclear–hydrogen system in the Pennsylvania-New Jersey-Maryland Interconnection (PJM) region over a full year. The system departs from a traditional baseload profile, exhibiting fluctuations exceeding 100 MW. Output closely follows grid demand, with near-maximum generation during morning and evening peaks and reduced output during off-peak hours, indicating strong load-following capability. **b**, Annual energy flow within the system. Reactor thermal output remains constant, primarily powering the turbine, with a smaller portion directed to the high-temperature electrolyzer (HTE). In the secondary energy allocation, most turbine-generated electricity is exported to the grid, with the remainder used to power the HTE, supply ancillary services, and meet balance of plant (BOP) demand. **c**, Hourly energy distribution breakdown. Consistent with the annual trend, most reactor energy is converted to electricity for export, followed by hydrogen production, ancillary services, and BOP, demonstrating efficient intra-system energy management. **d**, Average share of reactor energy used for ancillary services across regions. Most regions maintain a 5–8% share, reflecting the system's active participation in ancillary markets. In contrast, ISONE exhibits a lower share (2.7%) due to limited ancillary service offerings.

consistently selects the highest allowable value, the system response changes significantly. As the capacity limit increases, peak hourly hydrogen sales rise from 2,217 kg/h to 4,762 kg/h. When the limit is reduced below 200 MW, both the optimal hydrogen tank size and hydrogen sales volume decline. Increasing the limit beyond 200 MW leads to only marginal changes in tank size, but hourly hydrogen output remains high. Smaller HTE limits push the system to maximize storage utilization to sustain output. Conversely, larger HTE limits allow higher production rates that offset the need for extensive storage, even as utilization factors decline from 0.98 to 0.83 due to reactor energy constraints (Fig. 5.5**b**).

Total system revenue increases with higher HTE capacity limits, growing from $187 million at 100 MW to over $318 million at 300 MW. The share of hydrogen-related revenue also rises initially but drops slightly at 300 MW due to decreased utilization. In contrast, ancillary service revenue increases non-linearly, from 2.4% to 7.5% of total income, driven by enhanced system flexibility and market participation. This divergence reflects how HTE scaling not only affects energy production but also alters the balance of revenue sources, especially under flexibility-constrained scenarios (Fig. 5.5**c**).

As HTE capacity limits increase, the system bids more aggressively in ancillary service markets. Bid volumes grow across all service types, particularly for high-value regulation services. Beyond 200 MW, the bidding strategy prioritizes services with high deploy rates and economic returns, while maintaining reasonable bids for lower-value services. Even though bid volumes for some products decrease, actual deployment continues to rise, indicating that the system leverages its enhanced flexibility to pursue profit-optimized dispatch modes (Fig. 5.5**d**).

Net grid output declines from 273 MW to 154 MW as more energy is redirected to hydrogen production. However, the output range expands from 39 MW to 120 MW, with maximum flexibility achieved at the 250 MW limit. This behavior confirms that higher HTE capacities improve dispatchability, although further gains are limited by total system energy availability beyond this point (Fig. 5.5**e**).

HTE ramp rates rise with capacity, increasing from 0.89 MW/hr to 2.18 MW/hr. Turbine ramp rates also initially rise, but peak at 200 MW and then decrease from 0.20 MW/hr to 0.16 MW/hr. This shift indicates that flexibility responsibilities increasingly shift to the HTE, relieving mechanical stress on the turbine and allowing more dynamic system response. At high capacities, total system energy constraints cap further improvements in ramp performance (Fig. 5.5**f**).

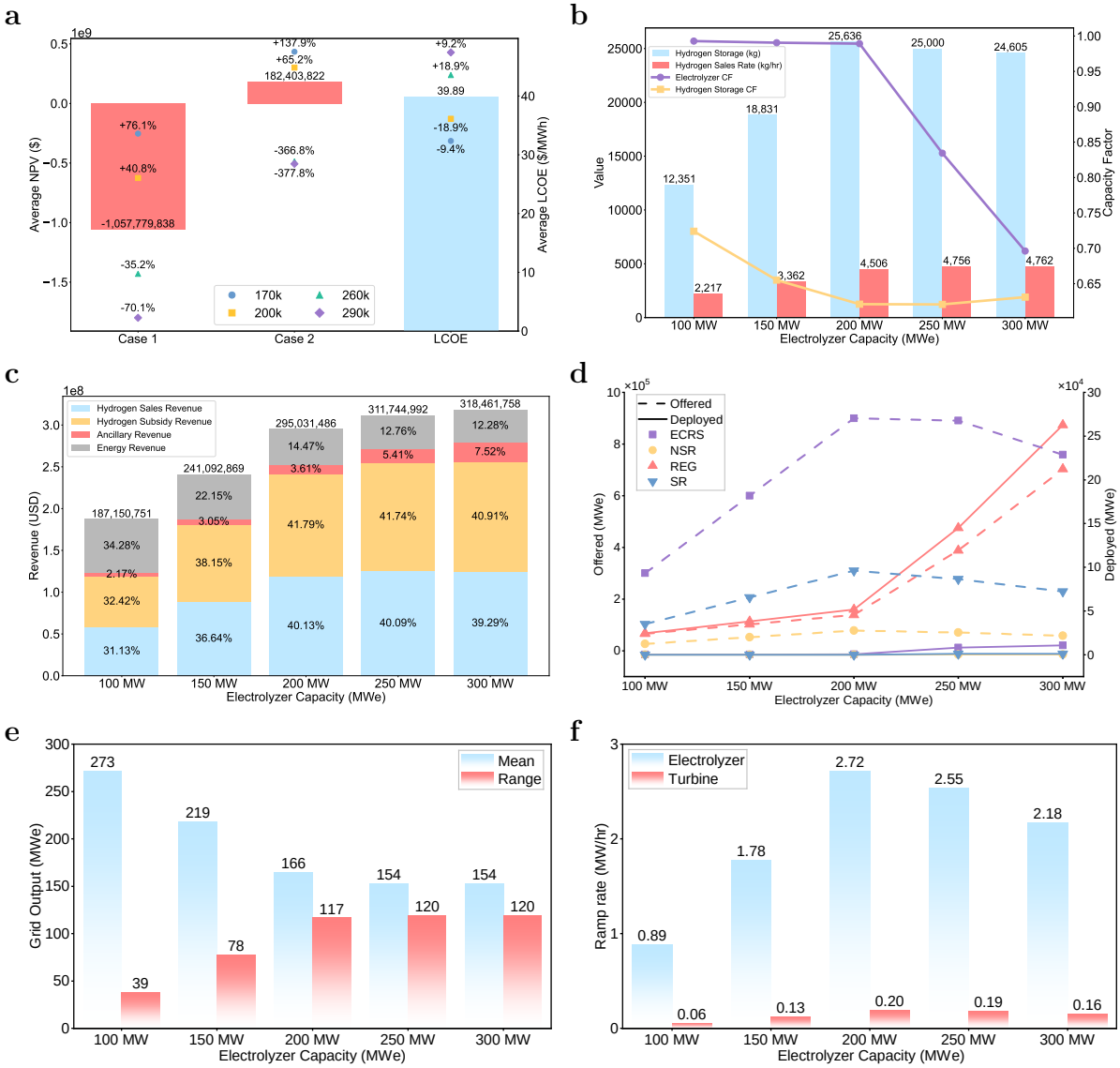


Figure 5.5: Sensitivity analysis of key system parameters. **a**, Nuclear fixed O&M and NPV. In BAU, NPV remains negative even as O&M falls from $230k/MW to $170k/MW. In the hybrid case, NPV rises 130% at $170k/MW but falls 370% at $290k/MW. **b**, HTE capacity limits. Relative to the 200 MW baseline, lower limits cut tank size and sales, while higher limits sustain output despite lower utilization. **c**, Revenues. Greater HTE capacity increases total and hydrogen revenues, though hydrogen peaks at 250 MW before declining. Ancillary revenues rise sharply with added flexibility. **d**, Ancillary services. Larger HTEs allow higher bids, especially beyond 200 MW, with regulation prioritized. Other bids shrink, but deployment rises. **e**, Grid output. Average output falls with larger HTEs, but variability grows, peaking at 120 MW under 250 MW, highlighting flexibility until system limits bind. **f**, Ramp rates. Higher HTE capacity raises ramp rates of both HTE and turbine; beyond a threshold, HTE slows from energy limits while turbine declines as flexibility shifts to HTE.

5.3 Summary

The U.S. nuclear fleet faces growing economic pressure in energy-only markets, where the inflexible nature of conventional baseload operation limits its ability to adapt to increasing renewable penetration and price volatility [90]. Our findings highlight that nuclear–hydrogen hybridization—specifically through HTE offers a viable pathway to enhance both the operational flexibility and economic viability of these assets [11]. By enabling dynamic reallocation of thermal output among electricity generation, hydrogen production, and ancillary services, hybrid systems allow nuclear plants to respond to market signals and provide multi-vector energy services. This integrated configuration not only diversifies revenue streams but also repositions nuclear power as a flexible, low-carbon energy platform capable of supporting both grid reliability and clean fuel production.

Our analysis demonstrates that retrofitting existing reactors with HTE can substantially improve investment performance compared to the baseline case. The addition of hydrogen production reduces reliance on low wholesale power prices and captures emerging hydrogen market value, resulting in more favorable financial outcomes. While standalone hydrogen systems also show strong economic potential, particularly where low-costelectricity is available, integrated nuclear–hydrogen systems maximize synergies by using the stable, continuous thermal and electrical output of reactors. Federal incentives such as 45U, 45V, 45Y, and 48E play a critical role in narrowing cost gaps, but their effectiveness varies by configuration and region, highlighting the importance of both technology improvements and supportive market mechanisms.

A key insight from this study is that flexibility is as important as cost reduction in achieving commercial viability. By enabling dynamic operation, integrated systems can participate in ancillary services, mitigate price volatility, and reduce curtailment, which collectively enhance total project value even if the levelized cost of electricity rises due to additional investments. This value-stacking capability demonstrates that the profitability of hybrid nuclear–hydrogen projects is determined not by energy cost alone but by their ability to provide system-level services that are increasingly valuable in high-renewable grids.

Regional market characteristics strongly influence the achievable benefits of nuclear hydrogen integration. Markets with robust ancillary service mechanisms and price variability offer greater opportunities for revenue diversification, while regions with suppressed power prices benefit from converting excess generation into clean hydrogen. These regional dynamics indicate that deployment strategies must be tailored to specific market conditions, and that

regulatory frameworks should evolve to reward the flexibility and reliability that hybrid nuclear systems provide.

Sensitivity analysis underscores the importance of cost control and system design. Fixed operations and maintenance costs of nuclear reactors and the sizing of HTE capacity emerge as dominant drivers of project viability. Reducing O&M costs and optimizing electrolyzer sizing can significantly enhance returns, while misalignment between design choices and market conditions can erode value. These findings emphasize the need for integrated planning that considers both economic and technical factors when deploying hybrid systems.

Looking forward, a phased deployment strategy is essential. Initial projects should focus on sites with favorable economic conditions, established hydrogen demand, and active ancillary service markets. Early deployments will provide critical operational experience, reduce perceived risk, and generate cost learning effects that can be leveraged in subsequent projects. Over time, scaling nuclear–hydrogen systems will contribute to lowering overall energy transition costs by offering firm, flexible, and reliable energy supply, as well as producing affordable hydrogen for industrial and transportation sectors.

At the system level, hybrid nuclear–hydrogen plants can deliver multiple benefits beyond individual project economics. They can stabilize renewable-heavy grids, reduce reliance on fossil backup, and supply clean hydrogen for industry and transportation, effectively bridging the gap between the power and hydrogen sectors. These contributions are particularly valuable during the transition to a fully integrated energy system, where flexible, dispatchable, and carbon-free resources are critical.

Nevertheless, this study has limitations that should guide future research. Hydrogen price trajectories, regional demand profiles, and policy environments remain uncertain, and our modeling does not fully capture the potential impacts of future market evolution or broader sectoral integration (e.g., ammonia, synthetic fuels, or carbon capture). Further engineering assessments and lifecycle analyses of HTE systems are needed to refine cost and performance assumptions.

Nuclear–hydrogen hybridization offers a compelling strategy to enhance the economic resilience and strategic role of nuclear power in a decarbonized future. Realizing this potential will require a combination of cost reduction, flexible operation, targeted incentives, and market designs that reward both low-carbon reliable energy and grid services. By redefining nuclear power as a versatile energy hub rather than a static baseload source, this approach can strengthen the pathway to a a more integrated energy system while unlocking new value streams for legacy and future nuclear assets.

CHAPTER 6

CONCLUSIONS AND FUTURE WORK[1][2]

The findings of this dissertation collectively highlight hydrogen's potential as a critical enabler in unlocking the flexibility, scalability, and economic viability of clean energy systems. By examining hydrogen integration from multiple perspectives—renewable co-location, grid-level optimization, and nuclear hybridization—this research demonstrates that hydrogen's value lies not only in its role as a long-duration energy storage medium but also in its capacity to enhance the effectiveness of other low-carbon technologies. The discussion and conclusions presented here draw together insights from the three analytical frameworks, evaluating their implications for technology development, energy system design, market structures, and policy support.

One of the central themes emerging from the study is the complementarity between hydrogen and variable renewable energy. The first framework demonstrated that hydrogen integration at the project level can significantly reduce wind curtailment, improve system utilization, and lower costs under favorable market conditions. However, the analysis also revealed trade-offs, such as increased electrolyzer capacity requirements leading to higher LCOH. These findings underscore the importance of carefully balancing the size and utilization rate of hydrogen infrastructure in co-located systems. The results suggest that hydrogen becomes most valuable when electricity prices and renewable availability exhibit large temporal fluctuations, conditions increasingly common in high-renewable systems. Thus, project-level hydrogen integration offers a pathway to transform excess renewable generation from a liability into a source of value creation, both economically and environmentally.

At the system level, the second framework demonstrated that hydrogen can address some of the most pressing challenges of large-scale renewable deployment. By designing a hydrogen network within the ERCOT grid, the study showed how inter-regional transport and storage can alleviate geographic mismatches between supply and demand, while providing additional capacity to support reliability. Hydrogen's contribution to decarbonization was particularly significant, as its ability to substitute fossil-based generation and reduce curtailment enabled

[1]©2024 ASME. Reprinted, with permission, from Li, H. and Zhang, J., 2024. Towards sustainable integration: Techno-economic analysis and future perspectives of co-located wind and hydrogen energy systems. Journal of Mechanical Design, 146(2), p.020903.

[2]Li, H. and Zhang, J., 2025. Hydrogen's role in expanding renewable energy and reducing carbon emissions in Texas. International Journal of Hydrogen Energy, 113, pp.77-89.

notable carbon reductions. Nevertheless, the results also revealed limitations: system performance remained sensitive to electricity prices, carbon costs, and hydrogen equipment costs, with higher natural gas tariffs shifting the balance of emissions and efficiency. This highlights hydrogen's dual dependence on technological progress and market conditions. The sensitivity analyses further showed that even substantial cost reductions in hydrogen technologies alone may not guarantee large-scale adoption unless complemented by supportive policy frameworks and infrastructure investment. Importantly, the grid-level analysis demonstrated that hydrogen is not just an alternative storage option, but a systemic solution that interlinks electricity, industrial, and transportation sectors.

The third framework extended the analysis to nuclear energy, traditionally considered an inflexible baseload technology. By integrating hydrogen production and storage, nuclear plants can be reconfigured as flexible assets capable of participating in ancillary service markets and providing new revenue streams. This hybridization enhances nuclear economics by diversifying output beyond electricity, thereby improving the competitiveness of existing reactors in markets increasingly dominated by renewables. Results from reactor-level case studies indicated that hydrogen integration can improve plant profitability under current market conditions and that policy incentives such as the 45U production tax credit and 48E investment tax credit are critical in making such systems financially attractive. Beyond economics, the findings emphasize hydrogen's role in redefining nuclear's contribution to clean energy: instead of being limited by its traditional baseload role, nuclear power can evolve into a multi-service platform that simultaneously supplies electricity, grid services, and clean hydrogen.

Taken together, these three frameworks reveal a consistent narrative: hydrogen is not merely an independent energy vector, but a transformative enabler that unlocks the potential of other clean energy technologies. In renewable-hydrogen systems, it mitigates curtailment and stabilizes revenues. At the grid level, it provides balancing mechanisms and cross-sectoral linkages. In nuclear-hydrogen systems, it enhances flexibility and profitability. The logical progression across these contexts reflects hydrogen's unique ability to integrate with multiple technologies and address challenges at different scales of the energy system.

Several broader implications arise from these findings. First, the economic feasibility of hydrogen integration depends heavily on the interaction between technology costs, market dynamics, and policy environments. Declining electrolyzer and storage costs, coupled with carbon pricing and tax incentives, substantially improve the outlook for hydrogen-enabled systems. Second, the results highlight the importance of system design choices, including the scale, location, and configuration of hydrogen infrastructure. Optimal solutions vary

across regions and technologies, emphasizing the need for context-specific planning. Third, the findings underscore the importance of complementary infrastructure, such as pipelines, storage facilities, and interconnections, without which hydrogen's full system value cannot be realized.

This dissertation also contributes methodologically by demonstrating how TEA can be structured to capture both operational dynamics and lifecycle economics. By combining mixed-integer optimization, stochastic modeling, and discounted cash flow analysis, the frameworks provide a flexible toolkit that can be applied to diverse contexts. The methodological rigor ensures that results are both technically grounded and economically relevant, bridging the gap between engineering feasibility and market realities. Future research can extend these models by incorporating uncertainty analysis, carbon pricing mechanisms, and multi-sector integration to further refine the understanding of hydrogen's role.

Despite the promising results, several limitations merit explicit acknowledgment and motivate concrete directions for future work. First, the analysis omits end-of-life and decommissioning costs for renewable assets (e.g., dismantling, site restoration, recycling logistics), and—although nuclear waste management costs are included—it does not account for nuclear plant decommissioning expenditures, timing, or associated financing structures. Excluding these cash flows likely biases lifecycle metrics (e.g., NPV, LCOE/LCOH) and understates capital at risk over long horizons. Second, the study is U.S.-centric. It does not examine cross-country heterogeneity in technology costs, policy regimes, permitting timelines, or financing conditions, nor does it endogenize cost and lead-time variability induced by international supply chains (e.g., equipment sourcing, currency risks, tariffs, shipping, and critical-materials constraints). Third, storage is modeled with technology and market conditions that are effectively static; the framework does not capture co-evolution of storage supply and demand, changing ancillary-service designs, or emerging demands from electrified industry, transport, and data centers that will reshape price signals and storage value.

Future research should therefore: (i) integrate cradle-to-grave costing for VRE and explicit nuclear decommissioning modules (including schedules, regulatory contingencies, and recycling scenarios) and propagate these through lifecycle financial metrics; (ii) extend the scope to multi-country comparative cases with an explicit trade and supply-chain layer that maps cost shocks and policy differences into project economics; (iii) model storage as an endogenous, multi-technology capacity expansion problem coupled to market evolution—allowing batteries, hydrogen, thermal, and other long-duration options to compete for energy, capacity, and ancillary revenues under scenario-based policy and demand growth; (iv) embed energy-equity

considerations via distributional metrics (e.g., energy burden, bill impacts by income/region), siting externalities, and community-benefit constraints; and (v) evaluate hydrogen's integration with additional pathways—either as a vector co-produced with other technologies (e.g., CCUS, industrial heat, district energy) or via alternative carriers such as ammonia and methanol—quantifying conversion losses, logistics, safety, and infrastructure interoperability to assess system-level value stacking. Methodologically, introducing stochastic/robust optimization and real-options analysis would better reflect policy, fuel, and supply-chain uncertainty.

In conclusion, this dissertation demonstrates that hydrogen integration, through distinct techno-economic frameworks, offers transformative opportunities to overcome key bottlenecks in renewable, grid, and nuclear systems. The research shows that hydrogen not only provides technical solutions to intermittency and inflexibility but also creates new economic pathways that enhance the viability of clean energy. The results reinforce the view that hydrogen should not be evaluated in isolation, but as part of hybrid systems where its true value emerges. Looking forward, the widespread adoption of hydrogen will depend on continued cost declines, strategic infrastructure development, and robust policy support. With these conditions in place, hydrogen has the potential to serve as a cornerstone of resilient, flexible, and carbon-neutral energy systems, accelerating the global transition toward sustainability.

APPENDIX A

NOMENCLATURE

Table A.1: Nomenclature of Chapter 3

Symbol	Definition	Units
A. Sets and Collections		
$\mathcal{B}$	Storage systems	—
$\mathcal{H}$	Time steps	—
$\mathcal{T}$	Technologies	—
$\mathcal{T}^{\mathrm{gh}} \subseteq \mathcal{T}$	Technologies that generate hydrogen	—
$\mathcal{T}^{\mathrm{h}} \subseteq \mathcal{T}$	Technologies that burn hydrogen	—
$\mathcal{T}_b \subseteq \mathcal{T}$	Technologies that can charge storage system b	—
B. Parameters (Constants)		
c_t^{cm}	Slope of capital cost curve for technology t	\$/kW
c_t^{cb}	y-intercept of capital cost curve for technology t	\$
c_b^{kW}	Capital cost of power capacity for storage system b	\$/kW
c_b^{bkWh}	Capital cost of energy capacity for storage system b	\$/kWh
c_b^{omb}	O&M cost of storage system b per unit of energy rating	\$/kWh
$c_t^{\mathrm{om}\sigma}$	O&M cost of technology t per unit of power rating	\$/kW
c_t^{omb}	O&M cost of hydrogen-using technologies t per unit of energy rating	\$/kWh
c^{ome}	O&M cost of electrolyzer per unit of energy rating	\$/kg
c_h^{e}	Export rate for energy in time step h	\$/kWh
c_h^{hts}	Export rate for hydrogen in time step h	\$/kg
$\bar{\delta}_h^{\mathrm{g}}$	Grid interconnection limit	kW
δ_h^{d}	Grid power demand	kW
i_t^{r}	Incentive rate for technology t	\$/kWh
$\bar{l}_t^{\sigma}$	Upper incentive limit for technology t	\$
f^{tow}	Tax rate factor for owner	fraction
f^{om}	O&M present worth factor	unitless
f^{e}	Energy present worth factor	unitless

Continued on next page

Table A.1: continued from previous page

Symbol	Definition	Units
f_t^{pi}	Present worth factor for incentives for technology t	unitless
f_t^{li}	Levelization factor of production incentive for technology t	fraction
f_{th}^{p}	Production factor of technology t at time step h	unitless
f_e^{l}	Levelization factor of technology t	fraction
f_{eh}^{p}	Production factor of electrolyzer at time step h	unitless
$\bar{b}_t^{\sigma}$	Maximum power rating for technology t	kW
η_{bt}^{+}	Efficiency of charging storage system b using technology t	fraction
η_b^{-}	Efficiency of discharging storage system b	fraction
$\underline{w}_b^{\mathrm{bkWh}}$	Minimum energy capacity of storage system b	kWh
$\bar{w}_b^{\mathrm{bkWh}}$	Maximum energy capacity of storage system b	kWh
$\bar{w}_b^{\mathrm{bkW}}$	Maximum power output of storage system b	kW
$\underline{w}_b^{\mathrm{bkW}}$	Minimum power output of storage system b	kW
$\bar{w}_b^{\mathrm{mcp}}$	Maximum percent state of charge of storage system b	fraction
w_b^0	Initial percent state of charge of storage system b	fraction
m_f	Slope of the hydrogen rate curve for fuel cells	kg/kW
m_e	Slope of the power curve for electrolyzer	kW/kg
M	Arbitrary large number	unitless
C. Decision Variables (Continuous)		
X_t^{σ}	Power rating of technology t	kW
X_b^{kWh}	Energy rating for storage system b	kWh
X_b^{kW}	Power rating for storage system b	kW
X_{th}^{rp}	Rated production of technology t during time step h	kW
X_{eh}^{rp}	Rated production of electrolyzer during time step h	kg/h
X_{bh}^{stg}	Exports from storage b to the grid during time step h	kW
X_{th}^{ptg}	Exports from technology t to the grid during time step h	kW
X_{eh}^{sell}	Hydrogen sold during time step h	kg
X_t^{pi}	Production incentive collected for technology t	\$
$X_{b,0}^{\mathrm{se}}$	State of charge of storage system b at the end of time step 0	kWh
X_{bh}^{se}	State of charge of storage system b at the end of time step h	kWh
X_{bth}^{pts}	Power from technology t used to charge storage system b during time step h	kW

Continued on next page

Table A.1: continued from previous page

Symbol	Definition	Units
X_{bh}^{dfs}	Power discharged from storage system b during time step h	kW
X_{th}^{pte}	Power from technology t supplied to the electrolyzer during time step h	kW
X_{th}^{ptc}	Curtailed power from technology t during time step h	kW
X_{bh}^{ste}	Power from storage b supplied to the electrolyzer during time step h	kW
X_{e}^{kg}	Capacity of electrolyzer	kg/h
X_{th}^{sh}	State of charge of hydrogen tank during time step h	kg
X_{eh}^{etf}	Hydrogen to fuel cells during time step h	kg
X_{fh}^{rp}	Rated production of fuel cells during time step h	kW
X_{fh}^{ftg}	Power to grid from fuel cells during time step h	kW
X_{f}^{kW}	Capacity of fuel cells	kW
D. Binary / Logical Variables		
Z_{th}^{to}	1 if technology t is operating in time step h; 0 otherwise	unitless
Z_{t}^{pi}	1 if production incentive is available for technology t; 0 otherwise	unitless

Table A.2: Nomenclature of Chapter 4

Symbol	Definition	Units
A. Sets and Collections		
I	Set of regions i	—
K	Set of technologies k	—
T	Set of time periods t	—
S	Set of scenarios s	—
B. Parameters (Constants)		
c^{ins}	Installation cost per technology at each node	k$
c^{om}	Fixed O&M cost per technology per year	k$
c^{tr}	Transportation cost per unit	k$
c^{w}	Water cost per ton	k$

Continued on next page

Table A.2: continued from previous page

Symbol	Definition	Units
c^{pen}	Penalty cost per MWh	k$
c^{p}	CCS cost per ton	k$
c^{s}	SMR carbon cost per ton	k$
δ	Discount rate	—
lifetime	Lifetime of technologies	years
λ^{e2h}	Efficiency from electricity to hydrogen	—
λ^{h2e}	Efficiency from hydrogen to electricity	—
η^{cha}	Charging efficiency	—
η^{dis}	Discharging efficiency	—
h^{cost}	Hydrogen price of SMR	k$
hd_i	Zonal hydrogen demand	tons
f^{power}	Gas power emission factor	ton/MWh
f^{smr}	SMR emission factor	ton/ton
ρ^{h}	Hydrogen price	k$
ρ^{o}	Oxygen price	k$
r^{w}	Water rate	tons
r^{o}	Oxygen rate	tons
χ	Hourly electricity demand	MWh
κ	Hourly hydrogen demand	tons
ϵ^{r}	Hourly generation	MWh
β	Battery capacity	MWh
C. Decision Variables		
$x_{i,k}$	Technology installation in region i and technology k	MW
$h^{\text{tr}}_{i,j,t,s}$	Hydrogen transfer from region i to j at time t, scenario s	tons
$\epsilon^{\text{h}}_{i,t,s}$	Electricity from hydrogen in region i, time t, scenario s	MWh
$\epsilon^{\text{dis}}_{i,t,s}$	Discharging in region i, time t, scenario s	MWh
$\epsilon^{\text{n}}_{i,t,s}$	Electricity purchase in region i, time t, scenario s	MWh
$\epsilon^{\text{cha}}_{i,t,s}$	Charging in region i, time t, scenario s	MWh
$\epsilon^{\text{e2h}}_{i,t,s}$	Electricity to hydrogen in region i, time t, scenario s	MWh
$h^{\text{se}}_{i,t,s}$	Hydrogen sold in region i, time t, scenario s	tons
$h^{\text{smr}}_{i,t,s}$	Hydrogen generated by SMR in region i, time t, scenario s	tons

Continued on next page

Table A.2: continued from previous page

Symbol	Definition	Units
$w_{i,t,s}$	Water usage in region i, time t, scenario s	tons
$o_{i,t,s}$	Oxygen usage in region i, time t, scenario s	tons
$\theta^{\mathrm{h}}_{i,t,s}$	Hydrogen tank state of charge in region i, time t, scenario s	tons
$\theta^{\mathrm{b}}_{i,t,s}$	Battery state of charge in region i, time t, scenario s	MWh
ψ_i	Hydrogen demand satisfaction rate in region i	—

Table A.3: Nomenclature of Chapter 5

Symbol	Definition	Units
A. Sets and Indices		
$t \in T$	Index and set of time periods in the optimization horizon.	–
$k \in K_{turb}$	Index and set of breakpoints for the turbine piecewise efficiency curve.	–
$j \in K_{elec}$	Index and set of breakpoints for the electrolyzer piecewise efficiency curve.	–
$c \in C$	Set of components that can provide ancillary services; $C = \{\text{Turbine, Electrolyzer, Battery}\}$.	–
$s \in S$	Set of modeled ancillary services; $S = \{\text{RegUp, RegDown, SR, NSR, ECRS, } \ldots\}$.	–
B. Parameters		
General and Market Parameters		
Δt	Duration of a single time period.	hr
λ^{E}_{t}	Energy market electricity price at time t.	\$/MWh
λ^{H_2}	Market price of hydrogen.	\$/kg
$\lambda^{H_2,sub}$	Government subsidy for hydrogen production.	\$/kg
$\lambda^{AS,cap}_{t,s}$	Market clearing price for ancillary-service capacity of service s at time t.	\$/MW
$w_{t,s}$	Winning rate for the ancillary-service bid of service s at time t.	–
$\delta_{t,s}$	Deployment factor for ancillary reserve service s at time t.	–

Continued on next page

Table A.3: continued from previous page

Symbol	Definition	Units
$M_{t,s}$	Mileage factor for ancillary regulation service s at time t.	–
$P_{t,s}$	Performance factor for ancillary regulation service s at time t.	–
τ^{AS}	Assumed duration of ancillary-service deployment for energy capacity check.	hr
Nuclear Turbine Parameters		
$Q^{steam,total}$	Total thermal power produced by the nuclear reactor.	MWth
P^{turb}_{max}, P^{turb}_{min}	Maximum and minimum electrical power output of the turbine.	MW
Q^{turb}_{max}, Q^{turb}_{min}	Maximum and minimum steam flow to the turbine.	MWth
$R^{turb,up}_{max}$, $R^{turb,down}_{max}$	Maximum hourly ramp-up and ramp-down rate of the turbine.	MW/hr
$C^{turb,vom}$	Variable O&M cost for the turbine.	\$/MWh
Electrolyzer Parameters		
P^{elec}_{max}, P^{elec}_{min}	Maximum and minimum power consumption of the electrolyzer (can be variable or parameter).	MW
$P^{elec,on}_{min}$	Minimum power consumption when the electrolyzer is online.	MW
$R^{elec,up}_{max}$, $R^{elec,down}_{max}$	Maximum hourly ramp-up and ramp-down rate as a fraction of max capacity.	%/hr
U^{elec}_{init}	Initial on/off status of the electrolyzer.	binary
$T^{elec,up}_{min}$, $T^{elec,down}_{min}$	Minimum up-time and down-time for the electrolyzer.	hr
$C^{elec,vom}$	Variable O&M cost for the electrolyzer.	\$/MWh
$C^{elec,su}$	Cost per startup event for the electrolyzer.	\$
C^{H_2O}	Cost of water per unit of hydrogen produced.	\$/kg
$C^{elec,capex}$	Annualized capital cost of the electrolyzer.	\$/MW-year
D_{op}, D_{su}	Degradation factors from operation and startups.	–
$CF^{H_2}_{target}$	Target minimum capacity factor for hydrogen production.	–
Battery Storage Parameters		
E^{b}_{max}, E^{b}_{min}	Maximum and minimum state of charge of the battery (can be variable or parameter).	MWh

Continued on next page

Table A.3: continued from previous page

Symbol	Definition	Units
P^{b}_{max}	Maximum charge/discharge power of the battery (can be variable or parameter).	MW
$\eta^{b,ch}$, $\eta^{b,dis}$	Battery charge and discharge efficiency.	–
E^{b}_{init}	Initial state of charge of the battery.	MWh
SOC_{min}	Minimum state of charge as a fraction of total capacity.	–
R^{b}_{max}	Maximum ramp rate as a fraction of capacity per hour.	1/hr
$C^{b,vom}$	Variable O&M cost for battery cycling.	$/MWh
$C^{b,capex,E}$	Annualized capital cost of battery energy capacity.	$/MWh-year
$C^{b,capex,P}$	Annualized capital cost of battery power capacity.	$/MW-year
Hydrogen Storage Parameters		
M^{stor}_{max}, M^{stor}_{min}	Maximum and minimum mass of hydrogen in storage (can be variable or parameter).	kg
$\dot{M}^{stor,ch}_{max}$, $\dot{M}^{stor,dis}_{max}$	Maximum charge and discharge rate of hydrogen storage.	kg/hr
$\eta^{stor,ch}$, $\eta^{stor,dis}$	Hydrogen storage charge and discharge efficiency.	–
M^{stor}_{init}	Initial mass of hydrogen in storage.	kg
$C^{stor,vom}$	Variable O&M cost for hydrogen storage cycling.	$/kg
$C^{stor,capex}$	Annualized capital cost of hydrogen storage capacity.	$/kg-year
C. Decision Variables		
Continuous Variables		
p^{IES}_{t}	Net power exchanged with the grid at time t (positive: sale; negative: purchase).	MW
p^{sale}_{t}, p^{buy}_{t}	Power sold to and purchased from the grid at time t.	MW
p^{turb}_{t}	Electrical power generated by the turbine at time t.	MW
q^{turb}_{t}	Steam consumed by the turbine at time t.	MWth
p^{elec}_{t}	Actual power consumed by the electrolyzer at time t.	MW
$p^{elec,sp}_{t}$	Power setpoint for the electrolyzer at time t.	MW
$\dot{m}^{H_2}_{t}$	Mass flow rate of hydrogen produced by the electrolyzer at time t.	kg/hr
q^{elec}_{t}	Steam consumed by the HTE electrolyzer at time t.	MWth
d_t	State of degradation of the electrolyzer at time t.	–

Continued on next page

Table A.3: continued from previous page

Symbol	Definition	Units
$p_t^{b,ch}$, $p_t^{b,dis}$	Battery charging and discharging power at time t.	MW
e_t^b	State of charge (energy level) of the battery at time t.	MWh
m_t^{stor}	Mass of hydrogen in storage at time t.	kg
$\dot{m}_t^{stor,in}$, $\dot{m}_t^{stor,out}$	Mass flow rate of hydrogen into and out of storage at time t.	kg/hr
$\dot{m}_t^{H_2,market}$	Mass flow rate of hydrogen sold directly to market at time t.	kg/hr
$\dot{m}_{const}^{H_2,sale}$	Constant hydrogen sales rate when optimal storage sizing is enabled.	kg/hr
$b_{t,s}^c$	Bid capacity for ancillary service s from component c at time t.	MW
$d_{t,s}^c$	Deployed capacity for ancillary service s from component c at time t.	MW
$\lambda_{t,k}$, $\lambda_{t,j}$	SOS2 weights for piecewise-linear approximations.	–
Component Sizing Variables		
P_{max}^{elec}	Optimized maximum power capacity of the electrolyzer.	MW
E_{max}^b	Optimized energy capacity of the battery.	MWh
P_{max}^b	Optimized power capacity of the battery.	MW
M_{max}^{stor}	Optimized capacity of the hydrogen storage.	kg
Binary Variables		
u_t^{elec}	On/off status of the electrolyzer at time t (1 if on, 0 if off).	binary
v_t^{elec}, w_t^{elec}	Startup and shutdown indicators for the electrolyzer at time t.	binary
$u_t^{b,ch}$, $u_t^{b,dis}$	Charge/discharge status of the battery at time t.	binary

APPENDIX B

SYSTEM PARAMETERS OF CHAPTER 5

Table B.1: Advanced system parameters [151, 11, 64, 65, 66, 90, 50, 9, 98, 103, 37, 18, 154]

Parameter	**Value**
delT_minutes	60.0
plant_lifetime_years	30
discount_rate	0.06
pIES_min_MW	-1,000.0
pIES_max_MW	3,000.0
qSteam_Total_MWth	1000.0
qSteam_Turbine_min_MWth	100.0
qSteam_Turbine_max_MWth	1,000.0
pTurbine_min_MW	38.0
pTurbine_max_MW	380.0
Turbine_RampUp_Rate_ Percent_per_Min	2.0
Turbine_RampDown_Rate_ Percent_per_Min	2.0
pTurbine_LTE_setpoint_MW	380.0
Turbine_Thermal_Elec_ Efficiency_Const	0.38
qSteam_Turbine_ Breakpoints_MWth	100.0, 550.0, 1,000.0, 10,000.0
pTurbine_Outputs_ at_Breakpoints_MW	38.0, 209.0, 380.0, 3800.0
vom_turbine_USD_per_MWh	2.0
pElectrolyzer_max_ upper_bound_MW	200.0
pElectrolyzer_max_ lower_bound_MW	0.0
pElectrolyzer_min_MW	50.0
pElectrolyzer_ Breakpoints_MW	50.0, 100.0, 250.0, 500.0
cost_water_USD_per_kg_h2	0.03

Continued on next page

Table B.1: continued from previous page

Parameter	Value
uElectrolyzer_initial_status_0_or_1	0
DegradationStateInitial_Units	0.0
h2_target_capacity_factor_fraction	0.0
hydrogen_subsidy_value_usd_per_kg	3.0
hydrogen_subsidy_duration_years	10
aux_power_consumption_per_kg_h2	0.0005
H2_value_USD_per_kg	3.0
cost_electrolyzer_ramping_USD_per_MW_ramp	0.5
Ramp_qSteam_Electrolyzer_limit_MWth_per_Hour	500.0
pElectrolyzer_min_MW_HTE	50.0
Electrolyzer_RampUp_Rate_Percent_per_Min_HTE	2.0
Electrolyzer_RampDown_Rate_Percent_per_Min_HTE	2.0
pElectrolyzer_Breakpoints_MW_HTE	50.0, 100.0, 250.0, 500.0
ke_H2_Values_MWh_per_kg_HTE	0.04400, 0.04300, 0.04200, 0.04100
kt_H2_Values_MWth_per_kg_HTE	0.00800, 0.00800, 0.00800, 0.00800
vom_electrolyzer_USD_per_MWh_HTE	6.9
cost_electrolyzer_capacity_USD_per_MW_year_HTE	130,912.5
cost_startup_electrolyzer_USD_per_startup_HTE	700.0
MinUpTimeElectrolyzer_hours_HTE	4
MinDownTimeElectrolyzer_hours_HTE	2
DegradationFactorOperation_Units_per_Hour_at_MaxLoad_HTE	0.0003

Continued on next page

Table B.1: continued from previous page

Parameter	Value
DegradationFactorStartup_Units_per_Startup_HTE	1.5
H2_storage_capacity_max_kg	100,000.0
H2_storage_capacity_min_kg	5,000.0
H2_storage_level_initial_kg	0.0
H2_storage_charge_rate_max_kg_per_hr	5,000.0
H2_storage_discharge_rate_max_kg_per_hr	5,000.0
storage_charge_eff_fraction	0.98
storage_discharge_eff_fraction	0.98
vom_storage_cycle_USD_per_kg_cycled	0.01
cost_h2_storage_capex_USD_per_kg_year	13.964
BatteryCapacity_min_MWh	0.0
BatteryCapacity_max_MWh	1000.0
BatteryPowerRatio_MW_per_MWh	0.25
BatteryChargeEff	0.92
BatteryDischargeEff	0.92
BatterySOC_min_fraction	0.1
BatterySOC_initial_fraction	0.5
BatteryRequireCyclicSOC	True
BatteryRampRate_fraction_per_hour	1.0
BatteryCapex_USD_per_MWh_year	0.0
BatteryCapex_USD_per_MW_year	183,277.5
BatteryFixedOM_USD_per_MWh_year	0.0
BatteryFixedOM_USD_per_MW_year	48168

Continued on next page

Table B.1: continued from previous page

Parameter	Value
user_specified_electrolyzer_capacity_MW	
user_specified_battery_power_MW	
user_specified_battery_energy_MWh	
45u_ptc_rate_per_mwh	15.0
45u_ptc_start_year	2024
45u_ptc_end_year	2032
45y_ptc_rate_per_mwh	30.0
45y_ptc_duration_years	10
48e_itc_rate	0.50
48e_itc_depreciation_basis_reduction_rate	0.50
npp_fixed_om_cost	230,000.0
npp_fuel_cost	10.0

APPENDIX C

TECHNO-ECONOMIC ANALYSIS PARAMETERS OF CHAPTER 5

Table C.1: Core data and parameters for the TEA framework [151, 11, 64, 65, 66, 90, 33, 9, 98, 103, 37, 18, 49, 77]

Parameter	Value
General Project Parameters	
Project Lifetime	30 years
Discount Rate	6.0%
Construction Years	2 years (Retrofit) 8 years (New Nuclear)
Corporate Tax Rate	21.0%
Construction Financing Interest Rate	6.0%
Hours in Year	8760 hours
Capital Expenditures (CAPEX) - Non-Nuclear Components	
Electrolyzer System	Base Cost: $75,000,000 Ref. Capacity: 50 MW Payment: -2yr: 50%, -1yr: 50%
H2 Storage System	Base Cost: $16,000,000 Ref. Capacity: 100,000 kg Payment: -2yr: 50%, -1yr: 50%
Battery System (Energy)	Base Cost: $0 Ref. Capacity: 100 MWh
Battery System (Power)	Base Cost: $23,600,000 Ref. Capacity: 25 MW Payment: -1yr: 100%
Grid Integration	Base Cost: $5,000,000 (Fixed Cost)

Continued on next page

Table C.1: continued from previous page

Parameter	Value
NPP Modifications	Base Cost: $2,000,000 (Fixed Cost)
CAPEX - Greenfield Nuclear Components	
Nuclear Power Plant	Base Cost: $6,000,000,000 Ref. Capacity: 1000 MW Learning Rate: 5.0%
Nuclear Site Preparation	Base Cost: $300,000,000 Ref. Capacity: 1000 MW Learning Rate: 2.0%
Nuclear Safety Systems	Base Cost: $1,500,000,000 Ref. Capacity: 1000 MW Learning Rate: 3.0%
Nuclear Grid Connection	Base Cost: $200,000,000 Ref. Capacity: 1000 MW
Operating Expenditures (OPEX)	
Fixed O&M (General)	2.0% of total CAPEX per year
Fixed O&M (Battery)	$48,168.0 per MW-year
Variable O&M (Electrolyzer)	$6.9 per MWh
Variable O&M (H2 Storage)	$0.01 per kg cycled
Nuclear Fixed O&M	$15,000 per MW-month
Nuclear Variable O&M	$1.0 per MWh
Nuclear Fuel Cost	$10.0 per MWh
Nuclear Additional Costs	$50,000 per MW-year
Replacement Costs	
Electrolyzer Stack	30% of initial electrolyzer CAPEX Years: 10, 20

Continued on next page

Table C.1: continued from previous page

Parameter	Value
H2 Storage Components	$5,000,000 Years: 15
Battery Augmentation	60% of initial battery CAPEX Years: 10
Nuclear Steam Generator	8% of initial nuclear CAPEX Years: 25
Nuclear Control Rods	1.5% of initial nuclear CAPEX Years: 18, 36, 54
MACRS Depreciation	
Nuclear Equipment	15-year schedule
Hydrogen Equipment	7-year schedule
Battery Systems	7-year schedule
Grid Infrastructure	15-year schedule
Federal Tax Incentive Policies	
45U PTC (Existing Plants)	Rate: $15.0/MWh Period: 2024-2032
45Y PTC (New Plants)	Rate: up to $30.0/MWh Duration: First 10 years of operation
48E ITC (New Plants)	Rate: up to 50% of qualified CAPEX Basis Reduction: 50% of credit value
System Technical & Economic Parameters	
H2 Market Value	$3.0 per kg
H2 Subsidy Value	$3.0 per kg Duration: 10 years
Electrolyzer Efficiency (HTE)	41.0 - 44.0 kWh/kg
Battery Round-trip Efficiency	84.6% (92% charge, 92% discharge)

Continued on next page

Table C.1: continued from previous page

Parameter	**Value**
Turbine Thermal Efficiency	38.0%

APPENDIX D

ANCILLARY SERVICES LIST OF CHAPTER 5

Table D.1: Ancillary services across U.S. ISOs [17, 39, 96, 100, 71, 129, 113]

ISO	**Abbreviation**	**Service Description**
SPP	RegU	Regulation Up
	RegD	Regulation Down
	RamU	Ramp Up
	RamD	Ramp Down
	Spin	Spinning Reserve
	Sup	Supplemental Reserve
	UncU	Uncertainty Up (may relate to ramp/reserves)
CAISO	RegU	Regulation Up
	RegD	Regulation Down
	Spin	Spinning Reserves
	NSpin	Non-Spinning Reserves
	RMU	Ramp Up
	RMD	Ramp Down
ERCOT	RegU	Regulation Up
	RegD	Regulation Down
	Spin	Responsive Reserves (mapped to Spin)
	NSpin	Non-Spinning Reserves
	ECRS	ERCOT Contingency Reserve Service
PJM	Rse	Primary Reserve
	Reg	Regulation
	Syn	Synchronized Reserve
	TMR	Thirty Minute Reserve
NYISO	Spin10	10-Minute Spinning Reserves
	NSpin10	10-Minute Non-Spinning Reserves
	Res30	30-Minute Reserves
	RegC	Regulation Capacity
ISONE	Spin10	Ten Minute Spinning Reserve (TMSR)

Continued on next page

Table D.1: continued from previous page

ISO	Abbreviation	Service Description
	NSpin10	Ten Minute Non-Spinning Reserve (TMNSR)
	OR30	Thirty Minute Operating Reserve (TMOR)
MISO	RamU	Ramp Up
	RamD	Ramp Down
	Spin	Spinning Reserve
	STR	Short-term Reserve
	Sup	Supplemental Reserve
	Reg	Regulation

APPENDIX E

ABBREVIATIONS

Table E.1: List of abbreviations used in the main text

Abbreviation	**Full Name**
45U	Nuclear Production Tax Credit (Section 45U)
45V	Clean Hydrogen Production Tax Credit (Section 45V)
45Y	Technology-Neutral Clean Electricity Production Tax Credit (Section 45Y)
48E	Technology-Neutral Clean Electricity Investment Tax Credit (Section 48E)
AS	Ancillary Service
ASEAN	Association of Southeast Asian Nations
ATB	Annual Technology Baseline (NREL)
BAU	Business-as-Usual
BESS	Battery Energy Storage System
BOP	Balance of Plant
CAISO	California Independent System Operator
CAPEX	Capital Expenditure
CCGT	Combined-Cycle Gas Turbine
CCUS	Carbon Capture, Utilization, and Storage
CO_2	Carbon Dioxide
CRF	Capital Recovery Factor
DCF	Discounted Cash Flow
DOE	U.S. Department of Energy
EOR	Enhanced Oil Recovery
ERCOT	Electric Reliability Council of Texas
H_2	Hydrogen
H2P	Hydrogen-to-Power
HTE	High-Temperature Electrolyzer
IES	Integrated Energy System
IRR	Internal Rate of Return

Continued on next page

Table E.1: continued from previous page

Abbreviation	**Full Name**
ISO	Independent System Operator
ISONE	ISO New England
ITC	Investment Tax Credit
LCOE	Levelized Cost of Energy
LCOH	Levelized Cost of Hydrogen
LCOS	Levelized Cost of Storage
LMP	Locational Marginal Price
MACRS	Modified Accelerated Cost Recovery System
MCMC	Markov Chain Monte Carlo
MISO	Midcontinent Independent System Operator
NETL	National Energy Technology Laboratory
NPP	Nuclear Power Plant
NPV	Net Present Value
NREL	National Renewable Energy Laboratory
NYISO	New York Independent System Operator
O&M	Operations and Maintenance
OPEX	Operating Expenditure
P2H	Power-to-Hydrogen
PJM	PJM Interconnection
PTC	Production Tax Credit
PV	Photovoltaic
SMR (hydrogen)	Steam Methane Reforming
SMR (nuclear)	Small Modular Reactor
SOC	State of Charge
SPP	Southwest Power Pool
TEA	Techno-Economic Analysis
VaR	Value at Risk
VRE	Variable Renewable Energy

REFERENCES

[1] (2024). Techno-economic assessment of hydrogen-based energy storage systems in determining the optimal configuration of the nuclear-renewable hybrid energy system. *Energy Reports*.

[2] Agreement, P. (2015). Paris agreement. In *report of the conference of the parties to the United Nations framework convention on climate change (21st session, 2015: Paris). Retrived December*, Volume 4, pp. 2017. HeinOnline.

[3] Alirahmi, S. M., A. R. Razmi, and A. Arabkoohsar (2021). Comprehensive assessment and multi-objective optimization of a green concept based on a combination of hydrogen and compressed air energy storage (caes) systems. *Renewable and Sustainable Energy Reviews 142*, 110850.

[4] analytics, M. (2021). Mileage ratio issue. [Online] Available at: `https://www.monitoringanalytics.com/reports/Presentations/2021/IMM_MRC_Mileage_Ratio_Issue_20210929.pdf`. [Accessed: May 28 2025].

[5] Andrade, G. A., J. G. García-Clúa, P. R. C. Mendes, and J. Normey-Rico (2019). Optimal control of a grid assisted photovoltaic-hydrogen production system. *IFAC-PapersOnLine*.

[6] Association, W. N. Economics of nuclear power. [Online] Available at: `https://world-nuclear.org/`. [Accessed: Jul. 2 2025].

[7] Badakhshan, S., S. Senemmar, H. Li, and J. Zhang (2022). Integrating offshore wind farms with unmanned hydrogen and battery ships. In *2022 IEEE Kansas Power and Energy Conference (KPEC)*, pp. 1–6. IEEE.

[8] Badea, G. et al. (2016). Techno-economical analysis of hybrid pv-wt-hydrogen fc system for a residential building.

[9] Bayramov, A. (2023). Comprehensive assessment of system efficiency and competitiveness of nuclear power plants in combination with hydrogen complex. *International Journal of Hydrogen Energy 48*(70), 27068–27078.

[10] Beacon Power, L. Overview of ferc order 755 and pay-for-performance regulation. [Online] Available at: `https://www.ercot.com/files/docs/2014/03/19/regulation_pay_for_performance_032114.pdf`. [Accessed: Jun. 2 2025].

[11] Boardman, R. D., T. L. Westover, S. J. Remer, and J. Cadogan (2022). Plan for scaling up hydrogen production with nuclear power plants. Technical report, Idaho National Laboratory (INL), Idaho Falls, ID (United States).

[12] Bockris, J. O. (1972). A hydrogen economy. *Science 176*(4041), 1323–1323.

[13] Bødal, E. F., D. Mallapragada, A. Botterud, and M. Korpås (2020). Decarbonization synergies from joint planning of electricity and hydrogen production: A texas case study. *International Journal of Hydrogen Energy 45*(58), 32899–32915.

[14] Borsboom-Hanson, T., S. R. Patlolla, O. E. Herrera, and W. Mérida (2022). Point-to-point transportation: the economics of hydrogen export. *International Journal of Hydrogen Energy 47*(74), 31541–31550.

[15] Bragg-Sitton, S. et al. (2014). An analysis of methanol and hydrogen production via high-temperature electrolysis using the sodium cooled advanced fast reactor. Technical report.

[16] CAISO. Informational report of the california independent system operator corporation. [Online] Available at: `https://www.caiso.com/Documents/Jul31_2014_Order755MarketDesignReport_ER12-1630_ER14-971.pdf`. [Accessed: Jun. 2 2025].

[17] California Independent System Operator (CAISO) (2025). Caiso official website. `https://www.caiso.com`. Accessed February 20, 2025.

[18] Chang, J.-H., Y.-W. Kim, K.-Y. Lee, Y.-W. Lee, W.-J. Lee, J.-M. Noh, M.-H. Kim, H.-S. Lim, Y.-J. Shin, K.-K. Bae, et al. (2007). A study of a nuclear hydrogen production demonstration plant. *Nuclear Engineering and Technology 39*(2), 111–122.

[19] Chatham House (2018). The power of flexibility. `https://www.chathamhouse.org/2018/08/power-flexibility/2-second-phase-transformations`. Accessed: May 22, 2025.

[20] Chen, X., L. Huang, J. Liu, D. Song, and S. Yang (2022). Peak shaving benefit assessment considering the joint operation of nuclear and battery energy storage power stations: Hainan case study. *Energy 239*, 121897.

[21] Choukulkar, A. (2022). *Don't Mess with Texas: Getting the Lone Star State to Net-Zero by 2050*. University of Colorado Boulder.

[22] Clúa, J., R. Mantz, and H. Battista (2011). Evaluation of hydrogen production capabilities of a grid-assisted wind-h2 system. *Applied Energy 88*, 1857–1863.

[23] COMMISSION, F. E. R. Comments of the independent market monitor for pjm. [Online] Available at: `https://www.monitoringanalytics.com/filings/2022/IMM_Comments_Docket_No_EL21-83_20221108.pdf`. [Accessed: Jun. 2 2025].

[24] Connelly, E., M. Penev, A. Milbrandt, B. Roberts, M. W. Melaina, and N. Gilroy (2020). Resource assessment for hydrogen production.

[25] Constellation Energy Corporation (2025, August). Constellation reports second quarter 2025 results. Press release; includes long-term clean energy offtake announcements.

[26] da Silva, G. N., P. R. Rochedo, and A. Szklo (2022). Renewable hydrogen production to deal with wind power surpluses and mitigate carbon dioxide emissions from oil refineries. *Applied Energy 311*, 118631.

[27] Dabar, O. A., M. O. Awaleh, M. M. Waberi, and A.-B. I. Adan (2022). Wind resource assessment and techno-economic analysis of wind energy and green hydrogen production in the republic of djibouti. *Energy reports 8*, 8996–9016.

[28] de Kleijne, K., M. A. Huijbregts, F. Knobloch, R. van Zelm, J. P. Hilbers, H. de Coninck, and S. V. Hanssen (2024). Worldwide greenhouse gas emissions of green hydrogen production and transport. *Nature Energy*, 1–14.

[29] Delbeke, J., A. Runge-Metzger, Y. Slingenberg, and J. Werksman (2019). The paris agreement. In *Towards a climate-neutral Europe*, pp. 24–45. Routledge.

[30] Denholm, P., D. J. Arent, S. F. Baldwin, D. E. Bilello, G. L. Brinkman, J. M. Cochran, W. J. Cole, B. Frew, V. Gevorgian, J. Heeter, et al. (2021). The challenges of achieving a 100% renewable electricity system in the united states. *Joule 5*(6), 1331–1352.

[31] Denholm, P. and M. Hand (2011). Grid flexibility and storage required to achieve very high penetration of variable renewable electricity. *Energy Policy 39*(3), 1817–1830.

[32] DOE. On the path to 100% clean electricity. [Online] Available at: `https://www.energy.gov/policy/articles/path-100-clean-electricity`. [Accessed: 25 Dec. 2023].

[33] Duan, L., R. Petroski, L. Wood, and K. Caldeira (2022). Stylized least-cost analysis of flexible nuclear power in deeply decarbonized electricity systems considering wind and solar resources worldwide. *Nature Energy 7*(3), 260–269.

[34] EIA. Hourly generation by energy source. [Online] Available at: `https://www.eia.gov/opendata/browser/electricity/rto/fuel-type-data`. [Accessed: 25 Aug. 2024].

[35] EIA. Solar capacity additions are changing the shape of daily electricity supply in texas. [Online] Available at: `https://www.eia.gov/todayinenergy/detail.php?id=61783`. [Accessed: 25 Jul. 2024].

[36] EIA. U.s. nuclear statistics. [Online] Available at: `https://www.eia.gov/energyexplained/nuclear/data-and-statistics.php`. [Accessed: Apr. 12 2025].

[37] El-Emam, R. and I. Khamis (2019). Advances in nuclear hydrogen production: Results from an iaea international collaborative research project. *International Journal of Hydrogen Energy 44*(35), 19080–19088.

[38] Elberry, A. M., J. Thakur, A. Santasalo-Aarnio, and M. Larmi (2021). Large-scale compressed hydrogen storage as part of renewable electricity storage systems. *International journal of hydrogen energy 46*(29), 15671–15690.

[39] Electric Reliability Council of Texas (ERCOT) (2025). Ercot official website. https://www.ercot.com. Accessed February 20, 2025.

[40] EPA. U.s. environmental protection agency. [Online] Available at: https://www.epa.gov/ghgreporting/ghgrp-emissions-location. [Accessed: 15 Aug. 2024].

[41] (EPA), U. E. P. A. Greenhouse gas reporting program (ghgrp). [Online] Available at: https://www.epa.gov/ghgreporting. [Accessed: 15 Aug. 2024].

[42] ERCOT. Combined wind and solar. [Online] Available at: https://www.ercot.com/gridmktinfo/dashboards/combinedwindandsolar. [Accessed: 15 Aug. 2024].

[43] ERCOT. Item 5: Ceo board update. [Online] Available at: https://www.ercot.com/files/docs/2024/04/22/5%20CEO%20Update.pdf. [Accessed: 15 Aug. 2024].

[44] ERCOT. Load forecast. [Online] Available at: https://www.ercot.com/gridinfo/load/forecast. [Accessed: 15 Aug. 2024].

[45] ERCOT. Maps. [Online] Available at: https://www.ercot.com/news/mediakit/maps. [Accessed: 25 Jul. 2024].

[46] ERCOT. Report on existing and potential electric system constraints and needs. [Online] Available at: https://www.ercot.com/files/docs/2022/12/22/2022_Report_on_Existing_and_Potential_Electric_System_Constraints_and_Needs.pdf. [Accessed: 25 Jul. 2024].

[47] ERCOT. Report on existing and potential electric system constraints and needs. [Online] Available at: https://www.ercot.com/files/docs/2023/12/22/2023-Report-on-Existing-and-Potential-Electric-System-Constraints-and-Needs.pdf. [Accessed: 25 Jul. 2024].

[48] Esteves, O. L. A. and H. A. Gabbar (2023). Implementing a nuclear-renewable hybrid energy system to reduce fossil fuel dependency in south africa: A case study. In *2023 IEEE 11th International Conference on Smart Energy Grid Engineering (SEGE)*, pp. 230–234.

[49] Fell, H., A. Gilbert, J. D. Jenkins, and M. Mildenberger (2022). Nuclear power and renewable energy are both associated with national decarbonization. *Nature Energy 7*(1), 25–29.

[50] Fernández-Arias, P., D. Vergara, and J. A. Orosa (2020). A global review of pwr nuclear power plants. *Applied Sciences 10*(13), 4434.

[51] Frew, B. A. et al. (2023). Analysis of multi-output hybrid energy systems interacting with the grid: Application of improved price-taker and price-maker approaches to nuclear-hydrogen systems. *Applied Energy*.

[52] Gao, B., Y. Teng, K. Liu, S. Wang, Z. Wu, B. Xu, H. Zhang, D. Wang, X. Yang, and F. Jiang (2024). Electric-hydrogen coupling system participation in grid peaking support capacity assessment. In *2024 4th International Conference on Energy Engineering and Power Systems (EEPS)*, pp. 627–631.

[53] Giampieri, A., J. Ling-Chin, and A. P. Roskilly (2023). Techno-economic assessment of offshore wind-to-hydrogen scenarios: A uk case study. *International Journal of Hydrogen Energy*.

[54] Gray, K. (2012, 12). Carbon utilization and storage atlas (fourth edition).

[55] Greene, S. R. (2018). Are current us nuclear power plants grid resilience assets? *Nuclear Technology 202*(1), 1–14.

[56] Hassanpouryouzband, A., E. Joonaki, K. Edlmann, and R. S. Haszeldine (2021). Offshore geological storage of hydrogen: is this our best option to achieve net-zero? *ACS Energy Letters 6*(6), 2181–2186.

[57] Homayouni, F. et al. (2017). Techno-economic and environmental analysis of an integrated standalone hybrid solar hydrogen system to supply cchp loads of a greenhouse in iran. *International Journal of Green Energy 14*, 295–309.

[58] Huang, Z., G. He, H. Yan, Z. Peng, and H. Yu (2017). Energy price sensitivity analysis of integrated energy system based on a parametric equation. In *Energy Procedia*, Volume 142, pp. 2905–2910.

[59] Idaho National Laboratory (2023, November). Technical economic assessment of LWR-supported hydrogen markets in gulf coast regions. Technical Report INL/RPT-23-75604, Idaho National Laboratory, Light Water Reactor Sustainability Program.

[60] IEA. Co2 emissions in 2023. [Online] Available at: `https://www.iea.org/reports/co2-emissions-in-2023`. [Accessed: 15 Aug. 2024].

[61] IEA. Wind. [Online] Available at: `https://www.iea.org/energy-system/renewables/wind`. [Accessed: 24 Jul. 2023].

[62] ifp. What does it cost to build nuclear power. [Online] Available at: `https://ifp.org/nuclear-power-plant-construction-costs/`. [Accessed: Jun. 16 2025].

[63] Internal Revenue Service (2023a). Publication 946: How To Depreciate Property. Accessed: 2025-07-24.

[64] Internal Revenue Service (2023b). Zero-Emission Nuclear Power Production Credit. Accessed: 2025-05-10.

[65] Internal Revenue Service (2024a). Clean Electricity Investment Credit. Accessed: 2025-05-10.

[66] Internal Revenue Service (2024b). Clean Hydrogen Production Tax Credit (45V) Resources. Accessed: 2025-05-10.

[67] International Atomic Energy Agency (2025). Nuclear power capacity trend (2005–2024). `https://pris.iaea.org/pris/worldstatistics/worldtrendnuclearpowercapacity.aspx`. Accessed: May 24, 2025.

[68] International Energy Agency (2024). United states 2024: Energy policy review. Technical report, IEA. Accessed: Mar. 26, 2025.

[69] International Energy Agency and Nuclear Energy Agency (2020). Projected costs of generating electricity – 2020 edition. Technical report, IEA & OECD NEA. Accessed: Mar. 24, 2025.

[70] IPCC. The numbers behind the science. in climate change 2014: Mitigation of climate change (cambridge univ. press, 2022). [Online] Available at: `https://www.ipcc.ch/assessment-report/ar6/`. [Accessed: 15 Jul. 2024].

[71] ISO New England (2025). Iso-ne official website. `https://www.iso-ne.com`. Accessed February 20, 2025.

[72] Jain, R., K. Nagasawa, S. Veda, and S. Sprik (2023). Grid ancillary services using electrolyzer-based power-to-gas systems with increasing renewable penetration. *e-Prime-Advances in Electrical Engineering, Electronics and Energy 6*, 100308.

[73] Jia, M., S. Huang, K. Tang, and C. Shen (2018). An investigation on the applicability of the integrated method for multi-carrier energy flow analysis. In *2018 IEEE Power Energy Society General Meeting (PESGM)*, pp. 1–5.

[74] Jodry, A., R. Girard, P. H. A. Nóbrega, R. Molinier, and M.-D. E. A. Faris (2023). Industrial hydrogen hub planning and operation with multi-scale optimisation. *Journal of Cleaner Production 426*, 138750.

[75] Kahlor, L. A., J. Yang, X. Li, W. Wang, H. C. Olson, and L. Atkinson (2020). Environmental risk (and benefit) information seeking intentions: The case of carbon capture and storage in southeast texas. *Environmental Communication 14*(4), 555–572.

[76] Klevstrand, Agnete (Hydrogen Insight) (2023). Indispensable tool for climate — first nuclear hydrogen produced in the us at new york pilot project.

https://www.hydrogeninsight.com/production/indispensable-tool-for-climate-first-nuclear-hydrogen-produced-in-the\/-us-at-new-york-pilot-project/2-1-1415744. Accessed: Mar. 14, 2025.

[77] Knighton, L. T., D. S. Wendt, J. D. Richards, C. Rabiti, A. Abou Jaoude, T. L. Westover, K. G. Vedros, S. Bates, A. Elgowainy, A. Bafana, et al. (2021). Techno-economic analysis of product diversification options for sustainability of the monticello and prairie island nuclear power plants. Technical report, Idaho National Lab.(INL), Idaho Falls, ID (United States).

[78] Knighton, W. B. and D. Wendt (2021). Techno-economic analysis of product diversification options for sustainability of the monticello and prairie island nuclear power plants. Technical report.

[79] Kong, L., L. Li, G. Cai, C. Liu, P. Ma, Y. Bian, and T. Ma (2021). Techno-economic analysis of hydrogen energy for renewable energy power smoothing. *International Journal of Hydrogen Energy 46*(3), 2847–2861.

[80] Li, H., J. H. Panchal, and X. Du (2023). Quantification model uncertainty of label-free machine learning for multidisciplinary systems analysis. In *International Design Engineering Technical Conferences and Computers and Information in Engineering Conference*, Volume 87318, pp. V03BT03A045. American Society of Mechanical Engineers.

[81] Li, H., J. Rahman, and J. Zhang (2022). Optimal planning of co-located wind energy and hydrogen plants: A techno-economic analysis. In *Journal of Physics: Conference Series*, Volume 2265, pp. 042063. IOP Publishing.

[82] Li, H., J. Yin, and X. Du (2022). Uncertainty quantification of physics-based label-free deep learning and probabilistic prediction of extreme events. In *International Design Engineering Technical Conferences and Computers and Information in Engineering Conference*, Volume 86236, pp. V03BT03A001. American Society of Mechanical Engineers.

[83] Li, H. and J. Zhang (2023). Towards sustainable integration: Techno-economic analysis and future perspectives of co-located wind and hydrogen energy systems. *Journal of Mechanical Design*.

[84] Li, H. and J. Zhang (2024). Towards sustainable integration: Techno-economic analysis and future perspectives of co-located wind and hydrogen energy systems. *Journal of Mechanical Design 146*(2).

[85] Liu, B., S. Liu, S. Guo, and S. Zhang (2020). Economic study of a large-scale renewable hydrogen application utilizing surplus renewable energy and natural gas pipeline transportation in china. *International Journal of Hydrogen Energy 45*(3), 1385–1398.

[86] Liu, H., P. Were, Q. Li, Y. Gou, and Z. Hou (2017). Worldwide status of ccus technologies and their development and challenges in china. *Geofluids 2017*(1), 6126505.

[87] Liu, Z., Z. Deng, S. J. Davis, and P. Ciais (2024). Global carbon emissions in 2023. *Nature Reviews Earth & Environment 5*(4), 253–254.

[88] L'Her, G., R. Kemp, M. Bazilian, and M. Deinert (2024). Potential for small and micro modular reactors to electrify developing regions. *Nature energy 9*(6), 725–734.

[89] Mahmud, S., B. Ponkiya, S. Katikaneni, S. Pandey, K. Mattimadugu, Z. Yi, V. Walker, C. Wang, T. Westover, A. Y. Javaid, et al. (2024). Design and optimization of a modular hydrogen-based integrated energy system to maximize revenue via nuclear-renewable sources. *Energy 313*, 133763.

[90] Mahmud, S., S. Sah, B. Ponkiya, S. Katikaneni, D. Raker, M. Heben, R. Khanna, A. Javaid, Z. Yi, T. Westover, et al. (2022). A transactive energy framework for hydrogen production with economically viable nuclear power. In *2022 IEEE/PES transmission and distribution conference and exposition (T&D)*, pp. 1–5. IEEE.

[91] Meckel, T. A., A. P. Bump, S. D. Hovorka, and R. H. Trevino (2021). Carbon capture, utilization, and storage hub development on the gulf coast. *Greenhouse Gases: Science and Technology 11*(4), 619–632.

[92] Medlock III, K. B. and K. Miller (2020). Carbon capture in texas: Comparative advantage in a low-carbon portfolio. *Rice University's Baker Institute for Public Policy*.

[93] Medlock III, K. B. and K. Miller (2021). Expanding carbon capture in texas. *Baker Institute Center for Energy Studies*.

[94] Meinshausen, M., J. Lewis, C. McGlade, J. Gütschow, Z. Nicholls, R. Burdon, L. Cozzi, and B. Hackmann (2022). Realization of paris agreement pledges may limit warming just below 2 c. *Nature 604*(7905), 304–309.

[95] Meraj, S. T., N. Z. Yahaya, B. Singh, and R. Kannan (2020). Implementation of a robust hydrogen-based grid system to enhance power quality. In *2020 IEEE International Conference on Power and Energy (PECon)*, pp. 153–158.

[96] Midcontinent Independent System Operator (MISO) (2025). Miso official website. `https://www.misoenergy.org`. Accessed February 20, 2025.

[97] Mishra, S., J. Pohl, N. Laws, D. Cutler, T. Kwasnik, W. Becker, A. Zolan, K. Anderson, D. Olis, and E. Elgqvist (2022). Computational framework for behind-the-meter der techno-economic modeling and optimization: Reopt lite. *Energy Systems 13*(2), 509–537.

[98] Naterer, G. F., I. Dincer, and C. Zamfirescu (2013). *Hydrogen production from nuclear energy*.

[99] National Association of Regulatory Utility Commissioners (NARUC) (2022). Nuclear energy as a keystone clean energy resource. Technical report, National Association of Regulatory Utility Commissioners (NARUC). Accessed: Apr. 24, 2025.

[100] New York Independent System Operator (NYISO) (2025). Nyiso official website. `https://www.nyiso.com`. Accessed February 20, 2025.

[101] Noyan, O. F., M. M. Hasan, and N. Pala (2023). A global review of the hydrogen energy eco-system. *Energies 16*(3), 1484.

[102] NRC. Operating nuclear power reactors (by location or name). [Online] Available at: `https://www.nrc.gov/info-finder/reactors/index.html`. [Accessed: Jul. 25 2025].

[103] NREL. Annual technology baseline. [Online] Available at: `https://atb.nrel.gov/`. [Accessed: 25 Jul. 2023].

[104] NucNet (2022). U.s. initiative aims for production with nuclear — davis-besse project. `https://www.nucnet.org/news/us-initiative-aims-for-productions-with-nuclear-energy-from-davis-besse-9-4-2022`. Accessed: Mar. 14, 2025.

[105] OECD Nuclear Energy Agency (2020). Unlocking reductions in the construction costs of nuclear: A practical guide for stakeholders. Technical report, OECD NEA. Accessed: Mar. 24, 2025.

[106] Offer, G. J., D. Howey, M. Contestabile, R. Clague, and N. Brandon (2010). Comparative analysis of battery electric, hydrogen fuel cell and hybrid vehicles in a future sustainable road transport system. *Energy policy 38*(1), 24–29.

[107] Ogbonnaya, C., C. Abeykoon, A. Nasser, and A. Turan (2021). Unitized regenerative proton exchange membrane fuel cell system for renewable power and hydrogen generation: Modelling, simulation, and a case study. *Cleaner Engineering and Technology 4*, 100241.

[108] Oskouei, M. Z. and H. Mehrjerdi (2022). Optimal allocation of power-to-hydrogen units in regional power grids for green hydrogen trading: Opportunities and barriers. *Journal of Cleaner Production*.

[109] Parks, G., R. Boyd, J. Cornish, and R. Remick (2014). Hydrogen station compression, storage, and dispensing technical status and costs: Systems integration. Technical report, National Renewable Energy Lab.(NREL), Golden, CO (United States).

[110] Pehl, M., A. Arvesen, F. Humpenöder, A. Popp, E. G. Hertwich, and G. Luderer (2017). Understanding future emissions from low-carbon power systems by integration of life-cycle assessment and integrated energy modelling. *Nature Energy 2*(12), 939–945.

[111] Peng, C., X. Dong, J. Yang, J. Ligao, S. Liu, and X. Zhu (2020). Economic evaluation method of integrated energy system. In *2020 10th Electrical Power, Electronics, Communications, Controls and Informatics Seminar (EECCIS)*, pp. 5–8.

[112] Peng, C., X. Dong, J. Yang, J. Ligao, X. Peng, and S. Liu (2020). Research on economic evaluation for typical integrated energy services. In *2020 IEEE 4th Conference on Energy Internet and Energy System Integration (EI2)*, pp. 961–964.

[113] PJM Interconnection (2025). Pjm official website. `https://www.pjm.com`. Accessed February 20, 2025.

[114] PJM Interconnection, L.L.C. (2025, January). 2025 pjm long-term load forecast report. Technical report.

[115] Price, J., I. Keppo, and P. E. Dodds (2023). The role of new nuclear power in the uk's net-zero emissions energy system. *Energy 262*, 125450.

[116] Products, A. Air products' u.s. gulf coast hydrogen network: Enhanced reliability from the world's largest hydrogen pipeline. [Online] Available at: `https://microsites.airproducts.com/h2-pipeline/pdf/air-products-us-gulf-coast-hydrogen-networkdatasheet.pdf`. [Accessed: 15 Aug. 2024].

[117] Raab, M., R. Körner, and R.-U. Dietrich (2022). Techno-economic assessment of renewable hydrogen production and the influence of grid participation. *International Journal of Hydrogen Energy*.

[118] Rand, J., N. Manderlink, W. Gorman, R. H. Wiser, J. Seel, J. M. Kemp, S. Jeong, and F. Kahrl (2024). Queued up: 2024 edition, characteristics of power plants seeking transmission interconnection as of the end of 2023.

[119] Rezaei, M., K. R. Khalilpour, and M. A. Mohamed (2021). Co-production of electricity and hydrogen from wind: A comprehensive scenario-based techno-economic analysis. *International Journal of Hydrogen Energy 46*(35), 18242–18256.

[120] Root, S. J., A. Shigrekar, and T. L. Westover (2023). Techno-economic analysis of a nuclear reactor system coupled with a liquid metal battery. Technical report, Idaho National Laboratory (INL), Idaho Falls, ID (United States).

[121] Ruth, M. F., P. Jadun, N. Gilroy, E. Connelly, R. Boardman, A. Simon, A. Elgowainy, and J. Zuboy (2020). The technical and economic potential of the h2@ scale hydrogen concept within the united states. Technical report, National Renewable Energy Lab.(NREL), Golden, CO (United States).

[122] Saur, G. (2008). Wind-to-hydrogen project: electrolyzer capital cost study. Technical report, National Renewable Energy Lab.(NREL), Golden, CO (United States).

[123] Schmidt, O., A. Gambhir, I. Staffell, A. Hawkes, J. Nelson, and S. Few (2017). Future cost and performance of water electrolysis: An expert elicitation study. *International journal of hydrogen energy 42*(52), 30470–30492.

[124] Service, C. R. Pipeline transportation of hydrogen: Regulation, research, and policy. [Online] Available at: `https://www.everycrsreport.com/files/2021-03-02_R46700_294547743ff4516b1d562f7c4dae166186f1833e.pdf`. [Accessed: 15 Aug. 2024].

[125] Shen, Y., X. Li, N. Wang, L. Li, and A. Hoseyni (2021). Introducing and investigation of a pumped hydro-compressed air storage based on wind turbine and alkaline fuel cell and electrolyzer. *Sustainable Energy Technologies and Assessments 47*, 101378.

[126] Sizaire, P., B. Lin, and E. Gençer (2024). A novel hydrogen supply chain optimization model–case study of texas and louisiana. *International Journal of Hydrogen Energy 78*, 401–420.

[127] Smola, T., J. Watson, S. Hancock, T. Westover, H. Yeh, and J. Umholtz (2023). Integrated thermohydraulic transient testing of steam extraction loop system to support joint electricity-hydrogen production using generic boiling water reactor. *Progress in Nuclear Energy 160*, 104692.

[128] Song, D., W. Meng, M. Dong, J. Yang, J. Wang, X. Chen, and L. Huang (2022). A critical survey of integrated energy system: Summaries, methodologies and analysis. *Energy Conversion and Management*.

[129] Southwest Power Pool (SPP) (2025). Spp official website. `https://www.spp.org`. Accessed February 20, 2025.

[130] Sovacool, B. K., P. Schmid, A. Stirling, G. Walter, and G. MacKerron (2020). Differences in carbon emissions reduction between countries pursuing renewable electricity versus nuclear power. *Nature Energy 5*(11), 928–935.

[131] SPP. Re: Informational report of southwest power pool, inc. in dockets no. er13-1748-000 and er13-1748-001. [Online] Available at: `https://www.spp.org/documents/37855/2016-05-02_informational%20report%20-%20order%20755%20compliance%20filing_er13-1748.pdf`. [Accessed: Jun. 2 2025].

[132] Stephens-Romero, S. D., T. M. Brown, J. E. Kang, W. W. Recker, and G. S. Samuelsen (2010). Systematic planning to optimize investments in hydrogen infrastructure deployment. *International journal of hydrogen energy 35*(10), 4652–4667.

[133] Su, H., E. Zio, and J. Zhang (2020). A method for the risk analysis of energy supply in integrated energy systems. In *Proceedings of the 30th European Safety and Reliability Conference and 15th Probabilistic Safety Assessment and Management Conference*.

[134] Su, H., E. Zio, J. Zhang, Z. Li, H. Wang, F. Zhang, L. Chi, L. Fan, and W. Wang (2020). A systematic method for the analysis of energy supply reliability in complex integrated energy systems considering uncertainties of renewable energies, demands and operations. *Journal of Cleaner Production 267*, 122117.

[135] Tavakoli, S., M. G. Dozein, V. A. Lacerda, M. C. Mañé, E. Prieto-Araujo, P. Mancarella, and O. Gomis-Bellmunt (2023). Grid-forming services from hydrogen electrolyzers. *IEEE Transactions on Sustainable Energy 14*, 2205–2219.

[136] The White House (2024, November). Biden–harris administration establishes bold u.s. government targets for safely and responsibly expanding u.s. nuclear energy. `https://www.google.com/search?q=Biden%E2%80%93Harris%20Administration%20Establishes%20Bold%20U.S.%20Government%20Targets%20for%20Safely%20and%20Responsibly%20Expanding%20U.S.%20Nuclear%20Energy`.

[137] Tizon, Z. A. M. et al. (2022). Hydrogen production via nuclear-renewable hybrid energy system: A feasibility study for decarbonization in asean region. In *22nd SGEM Int. Conf. on Energy and Clean Technologies*.

[138] Tools, H. North american merchant hydrogen plant production capacities. [Online] Available at: `https://h2tools.org/hyarc/hydrogen-data/merchant-hydrogen-plant-capacities-north-america`. [Accessed: 15 Aug. 2024].

[139] Tweed, K. Faster frequency regulation triples in pjm. [Online] Available at: `https://www.greentechmedia.com/articles/read/faster-frequency-regulation-triples-in-pjm`. [Accessed: Jun. 2 2025].

[140] Tzamalis, G. et al. (2013). Techno-economic analysis of res hydrogen technologies integration in remote island power system. *International Journal of Hydrogen Energy 38*, 11646–11654.

[141] U.S. Department of Energy (2023). The ultimate fast facts guide to nuclear energy. Technical report, Office of Nuclear Energy, U.S. Department of Energy. Accessed: Apr. 24, 2025.

[142] U.S. Department of Energy, Office of Nuclear Energy (2023). Nine mile point begins clean hydrogen production. `https://www.energy.gov/ne/articles/nine-mile-point-begins-clean-hydrogen-production`. Accessed: Mar. 14, 2025.

[143] U.S. Energy Information Administration (2021). U.s. nuclear electricity generation continues to decline as more retirements occur. `https://www.eia.gov/todayinenergy/detail.php?id=51978`. Accessed: Jul. 11, 2025.

[144] U.S. Energy Information Administration (2023). First new u.s. nuclear reactor since 2016 is now in operation. https://www.eia.gov/todayinenergy/detail.php?id=57280. Accessed: Jul. 11, 2025.

[145] U.S. Energy Information Administration (2025, July). We expect rapid electricity demand growth in texas and the mid-atlantic. Today in Energy.

[146] Vanatta, M., D. Patel, T. Allen, D. Cooper, and M. T. Craig (2023). Technoeconomic analysis of small modular reactors decarbonizing industrial process heat. *Joule 7*(4), 713–737.

[147] Verbruggen, A. (2008). Renewable and nuclear power: A common future? *Energy Policy 36*(11), 4036–4047.

[148] Vijayakumar, V., A. Jenn, and J. Ogden (2023). Modeling future hydrogen supply chains in the western united states under uncertainties: an optimization-based approach focusing on california as a hydrogen hub. *Sustainable Energy & Fuels 7*(5), 1223–1244.

[149] Wang, T., T. Xiang, B. Xu, and Y. Xiang (2022). Agent-based self-discipline operation of integrated energy system. In *2022 7th Asia Conference on Power and Electrical Engineering (ACPEE)*, pp. 2002–2007.

[150] Wendt, D., G. Neupane, J. G. Simpson, J. McTigue, and G. Zhu (2024). Techno-economic analysis of greenfield geothermal hybrid power plants using a solar or natural gas steam topping cycle. Technical report, National Renewable Energy Laboratory (NREL), Golden, CO (United States).

[151] Wendt, D. S., L. T. Knighton, and R. D. Boardman (2022). High temperature steam electrolysis process performance and cost estimates. Technical report, Idaho National Laboratory (INL), Idaho Falls, ID (United States).

[152] World Nuclear Association (2023). Economics of nuclear power. https://world-nuclear.org/information-library/economic-aspects/economics-of-nuclear-power.aspx. Accessed: May 22, 2025.

[153] World Nuclear Association (2024a). Nuclear power in the usa. https://world-nuclear.org/information-library/country-profiles/countries-t-z/usa-nuclear-power.aspx. Accessed: Mar. 26, 2025.

[154] World Nuclear Association (2024b). World nuclear performance report 2024. Accessed: July 24, 2025.

[155] Wu, Z., Y. Sun, and S. Yuan (2024). A bi-level optimization method for economic operation of integrated energy systems. In *2024 3rd International Conference on Energy, Power and Electrical Technology (ICEPET)*, pp. 477–480.

[156] Xiao, H., F. Long, L. Zeng, W. Zhao, J. Wang, and Y. Li (2023). Optimal scheduling of regional integrated energy system considering multiple uncertainties. *E3S Web of Conferences*.

[157] Xie, W. and X. Li (2023). Low-carbon economic operation of ies based on life cycle method and hydrogen energy utilization. *Frontiers in Energy Research*.

[158] Yan, L. (2020). An improved ε-constraint method for coordinated operation of integrated energy systems. In *2020 IEEE/IAS Industrial and Commercial Power System Asia (ICPS Asia)*, pp. 58–63.

[159] Yan, L. (2022). A planning method for airport ies with coordination of reliability and economy. In *2022 5th International Conference on Energy, Electrical and Power Engineering (CEEPE)*, pp. 1184–1192.

[160] Yue, X., S. Pye, J. DeCarolis, F. G. Li, F. Rogan, and B. Ó. Gallachóir (2018). A review of approaches to uncertainty assessment in energy system optimization models. *Energy strategy reviews 21*, 204–217.

[161] Zakaria, A., F. B. Ismail, M. H. Lipu, and M. A. Hannan (2020). Uncertainty models for stochastic optimization in renewable energy applications. *Renewable Energy 145*, 1543–1571.

[162] Zenith, F., M. N. Flote, M. Santos-Mugica, C. S. Duncan, V. Mariani, and C. Marcantonini (2022). Value of green hydrogen when curtailed to provide grid balancing services. *International Journal of Hydrogen Energy*.

[163] Zhang, T. (2022). Techno-economic analysis of a nuclear-wind hybrid system with hydrogen storage. *Journal of Energy Storage*.

[164] Zhao, Q., C. Yu, J. Liu, Y. Zhu, L. Yang, H. Zhao, H. Wang, and S. Gao (2021). The techno-economic evaluation of school integrated energy system based on g1-anti-entropy weight-topsis method. *IOP Conference Series: Earth and Environmental Science 675*.

BIOGRAPHICAL SKETCH

Honglin Li is a doctoral candidate in Mechanical Engineering at The University of Texas at Dallas. His doctoral research focuses on the techno-economic analysis of hydrogen-integrated sustainable energy systems, with an emphasis on the role of hydrogen in advancing clean energy transitions. His work systematically investigates three interconnected themes: the integration of hydrogen with renewable energy systems, the use of hydrogen as a pathway for deep decarbonization in the power sector, and the enhancement of nuclear flexibility through hydrogen production and participation in ancillary service markets. By combining mathematical optimization models with detailed techno-economic assessments, his research provides insights into the cost-effectiveness, operational feasibility, and policy adaptability of hydrogen-enabled energy pathways.

Before pursuing his PhD, Honglin earned master's degrees in industrial engineering and computer engineering, specializing in optimization algorithms, supply chain modeling, and machine learning. His broader research experience extends to floating photovoltaic systems, hydropower system, uncertainty analysis related to renewable energy and energy storage economics, reflecting a strong interdisciplinary foundation in clean energy technologies. His long-term goal is to contribute to the design of high-efficiency, low-emission, and economically viable energy systems that accelerate the global transition toward sustainability.

CURRICULUM VITAE

Honglin Li

September 10, 2025

Contact Information:

Department of Mechanical Engineering
The University of Texas at Dallas
800 W. Campbell Rd.
Richardson, TX 75080-3021, U.S.A.

Email: honglin.li@utdallas.edu

Educational History:

PhD, Mechanical Engineering, The University of Texas at Dallas, 2025
MS, Industrial Engineering, Texas State University, 2021
ME, Computer Technology, Dalian Maritime University, 2018
BA, English, Inner Mongolia University of Science and Technology, 2014

Employment History:

Energy System Intern, Idaho National Laboratory (INL), Feb. 2025 – Aug. 2025
Optimization Engineer Intern, FM, Aug. 2024 – Jan. 2025
Research Assistant, The University of Texas at Dallas, Aug. 2021 – Aug. 2024
Teaching Assistant, The University of Texas at Dallas, Aug. 2022 – Dec. 2022
Research Assistant, Texas State University, Aug. 2019 – Jul. 2021
Teaching Assistant, Texas State University, Aug. 2019 – Jul. 2021
Engineer, Shanghai Electric Power Construction Co., Ltd. (SEPC), Sep. 2014 – Apr. 2019

Recent Publications:

Li, H., and Jie Zhang, Towards sustainable integration: techno-economic analysis and future perspectives of co-located wind and hydrogen energy systems, *Journal of Mechanical Design*, 146(2), 2024.

Li, H., Gulai Shen, et al., Real-time greenhouse gas emission intensity informed demand-side load regulation for power grid decarbonization, *Cell Reports Sustainability*, 2025.

Li, H., Tongdan Jin, et al., Facility and microgrid location-allocation for integrated supply chain and transactive energy operations, *Applied Mathematical Modelling*, 119, 2023.

Li, H., Juha Kiviluoma, et al., Techno-economic analysis for co-located solar and hydrogen plants, *2023 19th International Conference on the European Energy Market (EEM)*, IEEE, 2023.

Li, H., Mingxin Li, et al., Techno-economic analysis incorporating intelligent operation and maintenance management: a case study of an integrated offshore wind and hydrogen energy system, *Journal of Physics: Conference Series*, 2767(6), 2024.

Jin, Tongdan, **Li, H.**, et al., Supply chain design for transactive energy operations in the nexus of manufacturing, microgrid and climate, *Journal of the Operational Research Society*, 73(11), 2022.

Conference Publications:

Li, H., Cong Feng, et al., A Multi-Fidelity Gaussian Process Regression Method for Probabilistic Wind Farm Power Curve Estimation, *ASME IDETC/CIE 2023*.

Li, H., Juha Kiviluoma, et al., Techno-economic analysis for co-located solar and hydrogen plants, *IEEE EEM 2023*.

Li, H., Jubeyer Rahman, et al., Optimal planning of co-located wind energy and hydrogen plants: a techno-economic analysis, *Journal of Physics: Conference Series*, 2022.

Badakhshan, S., S. Senemmar, et al., Integrating offshore wind farms with unmanned hydrogen and battery ships, *IEEE KPEC 2022*.

Li, H., Gulai Shen, et al., Locating and Allocating Warehouse Facilities and Prosumer Microgrid in Transactive Energy Paradigm, *2023 International Conference on Smart Electrical Grid and Renewable Energy (SEGRE)*.

Li, H., Huang, J., Poudel, B., et al., Rethinking the economics and flexibility of U.S. nuclear power through hydrogen integration and policy support. (under review).

Professional Services:

Journal Reviewer: Journal of Cleaner Production, International Journal of Hydrogen Energy, Journal of Mechanical Design, Scientific Reports, Journal of Energy Engineering, Energy Conversion and Management: X

Conference Reviewer: ASME-IDETC-2024, ASME-IDETC-2025